UNIVERSITY OF CALIFORNIA SAN DIEGO

SAN DIEGO STATE UNIVERSITY

Adaptive and Delay-Compensating Robot Controllers

A dissertation submitted in partial satisfaction of the
requirements for the degree
Doctor of Philosophy

in

Engineering Sciences (Mechanical and Aerospace Engineering)

by

Mostafa Bagheri

Committee in charge:

University of California San Diego

- Professor Miroslav Krstić, Chair
- Professor Maurício de Oliveira
- Professor Laurel Riek

San Diego State University

- Professor Peiman Naseradinmousavi, Co-Chair
- Professor Ping Lu

2019

The dissertation of Mostafa Bagheri is approved, and it is acceptable in quality and form for publication on microfilm and electronically:

_____

_____

_____

_____
Co-Chair

_____
Chair

University of California San Diego

San Diego State University

2019

DEDICATION

I dedicate this thesis to my parents Ardavan Bagheri and Soheila Javanmardi, and my siblings Sareh and Morteza, for their unwavering support and constant encouragement.

TABLE OF CONTENTS

LIST OF FIGURES

LIST OF TABLES

ACKNOWLEDGEMENTS

I would like to express the deepest appreciation to my advisors, Professor Miroslav Krstić and Professor Peiman Naseradinmousavi, whose experience and motivation have been instrumental in the successful completion of my Ph.D.

I would like to thank my committee members, Professor Miroslav Krstić, Professor Peiman Naseradinmousavi, Professor Ping Lu, Professor Maurício de Oliveira, and Professor Laurel Riek for their time and valuable comments.

I would like to thank Professor Thomas Bewley, Professor Robert Bitmead, Professor Jorge Cortés, Professor Raymond A. de Callafon, Professor Miroslav Krstic, Professor Maurício de Oliveira, Professor Stefan Llewellyn Smith, Professor Sanjoy Dasgupta, Professor Jiawang Nie, etc., for sharing their time and knowledge in the classes during the past years.

I feel fortunate being in the same research group with Shuxia Tang, Ulf Jakob Aarsnes, Leobardo Camacho-Solorio, Stephen Chen, Shumon Koga, Huan Yu, Imoleayo Abel, Drew Steeves, Alan Williams, Kevin Schmidt, Mark Burkhardt, Cenk Demir, Mohammad Al Suwaidanetc, etc. in Cymer Center for Control Systems and Dynamics at University of California San Diego, and Alex Bertino, Nathan Thomas, etc. in Dynamic Systems and Control Laboratory at San Diego State University. You friends make our labs like a home. I wish all of you the best of luck in the future.

This dissertation includes four chapters as follows; Chapter 1 discusses the motivation of this work along with background and literature review on what has been done in

this field. Chapter 2 contains reprints or adaptions of the following papers: 1) M. Bagheri, M. Krstić, and P. Naseradinmousavi, "Multivariable Extremum Seeking for Joint-Space Trajectory Optimization of a High-Degrees-of-Freedom Robot," *ASME Journal of Dynamic Systems, Measurement, and Control*, Vol. 140, Issue 11, pp. 111017-111017-13, 2018; 2) M. Bagheri, M. Krstić, and P. Naseradinmousavi, "Joint-Space Trajectory Optimization of a 7-DOF Baxter Using Multivariable Extremum Seeking," *IEEE American Control Conference (ACC 2018)*, pp. 2176-2181, June 27-29, Milwaukee, WI, USA, 2018; 3) M. Bagheri and P. Naseradinmousavi, "Novel Analytical and Experimental Trajectory Optimization of a 7-DOF Baxter Robot: Global Design Sensitivity and Step Size Analyses," *The International Journal of Advanced Manufacturing Technology*, Vol. 27, Issue 9, pp. 1-15, 2017. The dissertation author is the primary investigator and author of these papers, and would like to thank Miroslav Krstić and Peiman Naseradinmousavi for their contributions.

Chapter 3 contains reprints or adaptions of the following papers: 1) M. Bagheri, P. Naseradinmousavi, and M. Krstić, "Feedback Linearization Based Predictor for Time Delay Control of a High-DOF Robot Manipulator," *Automatica*, Vol. 108, Oct. 2019; 2) M. Bagheri, P. Naseradinmousavi, and M. Krstić, "Time Delay Control of a High-DOF Robot Manipulator Through Feedback Linearization Based Predictor," *ASME Dynamic Systems and Control Conference (DSCC 2019)*, Paper No. DSCC2019-8915, Oct. 8 - 11, Park City, UT, USA, 2019; 3) M. Bagheri, M. Krstić, and P. Naseradinmousavi, "Analytical and Experimental Predictor-Based Time Delay Control of Baxter Robot," *ASME Dynamic Systems and Control Conference (DSCC 2018)*, Paper No. DSCC2018-

9101, Sept. 30 - Oct. 3, Atlanta, GA, USA, 2018. The dissertation author is the primary investigator and author of these papers, and would like to thank Miroslav Krstić and Peiman Naseradinmousavi for their contributions.

Chapter 4 contains reprints or adaptions of the following papers: 1) M. Bagheri, I. Karafyllis, P. Naseradinmousavi, and M. Krstić, "Adaptive Control of a Two-Link Robot Using Batch Least-Square Identifier," *In preparation*, 2019. The dissertation author is the primary investigator and author of this paper, and would like to thank Iasson Karafyllis, Miroslav Krstić, and Peiman Naseradinmousavi for their contributions.

VITA

2010	Bachelor of Science in Mechanical Engineering *cum laude*, Amirkabir University of Technology (Tehran Polytechnic), Tehran, Iran
2013	Bachelor of Science in Chemical Engineering - Petrochemical Industry *cum laude*, Amirkabir University of Technology (Tehran Polytechnic), Tehran, Iran
2013	Master of Science in Mechanical Engineering - Applied Design, Amirkabir University of Technology (Tehran Polytechnic), Tehran, Iran
2013 - 2014	Graduate Researcher, Amirkabir University of Technology (Tehran Polytechnic), Tehran, Iran
2014	Researcher, Department of Advanced Robotics, Italian Institute of Technology (IIT), Genoa, Italy
2019	Doctor of Philosophy in Engineering Sciences (Mechanical and Aerospace Engineering), University of California San Diego and San Diego Sate University, La Jolla, USA

PUBLICATIONS

M. Bagheri, P. Naseradinmousavi, and M. Krstić, "Feedback Linearization Based Predictor for Time Delay Control of a High-DOF Robot Manipulator," *Automatica*, Vol. 108, Oct. 2019.

M. Bagheri, I. Karafyllis, P. Naseradinmousavi, and M. Krstić, "Adaptive Control of a Two-Link Robot Using Batch Least-Square Identifier," *In preparation*, 2019.

M. Bagheri, M. Krstić, and P. Naseradinmousavi, "Multivariable Extremum Seeking for Joint-Space Trajectory Optimization of a High-Degrees-of-Freedom Robot," *ASME Journal of Dynamic Systems, Measurement, and Control*, Vol. 140, Issue 11, pp. 111017-1 – 111017-13, 2018.

M. Bagheri and P. Naseradinmousavi, "Novel Analytical and Experimental Trajectory Optimization of a 7-DOF Baxter Robot: Global Design Sensitivity and Step Size Analyses," *The International Journal of Advanced Manufacturing Technology*, Springer, Vol. 93, Issue 9-12, pp 4153–4167, Dec. 2017.

P. Naseradinmousavi, H. Ashrafiuon, and **M. Bagheri**, "A Decentralized Neuro-Adaptive Control Scheme to Suppress Chaotic/Hyperchaotic Dynamics of Smart Valves Network," *ASME Journal of Computational and Nonlinear Dynamics*, Vol. 13, Issue 5, pp. 051008, Apr. 2018.

I. Kardan, M. Kabganian, R. Abiri, and **M. Bagheri**, "Stick-Slip Conditions in the General Motion of a Planar Rigid Body," *Journal of Mechanical Science and Technology*, Springer, Vol. 27, Issue 9, pp. 2577-2583, 2013.

M. Bagheri, M. Kabganian, and R. Nadafi, "Three-axis Attitude Control Design for a Spacecraft Based on Lyapunov Stability Criteria," *Scientia Iranica, Transaction B: Mechanical Engineering*, Vol. 20, Issue 4, pp. 1302–1309, 2013.

M. Bagheri, P. Naseradinmousavi, and M. Krstić, "Time Delay Control of a High-DOF Robot Manipulator Through Feedback Linearization Based Predictor," *ASME Dynamic Systems and Control Conference (DSCC 2019)*, Paper No. DSCC2019-8915, Oct. 8 - 11, Park City, UT, USA, 2019.

A. Bertino, **M. Bagheri**, M. Krstić, and P. Naseradinmousavi, "Experimental Autonomous Deep Learning-Based 3D Path Planning for a 7-DOF Robot Manipulator," *ASME Dynamic Systems and Control Conference (DSCC 2019)*, Paper No. DSCC2019-8951, Oct. 8 - 11, Park City, UT, USA, 2019.

M. Bagheri, M. Krstić, and P. Naseradinmousavi "Analytical and Experimental Predictor-Based Time Delay Control of Baxter Robot," *ASME Dynamic Systems and Control Conference (DSCC 2018)*, Paper No. DSCC2018-9101, Sept. 30 - Oct. 3, Atlanta, GA, USA, 2018.

M. Bagheri, M. Krstić, and P. Naseradinmousavi, "Joint-Space Trajectory Optimization of a 7-DOF Baxter Using Multivariable Extremum Seeking," *IEEE American Control Conference (ACC 2018)*, pp. 2176–2181, June 27-29, Milwaukee, WI, USA, 2018.

P. Naseradinmousavi, H. Ashrafiuon, and **M. Bagheri**, "Suppressing Chaotic and Hyperchaotic Dynamics of Smart Valves Network Using A Centralized Adaptive Approach," *IEEE American Control Conference (ACC 2018)*, pp. 1671–1676, June 27-29, Milwaukee, USA, 2018.

M. Bagheri, P. Naseradinmousavi, and R. Morsi, "Experimental and Novel Analytical Trajectory Optimization of a 7-DOF Baxter Robot: Global Design Sensitivity and Step Size Analyses," *ASME Dynamic Systems and Control Conference (DSCC 2017)*, Vol. 1, pp. V001T30A001, Paper No. DSCC2017-5004, Oct. 11-13, Tysons Corner, VA, USA, 2017.

M. Bagheri, P. Naseradinmousavi, M. Ashrafiuon, M. Canova, and D. B. Segala "Suppressing Chaotic/Hyperchaotic Dynamics of Smart Valves Network Using Decentralized and Centralized Schemes," *ASME Dynamic Systems and Control Conference (DSCC 2017)*, Vol. 3, pp. V003T42A001, Paper No. DSCC2017-5006, Oct. 11-13, Tysons Corner, VA, USA, 2017.

P. Naseradinmousavi, **M. Bagheri**, M. Krstić, and C. Nataraj, "Coupled Chaotic and Hyperchaotic Dynamics of Actuated Butterfly Valves Operating in Series," *ASME Dynamic Systems and Control Conference (DSCC 2016)*, Vol. 2, pp. V002T17A001, Paper No. DSCC2016-9601, Oct. 12-14, Minneapolis, MN, USA, 2016.

P. Naseradinmousavi, **M. Bagheri**, and C. Nataraj, "Coupled Operational Optimization of Smart Valve System Subject to Different Approach Angles of A Pipe Contraction," *ASME Dynamic Systems and Control Conference (DSCC 2016)*, Vol. 1, pp. V001T02A001, Paper No. DSCC2016-9627, Oct. 12-14, Minneapolis, MN, USA, 2016.

M. Bagheri, A. Ajoudani, J. Lee, D. Caldwell, and N. Tsagarakis, "Kinematic Analysis and Design Considerations for Optimal Base Frame Arrangement of Humanoid Shoulders," *IEEE International Conference on Robotics and Automation (ICRA 2015)*, pp. 2710–2715, May 26-30, Seattle, WA, USA, 2015.

M. Bagheri, M. Kabganian, and R. Nadafi, "Stable Design of Attitude Control for A Spacecraft," *IAA Conference on Dynamics and Control of Space System (DyCoSS 2012)*, Advances in the Astronautical Sciences, Vol. 145, pp. 777–788, Mar. 19-21, Porto, Portugal, 2012

M. Kabganian, R. Nadafi, Y. Tamhidi, and **M. Bagheri**, "A Novel Mechanical Attitude Simulator with Adaptive Control for Micro-Satellite," *IEEE International Conference on Control, Instrumentation, and Automation (ICCIA 2011)*, pp. 694–698, Dec. 27-29, Shiraz, Iran, 2011

M. Bagheri and P. Mottaghizadeh, "Analysis of Tool-Chip Interface Temperature with FEM and Empirical Verification," *International Journal of Mechanical, Aerospace, Industrial, Mechatronic and Manufacturing Engineering*, Vol. 6, No. 8, pp. 1766–1775, 2012.

P. Mottaghizadeh and **M. Bagheri**, "3D Modeling of Temperature by Finite Element in Machining With Experimental Authorization," *International Journal of Mechanical, Aerospace, Industrial, Mechatronic and Manufacturing Engineering*, Vol. 6, No. 8, pp. 1646–1652, 2012.

A. Fata, **M. Bagheri**, and P. Mottaghizadeh, "Tool Temperature Prediction during Machining by FEM with Experimental Validation," *Journal of Basic and Applied Scientific Research*, Vol. 2, Issue 12, pp. 12606–12610, 2012.

ABSTRACT OF THE DISSERTATION

Adaptive and Delay-Compensating Robot Controllers

by

Mostafa Bagheri

Doctor of Philosophy in Engineering Sciences (Mechanical and Aerospace Engineering)

University of California San Diego, 2019

San Diego State University, 2019

Professor Miroslav Krstić, Chair
Professor Peiman Naseradinmousavi, Co-Chair

The robot manipulators are used in network-based industrial units, and even homes, by expending a significant lumped amount of energy. Manipulators are also subject to large time delays like many engineering systems, which may lead to the lack of high precision required and could cause not only poor control performance, but also catastrophic instability. Hence designing control algorithms for such delay systems to compensate for the time delay and having a robust control law is a necessity. Another important point

which needs to be noticed in utilizing robots is environmental uncertainties, which may not be considered in the modeling. To summarize, parametric uncertainty and/or time-delay through manipulation along with optimal operation are important criteria for the operation of robotic systems.

One of the main contributions of this dissertation is focusing on the development of robust techniques for achieving optimal operation and control of the arm to attain perfect tracking. For the operational optimization, we examine a discrete-time multi-variable gradient-based Extremum Seeking (ES) scheme enforcing operational time and torque saturation constraints to minimize the lumped amount of energy consumed for a path given. Finally, the optimal trajectory is experimentally implemented to be thoroughly compared with the inefficient one.

Precise control of manipulators in the presence of delay or uncertainty and variation in their environments is also a prerequisite to feasibly utilize robot manipulators. Nonlinear control theorems for nonlinear systems (e.g. robotic systems) have been developed for a long period, however, implementing them, in reality, is one of the most challenging problems in engineering applications. Therefore, formulating novel robust and computationally efficient control approaches is still a necessity.

Another significant contribution of this work is a practical implementation of various control theories, with verifying all the necessary assumptions, for high-DOF manipulators. We formulate different computationally efficient control laws to implement real-time controllers for a high Degree-of-Freedom manipulator with uncertainties or in the presence of delay to move toward implementing those control laws in other engineering applications.

Chapter 1

Introduction

1.1 Motivation

The robot manipulators are used in network-based industrial units, and even homes, by expending a significant lumped amount of energy, and therefore, optimal trajectories need to be generated to address efficiency issues. These robots are typically operated for thousands of cycles resulting in a considerable cost of operation. Therefore, optimal trajectories need to be generated to address efficiency issues. Operational operation is an optimization process in which we try to find the best input parameter such that a cost function, for example, time and/or energy consumed, becomes minimum.

Manipulators are also subject to large time delays like many engineering systems, which may lead to the lack of high precision required and could cause not only poor control performance, but also catastrophic instability. Therefore, precise control of manipulators in the presence of delay or uncertainty and variation in their environments is a prerequisite

to feasibly utilize robot manipulators. Control theory tries to derive inputs such that system yields acceptable outputs. However, some interesting questions arise from practical implementation,

- How can a mechanical system be effectively modeled?
- What are the criteria defined for an acceptable response of the system?
- How can the optimal operation be determined subject to cost function and constraints?
- What type of controller can be applied to the system?
- How do the input parameters influence the system?
- Is it practically possible to implement the controller designed?

In this dissertation, we try to properly answer these questions with a focus on robot manipulators.

1.2 Robotics

Robotics is a branch of engineering that involves the conception, design, manufacturing, and operation of robots. This field is an interdisciplinary branch of engineering and science including mechanics, electronics, computer science, artificial intelligence, mechatronics, nanotechnology, and bioengineering. In robotics, machines are eventually

developed to be substituted for humans, with respect to both physical activity and decision making, and replicate human actions.

Robots are designed to replicate walking, lifting, speech, and anything a human can do and are usually utilized in dangerous environments (e.g. bomb detection and deactivation) or where humans cannot survive (e.g. in disasters or space). For instance, many robots are designed to do tasks being hazardous to people such as finding survivors in unstable ruins and exploring mines. To have the most efficient robot to be substituted with the human in dangerous environments, some robots are designed analogous to human, the so-called humanoid robots.

1.3 Humanoid Robots

A humanoid robot has the overall appearance of a human body, which is helping to interact properly with human and work with made-for-human tools as effective as possible. It is worth mentioning that as our concerns are operational optimization and the development of best control laws for robot manipulators, the history of humanoid robots is not thoroughly investigated in this dissertation, and it can be found in [76].

Humanoid robots have received much attention as research topics in several scientific fields, and scientists attempt to simulate the human body leading to a better understanding of it along with having more efficient robots. To enable robots to interact with complex environments and in different situations, planning and control processes must focus on self-collision detection, path planning, and obstacle avoidance. Through plan-

ning and control, the essential difference between humanoids and other kinds of robots (like industrial ones) is that the movement of the robot has to be human-like. Robots usually have redundancy in movements, i.e. more degrees of freedom than needed, and consequently have wide tasks availability. These characteristics are desirable to humanoid robots which bring more complexity and new problems to the planning and control.

In general, humanoid robots are made of a torso with a head, two arms, and two legs, although some humanoid robots may represent a part of the human body, the waist up (just manipulation) or down (just locomotion). In this dissertation, we focus on a dual-arm Baxter manipulator, whose each arm has 7 Degrees-oF-Freedom (DOF), to thoroughly study the dynamics and control of an arm. To this end, we briefly explain the kinematics and kinetics of manipulators and then carry out modeling of the Baxter's arm along with verifying the model.

Figure 1.1: Baxter research robot

1.4 Problem Statement and Contributions

As mentioned earlier, the robot manipulators are utilized in different work environments and consume a significant lumped amount of energy, while they are subject to time delay and uncertainties. Therefore, one of the important points, which needs to be noticed, is the modeling of manipulator subject to environmental uncertainties and/or time-delay along with operational optimization. Therefore, a systematic and general approach, namely, the Denavit-Hartenberg convention for robotic systems, in particular manipulators, is presented through this dissertation. Then, operational optimization and control of the Baxter manipulator are investigated using various simulations and experiments.

Precise control of manipulators in the presence of delay or uncertainty and variation in their environments is a prerequisite to feasibly employ robot manipulators. Nonlinear control theorems for nonlinear systems (e.g robotic systems) have been developed for a long time, however, implementing them, in reality, is one of the most challenging problems in engineering applications. First of all, some specific assumptions generally mentioned in a theorem are not necessarily valid for all engineering systems. Second, verifying those assumptions are analytically cumbersome to be carried out. Another important contribution of this work is the practical implementation of various control theories for high-DOF manipulators.

One of the main contributions of this dissertation is focusing on the development of robust techniques for achieving optimal operation and control of the arm to attain perfect tracking. To this end, coupled dynamic equations of the Baxter manipulator are derived

using the Lagrangian method and then experimentally validated to examine the accuracy of the model through Chapter 2.

For the operational optimization, we examine a discrete-time multi-variable gradient-based Extremum Seeking (ES) scheme enforcing operational time and torque saturation constraints to minimize the lumped amount of energy consumed for a path given. Therefore, global sensitivity analysis is performed to investigate the effects of changes in optimization variables on the cost function leading to select the most effective ones. The results are compared with those of a global heuristic genetic algorithm (GA) to discuss the locality/globality of optimal solutions. Finally, the optimal trajectory is experimentally implemented to be thoroughly compared with the inefficient one. We also carry out time-energy optimization using discrete-time multi-variable Extremum Seeking (ES) and its results are discussed.

The control of nonlinear systems, i.e. a manipulator, has received much attention during the last decays, however, there are still some challenges arising from their applications, which include dealing with uncertainties and time delays. Therefore, formulating novel robust and time-efficient control approaches is still a necessity and therefore, this research effort is another important contribution of this dissertation. We formulate different time-efficient control laws to implement real-time controllers for a high Degree-of-Freedom manipulator with uncertainties or in the presence of delay to move toward implementing those control laws in other engineering applications.

1.5 Organization

The rest of this dissertation is structured into three chapters. In Chapter 2, modeling and operational optimization of a 7-DOF Baxter manipulator are carried out. For this purpose, the coupled dynamic equations of the Baxter manipulator are symbolically derived using the Euler-Lagrangian method and then experimentally validated to examine the accuracy of the model. Then, the operational optimization is examined using discrete-time multi-variable gradient-based Extremum Seeking (ES) scheme to minimize the lumped amount of energy consumed for a path given. To this end, the global sensitivity analysis is also performed to investigate the optimization variables' effects on the cost function defined. The results are compared with those of a global heuristic genetic algorithm (GA) and then the optimal trajectory is experimentally implemented.

In Chapter 3, a predictor-based control scheme is formulated for the high-DOF manipulator in the presence of input delays. Our controller is adopted from a predictor-based control approach for a general nonlinear system subject to a couple of assumptions. We investigate the effects of time delay on the system, the Baxter manipulator, verify all the assumptions, and then utilize the control method proposed for our system. Finally, the controller is implemented on Baxter and results are thoroughly discussed. It is worth mentioning that our approach is extendable to any Euler-Lagrangian system.

In Chapter 4, a novel adaptive control approach, which is more computationally applicable/efficient in comparison with the classical one, is formulated for a general robotic system. The simulation results for a two-link manipulator are presented and the computa-

tional efficiency of the method, in particular for parameter estimation, is investigated. The significance of this method is its independence to the persistent excitation in input/output for the parameter estimation, which is a crucial concern in classical controllers.

Chapter 2

Modeling and Operational Optimization

2.1 Dynamic Modeling

The mechanical structure of a robot manipulator consists of a sequence of rigid bodies (links) dynamically interconnected through joints. A manipulator is characterized by an arm that ensures mobility and dexterity as well as an end-effector that performs the task defined for the robot. A prismatic joint creates a relative translational motion between the two links, whereas a revolute joint creates a relative rotational motion between the two links. In the Baxter manipulator, we have seven revolute joints, as shown in Fig. 2.1.

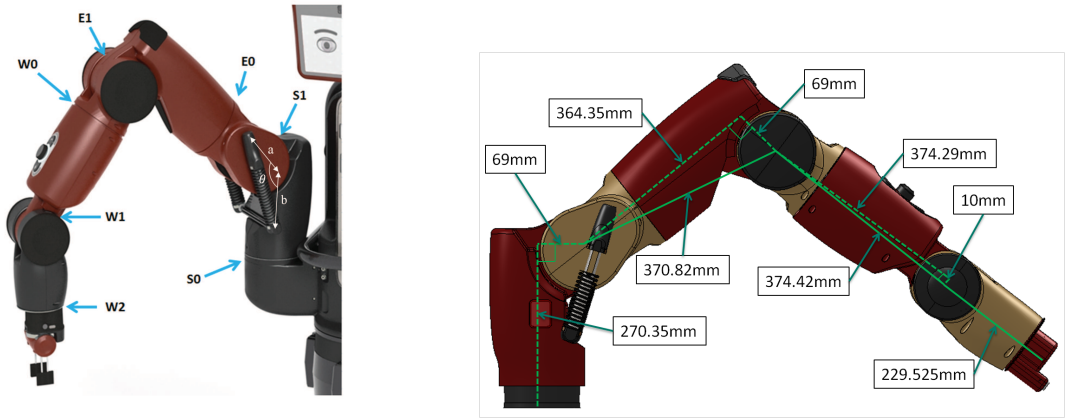

(a) (b)

Figure 2.1: Baxter's joints and link lengths: (a) Baxter's joints; (b) Baxter's link lengths

2.1.1 Kinematics

In a robot manipulator, the joints' variables are the angles between the links in the case of revolute or rotational joints. The forward kinematics equation relates joint space variables to operational space variables, while the inverse kinematic problem provides closed-form solutions for typical manipulation structures. Deriving forward/inverse kinematic equations are thoroughly discussed in [93].

We briefly introduce a systematic and general approach for the kinematics of a manipulator, which refers to the Denavit-Hartenberg (DH) convention. This convention provides a systematic procedure for performing kinematics analysis. The problem is calculating the coordinate transformations between two frames attached to the two links. Note that carrying out kinematic analysis of an n-link manipulator can be extremely complex

without utilizing this convention.

Frame i with respect to Frame $i-1$ are completely specified by the following parameters [93]:

- ✓ a_i is the distance between O_i and $O_{i'}$,
- ✓ d_i is the coordinate of $O_{i'}$ along z_{i-1},
- ✓ α_i is the angle between axes z_{i-1} and z_i about axis x_i to be taken positive when rotation is made counter-clockwise,
- ✓ θ_i is the angle between axes x_{i-1} and x_i about axis z_{i-1} to be taken positive when rotation is made counter-clockwise.

Through this convention, each homogeneous transformation is represented in terms of the four quantities θ_i, a_i, d_i, and α_i, which are the parameters associated with link i and joint i. The four parameters a_i, α_i, d_i, and θ_i, shown in Fig. 2.2, are calculated based on the length, twist, offset, and joint angle of a link, respectively, with respect to the relationship between two coordinate frames, as follows. Note that θ_i for a revolute joint and d_i for a prismatic joint are varying while the others are constant for a link.

We utilize this convention for modeling and subsequently kinematic and kinetic analyses of Baxter. For finding the robot's DH parameter, we need the arm's dimensions and geometrical parameters, which are provided by the Baxter's manufacturer.

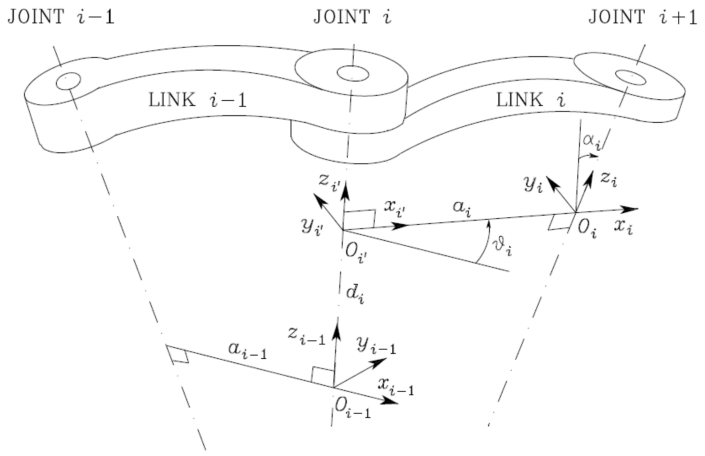

Figure 2.2: Denavit-Hartenberg frame assignment [93]

Table 2.1: Baxter's DH parameters

Link	d	a	α	θ
1	0.27035	0.069	$-\pi/2$	0
2	0	0	$\pi/2$	0
3	0.3644	0.069	$-\pi/2$	0
4	0	0	$\pi/2$	0
5	0.3743	0.01	$-\pi/2$	0
6	0	0	$\pi/2$	0
7	0.2295	0	0	0

2.2 Workspace

The shape and volume of the workspace depend on the kinematics and mechanical joints' limits of a manipulator. The workspace can be computed using the direct kinematic equation with a random search within the joint motion ranges, and then finding the end-effector position in the Cartesian space [6].

Table 2.2: Joints' ranges [88]

Joint	Range (Degrees)	Range (Radians)
S_0	from -97.494° to +97.494°: 194.998°	from -1.7016 to +1.7016: 3.4033
S_1	from -123° to +60°: 183°	from -2.147 to +1.047: 3.194
E_0	from -174.987° to +174.987°: 349.979°	from -3.0541 to +3.0541: 6.1083
E_1	from -2.864° to +150°: 153°	from -0.05 to +2.618: 2.67
W_0	from -175.25° to +175.25°: 350.5°	from -3.059 to +3.059: 6.117
W_1	from -90° to +120°: 210°	from -1.571 to +2.094: 3.6647
W_2	from -175.25° to +175.25°: 350.5°	from -3.059 to +3.059: 6.117

Fig. 2.3 presents the workspace of each arm and the common workspace of dual-arms. The common workspace is one of the most important manipulation indices in the dual-arm manipulations such as valve-turning and assembly tasks. Baxter can execute actions within the area shown, although Baxter performs tasks more efficiently when the objects are located close to the center of the workspace [88].

2.2.1 Kinetics

Kinetics provides a description of the relationship between the joints' actuator torques and the motions of links in a manipulator. In general, the Euler-Lagrange equation expectedly leads to a set of second-order ordinary differential equations:

$$\frac{d}{dt}\frac{\partial L}{\partial \dot{q}_i} - \frac{\partial L}{\partial q_i} = \tau_i \qquad i = 1, \cdots, n \tag{2.1}$$

where L denotes the Lagrangian and is obtained based on kinetic and potential energies ($L = K - P$), and q_i is the rotation angle of each link related to the previous one. The

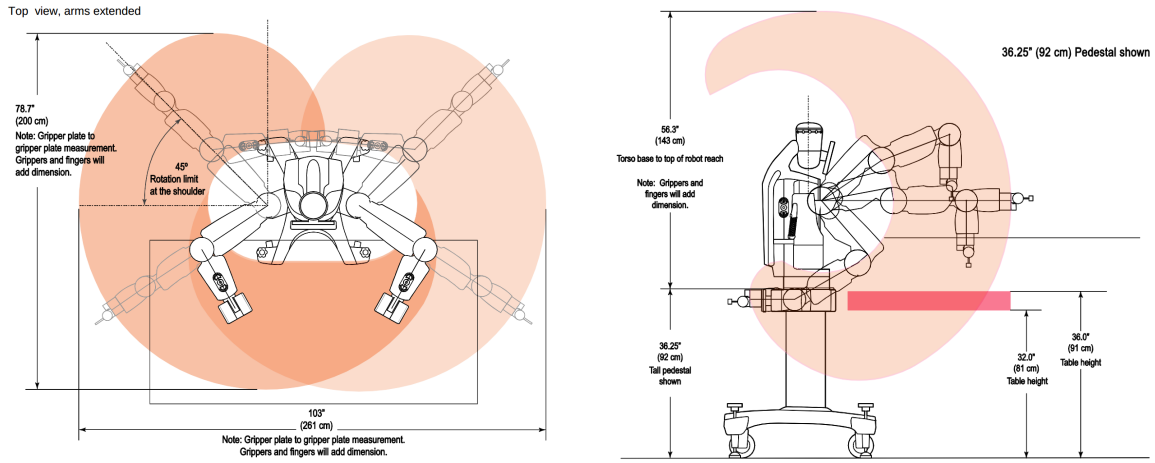

(a) (b)

Figure 2.3: Baxter's workspace [88]

kinetic energy of an n-link manipulator, which has n degrees of freedom, is a quadratic function of $\dot{q}$ (the vector of joints' angular velocities) as follows:

$$\begin{aligned} K =& \frac{1}{2}\dot{q}^T \sum_{i=1}^{n} \left[J_{\mathrm{v_i}}(q)^T m_i J_{\mathrm{v_i}}(q) + J_{\omega_\mathrm{i}}(q)^T R_i(q) I_i R_i(q)^T J_{\omega_\mathrm{i}}(q) \right] \dot{q} \\ =& \frac{1}{2}\dot{q}^T M(q)\dot{q} = \frac{1}{2}\sum_{i,j}^{n} d_{ij}(q)\dot{q}_i \end{aligned} \tag{2.2}$$

where, $J_{\mathrm{v_i}}$ and J_{ω_i} are $3 \times n$ matrices making the Jacobian of mass center of the i-th link. Also, m_i, r_i, and I_i are mass, the center of mass, and the moment of inertia of the i-th link, respectively, which are shown in Tables 2.3 and 2.4.

Table 2.3: Links' mass and center of mass

Link	Mass (kg)	Center of mass (m)
S_0	5.70044	[0.01783, 0.00086, 0.19127]
S_0	3.22698	[0.06845, 0.00269, -0.00529]
S_0	4.31272	[-0.00276, 0.00132, 0.18086]
S_0	2.07206	[0.02611, 0.00159, -0.01117]
W_0	2.24665	[-0.00168, 0.0046, 0.13952]
W_1	1.60979	[0.06041, 0.00697, 0.006]
W_2	0.35093	[0.00198, 0.00125, 0.01855]

The matrix $M(q)$ is consist of two kinds of elements: 1) constant terms including the mass and moment of inertia around the center of mass, which do not depend on the robot's configuration and 2) state/configuration dependent terms. Also, $M(q) : \mathbb{R}^n \to \mathbb{R}^{n\times n}$ is a symmetric positive definite matrix.

Note that the Baxter's arm has a set of springs (Fig. 2.1(a)) acting as a damper to absorb harmful vibration of the jerky motions as discussed earlier. The potential energy is hence obtained as follows:

$$P = \sum_{i=1}^{n} P_i + \frac{1}{2} k_{\mathrm{eq}} x^2 = \sum_{i=1}^{n} g^T r_{\mathrm{c_i}} m_i + \frac{1}{2} k_{\mathrm{eq}} x^2 \tag{2.3}$$

where, P_i is the potential energy of the i-th link, g is the gravitational acceleration, r_{c_i} indicates the coordinate of mass center of link i, k_{eq} stands for the stiffness of preloaded springs in joint S_1, and x is the spring displacement which is calculated as:

$$x = x_0 - \sqrt{a^2 + b^2 - 2ab\cos(\theta)} \tag{2.4}$$

Table 2.4: Links' moment of inertia

Link	I_{xx}	I_{xy}	I_{xz}	I_{yy}	I_{yz}	I_{zz}
Upper Shoulder	0.04709102262	0.00012787556	0.00614870039	0.03766976455	0.00078086899	0.03595988478
Lower Shoulder	0.01175209419	-0.00030096398	0.00207675762	0.0278859752	-0.00018821993	0.02078749298
Upper Elbow	0.02661733557	0.00029270634	0.00392189887	0.02844355207	0.0010838933	0.01248008322
Lower Elbow	0.00711582686	0.00036036173	0.0007459496	0.01318227876	-0.00019663418	0.00926852064
Upper Forearm	0.01667742825	0.00018403705	0.00018657629	0.01675457264	-0.00064732352	0.0037463115
Lower Forearm	0.00387607152	-0.00044384784	-0.00021115038	0.00700537914	0.00015348067	0.0055275524
Wrist	0.00025289155	0.00000575311	-0.00000159345	0.0002688601	-0.00000519818	0.0003074118

where x_0 is the free length of spring and $\theta = \frac{\pi}{2} + \psi$ ($\psi = -q_2$).

Using the energy terms shown in Eqs. (2.2) and (2.3), the general form of the Euler-Lagrange equation becomes:

$$M(q)\ddot{q} + C(q,\dot{q})\dot{q} + G(q) = \tau \tag{2.5}$$

where, $\dot{q} \in \mathbb{R}^n$ and $\ddot{q} \in \mathbb{R}^n$ indicate the vectors of angular velocity and acceleration of the joints, respectively, τ is the driving torques' vector. When the system is fully actuated we have $\tau \in \mathbb{R}^n$. Finally, $G(q) \in \mathbb{R}^n$ is the gravitational matrix as follows:

$$G_k = \frac{\partial P}{\partial q_k} \tag{2.6}$$

Utilizing the "Christoffel symbols" [100] would help us derive the elements of the Coriolis matrix ($C(q,\dot{q})$) as follows:

$$c_{ijk} = \frac{1}{2}\left\{\frac{\partial d_{kj}}{\partial q_i} + \frac{\partial d_{ki}}{\partial q_j} - \frac{\partial d_{ij}}{\partial q_k}\right\} \tag{2.7}$$

where the k,j-th element of $C(q,\dot{q})$ is calculated as the following:

$$c_{kj} = \sum_{i=1}^{n} c_{ijk}(q)\dot{q}_i = \sum_{i=1}^{n} \frac{1}{2}\left\{\frac{\partial d_{kj}}{\partial q_i} + \frac{\partial d_{ki}}{\partial q_j} - \frac{\partial d_{ij}}{\partial q_k}\right\}\dot{q}_i \tag{2.8}$$

2.2.2 Model Verification

The experimental validation of such a coupled nonlinear mathematical model is a necessity to be carried out in order to examine the accuracy of the formulation and then possibly refine the model [9, 10, 13]. We hence recorded the joints' torques to be compared with the ones computed through the interconnected equations, and the results are shown in Fig. 2.4 for all joints.

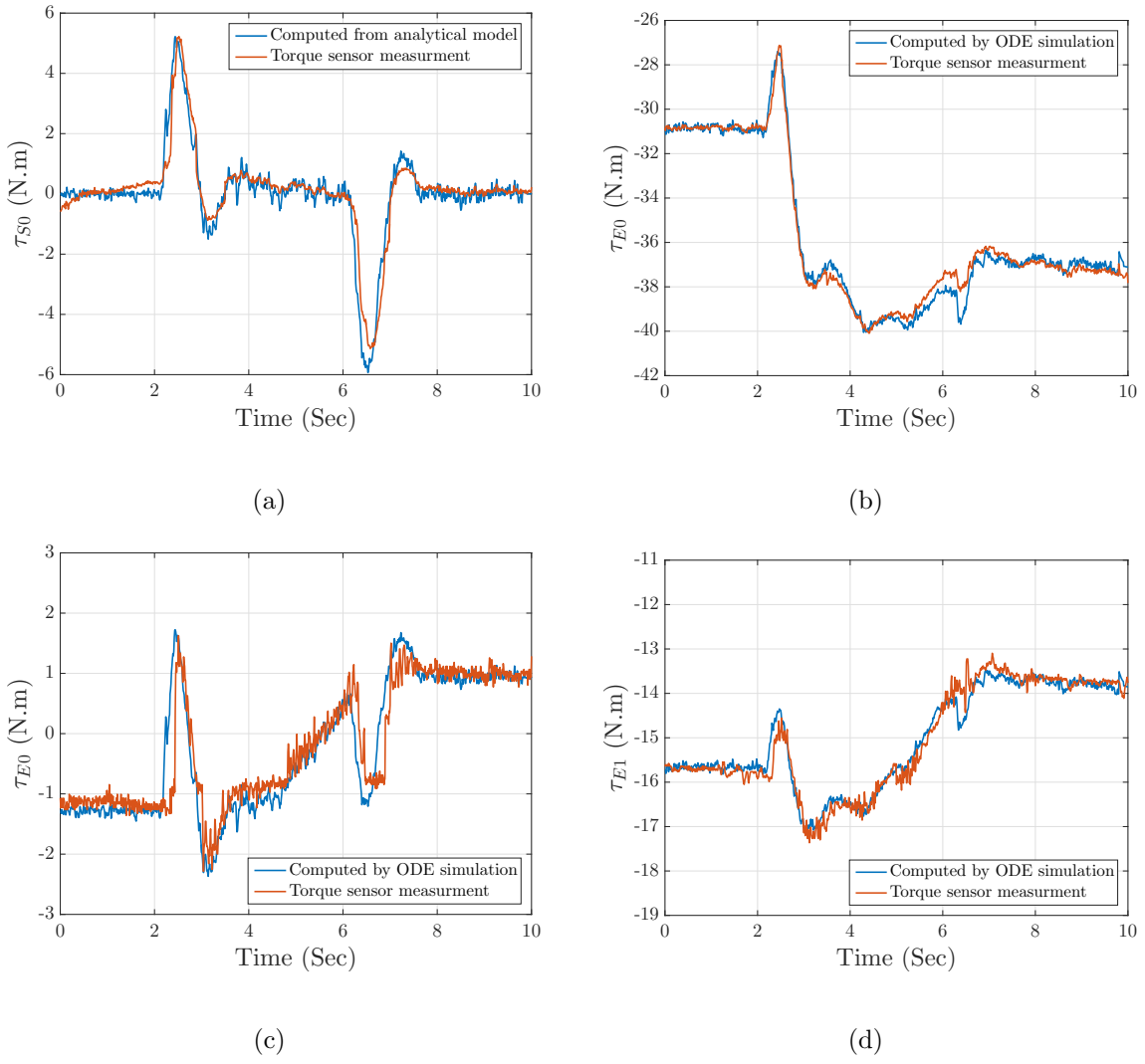

Figure 2.4: Comparison between the experimentally measured and nominal analytical torques used in driving the joints (a) S_0, (b) S_1, (c) E_0, (d) E_1, (e) W_0, (f) W_1, and (g) W_2; the non-zero torques at the initial point ($t = 0$) stand for holding torques against gravity

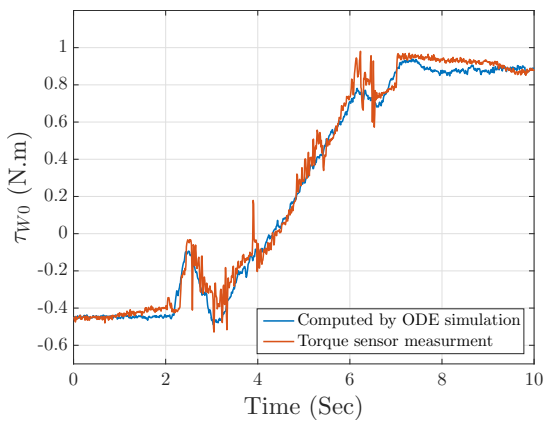

(e)

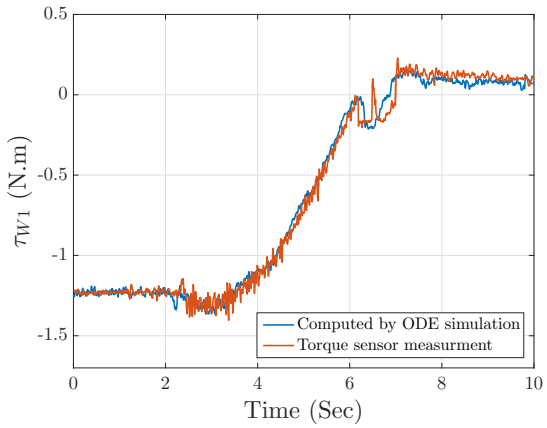

(f)

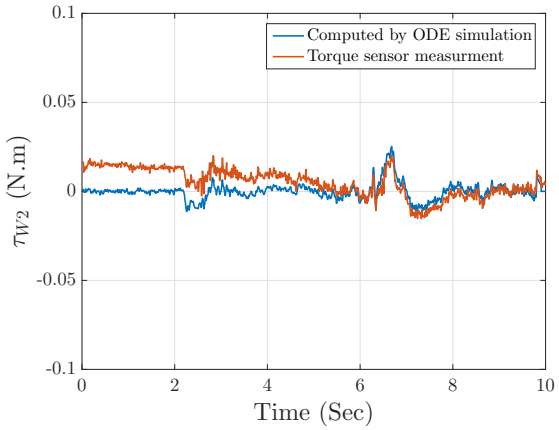

(g)

Figure 2.4: Comparison between the experimentally measured and nominal analytical torques used in driving the joints (a) S_0, (b) S_1, (c) E_0, (d) E_1, (e) W_0, (f) W_1, and (g) W_2; the non-zero torques at the initial point ($t = 0$) stand for holding torques against gravity, continued

Fig. 2.4 presents the experimental and analytically computed torques used in driving the joints, which reveal an acceptable consistency giving us the confidence to utilize

the model developed in the optimization process. Note that the negligible differences potentially root on the unmodeled friction and backlash of the joints.

Note that non-zero torques at the initial point, $t = 0$, stand for holding torques against gravity while the links are stationary leading to zero angular velocities/accelerations at the initial point.

2.3 Optimization Using Multi-Input Extremum Seeking

Through this Section, a novel analytical coupled trajectory optimization of a 7-DOF Baxter manipulator utilizing Extremum Seeking (ES) approach is presented. The robotic manipulators are used in network-based industrial units, and even homes, by expending a significant lumped amount of energy and therefore, optimal trajectories need to be generated to address efficiency issues. These robots are typically operated for thousands of cycles resulting in a considerable cost of operation.

The coupled dynamic equations, which were derived and then experimentally validated, along with the global sensitivity analysis, to select the most effective parameters, help us carry out a time-efficient operational optimization. We examine a discrete-time multivariable gradient-based extremum seeking scheme enforcing operational time and torque saturation constraints in order to minimize the lumped amount of energy consumed in a path given. The results are compared with those of a global heuristic genetic algorithm to discuss the locality/globality of optimal solutions. Finally, the optimal tra-

jectory is experimentally implemented to be thoroughly compared with the inefficient one. We also carry out time-energy optimization using discrete-time multi-variable Extremum Seeking (ES) and its results are discussed.

2.4 Background

Autonomous and non-autonomous operations of any electromechanical systems, in particular robots, have received considerable attention with respect to both the stability and, more importantly, the efficiency issues. Both the autonomous and the non-autonomous methods, which utilize online and offline/blind optimization and control schemes, respectively, have revealed some advantages and disadvantages. We here focus on the non-autonomous energy-efficient operation of the Baxter manipulator which would subsequently be used in nonlinear control schemes. The offline optimization/control of the robot will be gradually examined with respect to the autonomous practice to yield the most reliable and optimal configuration.

Robots are not necessarily operating in an energy-efficient way and hence consume a significant lumped amount of energy. The energy consumption and subsequently cost of operation considerably increase when thousands of robots are working together, for example in a factory, to carry out a network-based task for thousands of cycles. Based on the recent statistics published, industries are among the largest consumers of energy in which the robots take the biggest share of consumption [80]. It is worth mentioning that the robots used in the auto industry consume more than half of the total energy required

to produce a vehicle body.

The importance of the optimal operation can be visualized through a network of robots operating simultaneously to carry out a specific task defined. The robot manipulator, which is being analyzed in this research work, is operated for thousands of cycles in industries and even at homes as a reliable servant. A considerable lumped amount of energy is expectedly consumed in a trajectory given, as a part of the network-based operation, and it hence needs to be minimized resulting in a significant reduction of operational cost. Therefore, the issue of energy consumed by robots has become a major challenge for researchers and robot manufacturers.

The total mechanical energy consumed by the robot is expectedly affected by the required torque of each joint in addition to the joints' angular velocities. The high level of energy consumption is typically caused by jerky motions of robots. Many research efforts addressed design optimization [6, 85], path planning [50, 51, 54, 75, 86, 87, 90, 109, 110], and minimizing joints' torques [26, 42, 52, 55].

Garge and Kumar [42] developed an optimum path requiring the minimum amount of torque which expectedly leads to a minimal amount of energy consumption. They utilized genetic and simulated annealing algorithms by comparing their performance. Other efforts reported in [39, 77, 92] investigated smooth and time-optimal trajectories. Some researchers have focused on path smoothness and/or minimizing the execution time, which may not necessarily yield a minimal amount of energy consumption [15, 36, 79].

Extremum Seeking (ES) is a model-free optimization approach [5,64,71] for systems with unknown dynamics and with a measurable output which has been applied to a wide

range of technical applications [27, 34, 35, 44, 108]. The first proof of stability for an extremum seeking feedback scheme was provided by Krstić and Wang [71]. They utilized the tools of averaging and singular perturbations in revealing that solutions of the closed-loop system converge to a small neighborhood of the extremum of the equilibrium map. Note that the ES approach can yield fast convergence, in spite of being simple to implement by utilizing iterative (batch-to-batch) optimization of the cost function. Frihauf *et al.* [41] carried out optimization of a single-input discrete-time linear system using discrete-time ES.

Discrete-time extremum seeking with stochastic perturbation was studied without measurement noise in [78]. Stanković and Stipanović [104] investigated discrete-time extremum seeking with sinusoidal perturbation including measurement noise. Liu and Krstić [73] and Choi *et al.* [33] employed discrete-time ES for one-variable static system with an extremum using stochastic and sinusoidal perturbations, respectively.

Rotea [89] and Walsh [107] studied multivariable extremum seeking schemes for time-invariant plants. Ariyur and Krstić [4] investigated, for the first time, the multivariable extremum seeking scheme for general time-varying parameters. Li *et al.* [72] utilized the multivariable ES in optimizing the cooling power of a tunable thermoacoustic cooler. Other multivariable ES applications can be found in [46, 111, 112].

Through this research effort, the time-invariant discrete-time multivariable optimization [8, 9] of all joints' trajectories are presented in detail. To the best of our knowledge, the multivariable ES has not yet been utilized for the minimization of the energy consumed by robotic manipulators. Note that time-energy optimization would not be

beneficial by yielding, as expected, a lower amount of energy saved; although the operation time may potentially decrease which is not the immediate concern of this research work [39, 77, 92].

The contribution of our work in this Section is in employing the multivariable gradient-based discrete-time ES scheme as follows:

1. The scheme is being numerically applied for a 7-DOF manipulator and the results implemented experimentally;

2. The scheme's computational burden is significantly less than other optimization methods including Genetic Algorithm (GA) which we examine here.

To carry out the operational optimization, using the verified model, the cost function is formulated as 1) the lumped amount of mechanical energy consumption enforcing operational time and torque saturation constraints, and 2) the summation of operational time and consumed energy without any constraint. The effects of changes of optimization variables on the cost function are studied using the global sensitivity analysis in order to select the most effective ones, and a nominal "*S-Shaped*" trajectory is fitted for every joint for a collision-free trajectory given. We utilize both Extremum Seeking and Genetic Algorithms to improve the dynamic characteristics of the fitted (nominal) trajectories along with minimizing energy consumption. The optimal trajectory is experimentally implemented and thoroughly compared with the inefficient one.

2.4.1 Energy-Wise Trajectory Optimization

The Baxter uses a simple linear PID controller for every joint with respect to the initial and end points given in the joint space (while its gains are not adjustable), which yields the jerky motions and subsequently, the inefficient operation of the robot. The undesirable responses can be observed through the experimental work which we have carried out in our Dynamic Systems and Control Laboratory (DSCL). We observed that the robot collides with other objects close to the end point making the motion unreliable and inefficient. This is counted as a harmful dynamical behavior for both the industrial and home applications. As mentioned earlier, the robot operates using the PID controller which in turn generates energy-inefficient trajectories. Note that Baxter, which is being analyzed here, has been designed for research purposes and hence has no predefined nominal trajectory. Therefore, the coupled trajectory optimization of the robot, as a part of the nonautonomous approach, is a necessity to be carried out in order to considerably reduce the mechanical energy consumption along with removing the jerky motions to avoid such a harmful collision discussed earlier.

The optimization needs to be formulated enforcing the operational time and torque saturation constraints to avoid the expected singularities. The feasible joints' ranges along with the initial and end points are listed in Table 2.5. Note that one of the physical constraints, which needs to be implemented in the optimization formulation, is zero angular velocity/acceleration at the initial and zero angular velocity at the end points, indicating that the manipulator would remain stationary at those points. This constraint leads us

to *the well-known "S-Shaped" trajectories which would yield the robot's smooth dynamical behavior by mitigating the effects of jerky motions. Such a smooth trajectory obviously satisfies the initial/end point zero angular velocity condition.*

It is worth mentioning that the conventional polynomials, including Spline/Bézier ones, would yield considerably more variables to be optimized with respect to the joint-space optimization, which in turn would expectedly impose cumbersome computational costs. From another aspect, adding points between the initial and end points only imposes additional constraints with a cumbersome computational cost which would be meaningless with respect to the collision-free motion (except the collision between the robot's end-effector and other objects close to the end point due to the jerky motion).

Note that in experiments, the achievable Baxter joints' angles are as follows, which are slightly different from what reported by the manufacturer in Table 2.2.

Table 2.5: The ranges of joints' angles (degree)

Joints's Name	Range	Initial Point	End Point
S_0	from -97.5° to 90°	-87.0532°	-25.6510°
S_1	from -80° to 60°	-50.0156°	5.0300°
E_0	from -170° to 170°	-10.1733°	41.0350°
E_1	from 0° to 150°	20.1435°	65.1590°
W_0	from -170° to 170°	-30.1357°	-85.2770°
W_1	from -90° to 115°	9.2920°	-46.2050°
W_2	from -170° to 170°	-60.0735°	12.0360°

We fit the following nonlinear functions (nominal trajectories) to the joints' actual trajectories which are generated with respect to the initial/end points given in Table 2.5 using the Baxter's PID controller:

$$\theta_i(k) = A_i \tanh\left(B_i \left(k\Delta t\right)^{C_i}\right) + D_i \qquad i = 1, \cdots, 7 \tag{2.9}$$

where, $k = 0, 1, \cdots, N$, Δt indicates constant time step, $t_f = N\Delta t$ (operation time), and A_i's, B_i's, C_i's, and D_i's are calculated with respect to initial and end points and utilizing the least square method for the trajectory fitting process listed in Table 2.6. Note that we discretized the functions due to the discrete-time nature of the problem.

Table 2.6: The nominal trajectories' coefficients

Joint's Name	A	$B \times 10^2$	C	D
S_0	61.4022	1.532	2.9430	-87.0532
S_1	55.0456	1.489	2.9760	-50.0156
E_0	51.2083	1.504	2.9385	-10.1733
E_1	45.0155	1.510	2.9712	20.1435
W_0	-55.1413	1.490	2.9910	-30.1357
W_1	-55.9970	1.513	2.9293	9.2920
W_2	72.1095	1.495	2.9382	-60.0735

The A_i's and D_i's are constant/unique parameters for each joint and are easily calculated as follows,

$$A_i = \left(\text{Initial Points}\right)_i \tag{2.10}$$

$$D_i = \left(\text{End Points} - \text{Initial Points}\right)_i \tag{2.11}$$

where $(.)_i$ means the i-*th* element of a vector. The B_i's and C_i's are the optimization variables although a crucial issue to address is the number of parameters expectedly leading to a cumbersome computational cost. Therefore, the sensitivity of the optimization process to the variables of B_i's and C_i's needs to be carefully addressed.

2.4.2 Sensitivity Analysis

A global sensitivity analysis has to be carried out to examine the roles of B_i's and C_i's in the optimization process. Typically, the local and global sensitivity analyses are used in determining the effects of changes in the optimization variables on the cost function defined.

The local sensitivity analysis (one-at-a-time (OAT) method) evaluates the effect of one variable on the cost function at a time while keeping the other variables constant, although the global sensitivity analysis utilizes a set of random samples to search the design space concerning the bounds defined. The global analysis would be an efficient approach as the change of each variable affects the dynamic characteristics of all the joints/links, through the interconnected dynamic equations, and subsequently the lumped cost function.

To carry out the global sensitivity analysis, we need to numerically calculate the gradient of the cost function with respect to the optimization variables as follows:

$$\nabla E = \left[\frac{\partial E}{\partial B_i}, \frac{\partial E}{\partial C_i}\right]^T \qquad i = 1, \cdots, 7 \tag{2.12}$$

where,

$$E = \sum_{i=1}^{7} E_i = \sum_{i=1}^{7} \sum_{k=0}^{N-1} \left|\tau_i(k)\dot{\theta}_i(k)\right| \Delta t \tag{2.13}$$

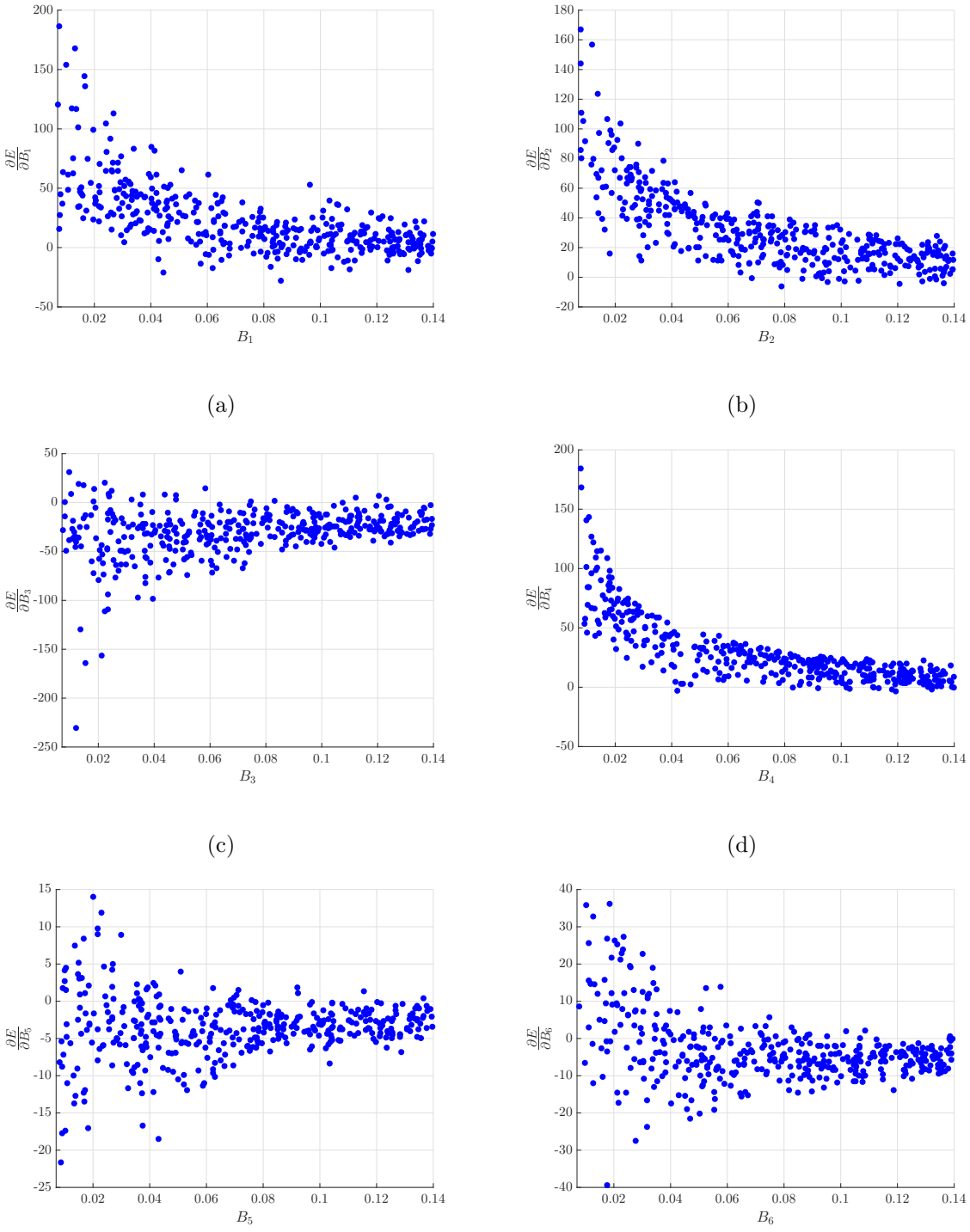

Figure 2.5: The global sensitivity analysis with respect to the B_i's

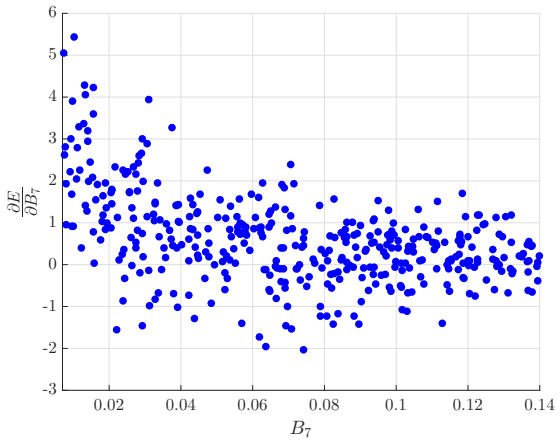

(g)

Figure 2.5: The global sensitivity analysis with respect to the B_i's, continued

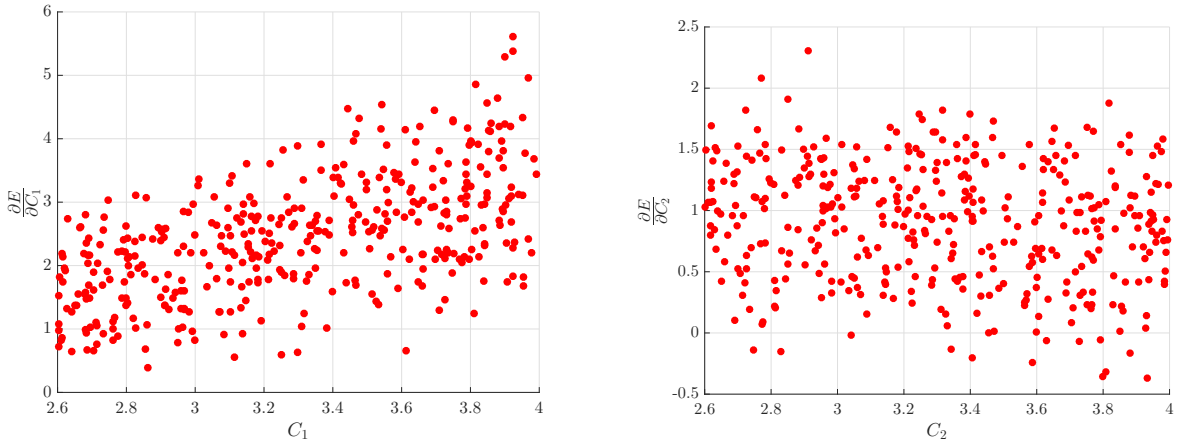

(a) (b)

Figure 2.6: The global sensitivity analysis with respect to the C_i's

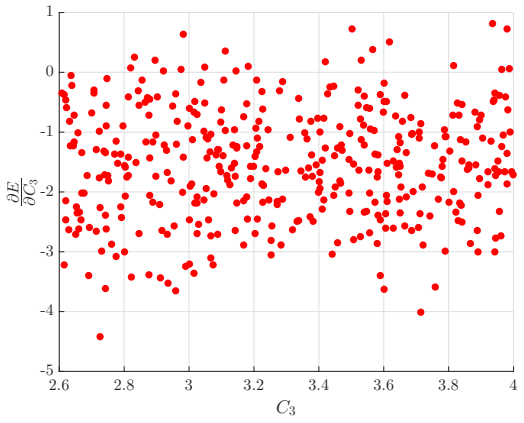

(c)

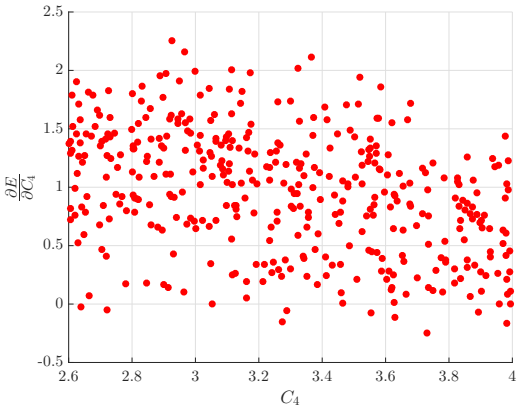

(d)

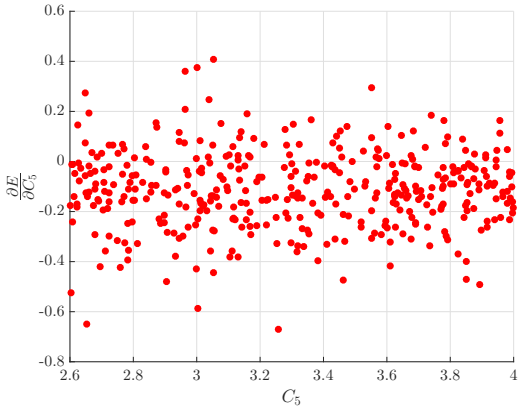

(e)

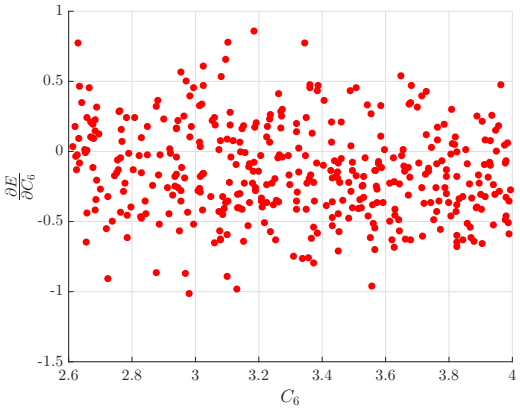

(f)

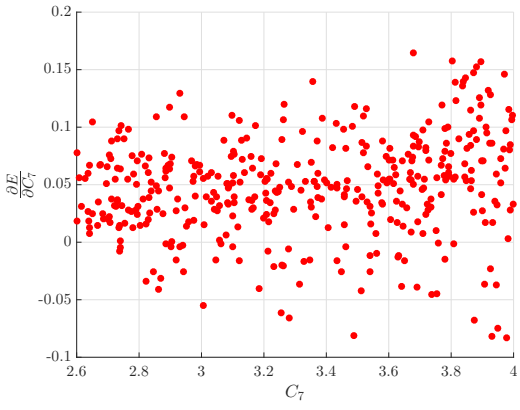

(g)

Figure 2.6: The global sensitivity analysis with respect to the C_i's, continued

Figs. 2.5 and 2.6 reveal that the roles of B_i's are more drastic than the C_i's. In other words, the effects of C_i's are negligible in comparison with those of B_i's on the changes of energy consumption. Therefore, all the B_i's are logically chosen to be optimized using both the ES and GA. The B_i's are optimized subject to the following lower and upper bounds determined through the constraints:

$$B = [B_1, B_2, B_3, B_4, B_5, B_6, B_7] \tag{2.14}$$

$$B_{\min} = [68, 69, 68.5, 69, 66.5, 69.3, 69] \times 10^{-4} \tag{2.15}$$

$$B_{\max} = [1385, 1368, 1372, 1368, 1383, 1390, 1386] \times 10^{-4} \tag{2.16}$$

The lower bound indicates the operational time, which we are willing to keep within $t_f = 8s$. Note that decreasing the lower bound would yield much slower motion which is not desirable and logical, in particular for the industrial applications. The upper bound is determined based on the practical torque saturation issue such that increasing the upper bound would yield abrupt torques leading to both the motors' failures and considerably fast motion.

It is worth mentioning that Eq. (2.9) is the nonlinear function of the B_i leading to:

$$q(B,k) = [\theta_1(B_1,k), \cdots, \theta_7(B_7,k)]^T \tag{2.17}$$

$$\dot{q}(B,k) = \left[\dot{\theta}_1(B_1,k), \cdots, \dot{\theta}_7(B_7,k)\right]^T \tag{2.18}$$

$$\ddot{q}(B,k) = \left[\ddot{\theta}_1(B_1,k), \cdots, \ddot{\theta}_7(B_7,k)\right]^T \tag{2.19}$$

Therefore, the joints' torques (Eq. (2.5)) and subsequently the mechanical energy consumed are the nonlinear functions of the B_i's,

$$E(B) = \sum_{i=1}^{7} \sum_{k=0}^{N-1} \left| \tau_i(B,k) \dot{\theta}_i(B,k) \right| \Delta t$$

$$= \sum_{i=1}^{7} \sum_{k=0}^{N-1} \left| \Big(M_i(B,k) \ddot{q}(B,k) + C_i(B,k) \dot{q}(B,k) + \Phi_i(B,k) \Big) \dot{\theta}_i(B,k) \right| \Delta t \qquad (2.20)$$

where $M_i(B,k)$ and $C_i(B,k)$ are the i-th rows of M and C matrices, respectively; and

$$q(B,k) = [\theta_1(B_1,k), \cdots, \theta_7(B_7,k)]^T \qquad (2.21)$$

$$\dot{q}(B,k) = [\dot{\theta}_1(B_1,k), \cdots, \dot{\theta}_7(B_7,k)]^T \qquad (2.22)$$

$$\ddot{q}(B,k) = [\ddot{\theta}_1(B_1,k), \cdots, \ddot{\theta}_7(B_7,k)]^T \qquad (2.23)$$

Therefore, the optimization problem is a constrained one, enforcing the mentioned lower and upper bounds, with the following cost function defined as the lumped amount of mechanical energy consumed in the robot:

$$\min_B E(B)$$

$$\text{Subject to : The Interconnected Equations} \qquad (2.24)$$

$$B_{\min} \leq B \leq B_{\max}$$

We hence need to optimize seven interconnected variables using both the ES and GA. One issue to consider is the small values of the variables resulting in serious numerical errors. We fixed this problem by conditioning them using a normalization scheme as

follows:

$$B_n = B \times 10^4 \tag{2.25}$$

Two optimization schemes, including both the ES and GA, are utilized to avoid being trapped in several possible local minima. The genetic method was developed based on a heuristic search to mimic the process of natural selection [37]. The genetic algorithm is typically more robust than other conventional schemes. It does not break down easily in the presence of slight changes of inputs, and noise. For large-scale state-space equations, the algorithm may potentially exhibit significantly better performance than typical optimization techniques.

Note that for the GA method we have utilized 1) "PopulationSize" of 200 for the size of population, 2) "Generations" of 400 which indicates the maximum number of iterations before the algorithm halts, 3) "MigrationFraction" of 0.2 specifying the fraction of individuals in each subpopulation that migrates to a different subpopulation, and 4) "MigrationInterval" of 20 standing for the number of generations that take place between migrations of individuals between subpopulations, and 5) Function (TolFun) and constraints (TolCon) tolerances of 10^{-6}.

2.5 Multivariable Optimization Using Gradient-Based Extremum Seeking

Our objective is to develop a iterative feedback mechanism minimizing the energy consumed (E), where its nonlinear static map is known to have an extremum. We utilize the multivariable extremum seeking scheme [3,43,45,47], developed from Krstić and Wang efforts [71], in obtaining optimal values $B^* = [B_1^*, \cdots, B_7^*]^T$.

The extremum seeking scheme estimates the gradient of the cost function defined in addition to driving it to zero. The gradient is estimated using a zero-mean external periodic perturbation (or dither signal) and a series of filtering and modulation operations. The convergence of the gradient algorithm is dictated by the second derivative (Hessian) of the cost function. The minimizer is the optimal parameters B^* obtained by driving the system with a $B(l) = [B_1(l), \cdots, B_7(l)]^T$ to determine the cost value $E(l)$ and then iterating the discrete-time extremum seeking to produce the $B(l+1)$; where l denotes the l-th iteration of the algorithm [41].

Shown in Fig. 2.7 is a schematic of the discrete-time ES algorithm. It is worth mentioning that the measured output passing through a washout (high-pass) filter $\left(W(z) = \frac{z-1}{z+h}\right)$, by having zero DC gain, expectedly helps better performance [33, 41].

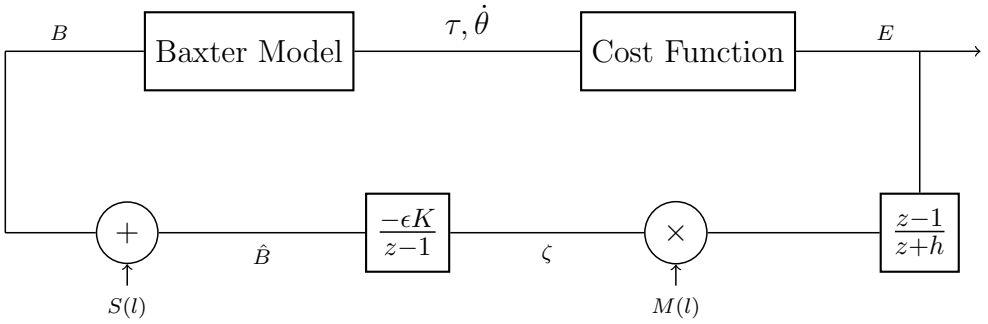

Figure 2.7: Discrete-time multivariable gradient-based extremum seeking using washout filter

Note that there is a map from the B_i's to the energy consumed (E) through Eq. 2.20. The extremum seeking-based optimization shown in Fig. 2.7 is governed by the following equations:

$$\hat{B}(l) = \frac{-\epsilon K}{z-1}\left[\zeta(l)\right] \tag{2.26}$$

$$\zeta(l) = M(l)\frac{z-1}{z+h}\left[E(l)\right] \tag{2.27}$$

$$B(l) = \hat{B}(l) + S(l) \tag{2.28}$$

where, $\hat{B}(l) = \left[\hat{B}_1(l), \cdots, \hat{B}_7(l)\right]^T$, ϵ is a small positive parameter, K is a positive diagonal matrix, and $0 < h < 1$. The notation $P(z)[q(l)]$ is used to denote the signal in the iteration domain that is the output of the transfer function $P(z)$ driven by $q(l)$, where $P(z)$ operates with respect to the iteration domain. Note that $q(l)$ is a signal in iteration domain, where l denotes the l-th iteration.

The perturbation signals $M(l)$ and $S(l)$ are given by

$$S(l) = \left[a_1 \cos(\omega_1 l), \cdots, a_7 \cos(\omega_7 l)\right]^T \tag{2.29}$$

$$M(l) = \left[\tfrac{2}{a_1} \cos(\omega_1 l - \phi_1), \cdots, \tfrac{2}{a_7} \cos(\omega_7 l - \phi_7)\right]^T \tag{2.30}$$

with $a_k > 0$ and the modulation frequencies are given by $\omega_k = b_k \pi$, where $|b_k| \in (0, 1)$ is a rational number and the probing frequencies are selected such that $\omega_i \neq \omega_j$ for all distinct $i, j, k \in \{1, \cdots, 7\}$. Also, phase values ϕ_k are selected such that $\mathrm{Re}\left\{e^{j\phi_k} W\left(e^{j\omega_k}\right)\right\} > 0$ for all $k \in \{1, \cdots, 7\}$ [41].

Using the Taylor series expansion of the cost function around the local minimum B^* ($\nabla E(B^*) = 0$), the cost function can be written as

$$E\left(B\right) = E\left(B^*\right) + \frac{1}{2}\left(B - B^*\right)^T H \left(B - B^*\right) \tag{2.31}$$

where H is a positive definite Hessian matrix $\left(H := \frac{\partial^2 E}{\partial B^2}\right)$. Note that cubic and higher order terms are eliminated since they are negligible for local stability analysis via averaging [33]. We then define

$$\tilde{B}(l) = \hat{B}(l) - B^* = B(l) - S(l) - B^* \tag{2.32}$$

Substituting Eq. (2.32) into Eq. (2.31) yields

$$E\left(\tilde{B}(l)\right) = E\left(B^*\right) + \frac{1}{2}\left(\tilde{B}(l) + S(l)\right)^T H \left(\tilde{B}(l) + S(l)\right) \tag{2.33}$$

$$= E\left(B^*\right) + \frac{1}{2}\tilde{B}^T H \tilde{B} + S^T H \tilde{B} + \frac{1}{2} S^T H S \tag{2.34}$$

Eq. (2.26) can be therefore rewritten as

$$\tilde{B}(l) = \frac{-\epsilon K}{z - 1}\left[\zeta(l)\right] - B^* \tag{2.35}$$

which leads to the following difference equation by utilizing Eq. (2.34) and $\left(W(z) = \frac{z-1}{z+h}\right)$:

$$\begin{aligned}\tilde{B}(l+1) =& \tilde{B}(l) - \epsilon KM(l)W(z)\left[E(l)\right] \\ =& \tilde{B}(l) - \epsilon KM(l)W(z)\left[E\left(B^*\right)\right] \\ & - \frac{1}{2}\epsilon KM(l)W(z)\left[\tilde{B}(l)^T H\tilde{B}(l) + S(l)^T HS(l)\right] \\ & - \epsilon KM(l)W(z)\left[S(l)^T H\tilde{B}(l)\right] \end{aligned} \tag{2.36}$$

We utilize the following lemmas [41] to carry out the convergence analysis.

Lemma 1. *The transfer function G(z) for any real ϕ can be written as:*

$$G(z)\left[\cos\left(\omega l - \phi\right)\nu(l)\right] = \mathrm{Re}\left\{e^{j(\omega l-\phi)}G\left(e^{j\omega}z\right)\left[\nu(l)\right]\right\} \tag{2.37}$$

Lemma 2. *The following is true for any two rational functions $P(\cdot)$ and $Q(\cdot,\cdot)$:*

$$\begin{aligned}& \mathrm{Re}\left\{e^{j(\omega_1 l-\phi_1)}P\left(e^{j\omega_1}\right)\right\}\mathrm{Re}\left\{e^{j(\omega_2 l-\phi_2)}Q\left(z,e^{j\omega_2}\right)\left[\nu(l)\right]\right\} \\ =& \frac{1}{2}\mathrm{Re}\left\{e^{j((\omega_2-\omega_1)l+\phi_1-\phi_2)}P\left(e^{-j\omega_1}\right)Q\left(z,e^{j\omega_2}\right)\left[\nu(l)\right]\right\} \\ & + \frac{1}{2}\mathrm{Re}\left\{e^{j((\omega_2+\omega_1)l-\phi_1-\phi_2)}P\left(e^{j\omega_1}\right)Q\left(z,e^{j\omega_2}\right)\left[\nu(l)\right]\right\} \end{aligned} \tag{2.38}$$

Lemma 3. *The following is true for any rational functions $Q(\cdot,\cdot)$:*

$$\begin{aligned}& \mathrm{Re}\left\{e^{j(\omega l-\phi)}Q\left(z,e^{j\omega}\right)\left[\nu(l)\right]\right\} \\ =& \cos(\omega l-\phi)\mathrm{Re}\left\{Q\left(z,e^{j\omega}\right)\left[\nu(l)\right]\right\} - \sin(\omega l-\phi)\mathrm{Im}\left\{Q\left(z,e^{j\omega}\right)\left[\nu(l)\right]\right\} \end{aligned} \tag{2.39}$$

Utilizing Lemma 1 to the last term of Eq. (2.36) results in

$$W(z)\left[S^T H\tilde{B}\right] = a\ \mathrm{Re}\left\{e^{j\omega}Q\left(z, e^{j\omega}\right)\left[H\tilde{B}\right]\right\} \tag{2.40}$$

where

$$a = \mathrm{diag}\left[a_1, \cdots, a_7\right] \tag{2.41}$$

$$\Omega\left(z, e^{j\omega}\right) = \mathrm{diag}\left[W\left(e^{j\omega_1}z\right), \cdots, W\left(e^{j\omega_7}z\right)\right] \tag{2.42}$$

Due to the fact that $\frac{2}{a'}\cos(\omega' l - \phi) = \frac{2}{a'}\mathrm{Re}\left\{e^{j(\omega' l - \phi)}\right\}$, and utilizing Lemmas 1 and 2, following holds,

$$\begin{aligned}
&\frac{2}{a'}\cos(\omega' l - \phi)W(z)\left[a\cos(\omega)H\tilde{B}\right] \\
&\quad = 2\frac{a}{a'}\mathrm{Re}\left\{e^{j(\omega' - \phi)}\right\}\mathrm{Re}\left\{e^{j\omega}W\left(e^{j\omega}z\right)\left[H\tilde{B}\right]\right\} \\
&\quad = \frac{a}{a'}\Bigg(\mathrm{Re}\left\{e^{j((\omega-\omega')l+\phi)}W\left(e^{j\omega}z\right)\left[H\tilde{B}\right]\right\} \\
&\qquad + \mathrm{Re}\left\{e^{j((\omega+\omega')l-\phi)}W\left(e^{j\omega}z\right)\left[H\tilde{B}\right]\right\}\Bigg)
\end{aligned} \tag{2.43}$$

Then, using Lemma 2 and Eq. (2.43) follows,

$$M(l)W(z)\left[S^T H\tilde{B}\right] = \begin{bmatrix} 1 & \cdots & \frac{a_1}{a_7} \\ \vdots & \ddots & \vdots \\ \frac{a_7}{a_1} & \cdots & 1 \end{bmatrix}$$

$$\times \left(\mathrm{Re}\left\{ \begin{bmatrix} e^{\phi_1} & \cdots & e^{j(\omega_1-\omega_7)+\phi_1} \\ \vdots & \ddots & \vdots \\ e^{j(\omega_7-\omega_1)+\phi_7} & \cdots & e^{\phi_7} \end{bmatrix} Q\left(z, e^{j\omega}\right)\left[H\tilde{B}\right] \right\} \right.$$

$$\left. + \mathrm{Re}\left\{ \begin{bmatrix} e^{2j\omega_1-\phi_1} & \cdots & e^{j(\omega_1+\omega_7)-\phi_1} \\ \vdots & \ddots & \vdots \\ e^{j(\omega_7+\omega_1)-\phi_7} & \cdots e^{2j\omega_7-\phi_7} & \end{bmatrix} Q\left(z, e^{j\omega}\right)\left[H\tilde{B}\right] \right\} \right) \tag{2.44}$$

Finally, we apply Lemma 3 for each $\mathrm{Re}\{.\}$ terms in Eq. (2.44) and we have,

$$\begin{aligned} M(l)W(z)\left[S(l)^T H\tilde{B}(l)\right] =& C^-(l)\mathrm{Re}\left\{\Omega\left(z, e^{j\omega}\right)\left[H\tilde{B}\right]\right\} \\ & - S^-(l)\mathrm{Im}\left\{\Omega\left(z, e^{j\omega}\right)\left[H\tilde{B}\right]\right\} \\ & + C^+(l)\mathrm{Re}\left\{\Omega\left(z, e^{j\omega}\right)\left[H\tilde{B}\right]\right\} \\ & - S^+(l)\mathrm{Im}\left\{\Omega\left(z, e^{j\omega}\right)\left[H\tilde{B}\right]\right\} \end{aligned} \tag{2.45}$$

where, C^-,S^-,C^+, and S^+ are 7×7 matrices whose k-th rows are given by

$$C_k^-(l) = \left[\frac{a_1}{a_k}\cos\left(\left(\omega_1 - \omega_k\right)l + \phi_k\right), \cdots, \frac{a_7}{a_k}\cos\left(\left(\omega_7 - \omega_k\right)l + \phi_k\right)\right] \tag{2.46}$$

$$S_k^-(l) = \left[\frac{a_1}{a_k}\sin\left(\left(\omega_1 - \omega_k\right)l + \phi_k\right), \cdots, \frac{a_7}{a_k}\sin\left(\left(\omega_7 - \omega_k\right)l + \phi_k\right)\right] \tag{2.47}$$

$$C_k^+(l) = \left[\frac{a_1}{a_k}\cos\left(\left(\omega_1 + \omega_k\right)l - \phi_k\right), \cdots, \frac{a_7}{a_k}\cos\left(\left(\omega_7 + \omega_k\right)l - \phi_k\right)\right] \tag{2.48}$$

$$S_k^+(l) = \left[\frac{a_1}{a_k}\sin\left(\left(\omega_1 + \omega_k\right)l - \phi_k\right), \cdots, \frac{a_7}{a_k}\sin\left(\left(\omega_7 + \omega_k\right)l - \phi_k\right)\right] \tag{2.49}$$

The diagonal elements of C^- and S^- are time-invariant. We define diagonal matrices C_D^- and S_D^- containing the diagonal elements of C^- and S^-, respectively, to highlight these time-invariant terms. Then, Eq. (2.45) can be rewritten as,

$$\begin{aligned} M(l)W(z)\left[S^T H\tilde{B}\right] =& \mathrm{Re}\left\{\bar{\Omega}\left(e^{j\phi}\right)\Omega\left(z, e^{j\omega}\right)\left[H\tilde{B}\right]\right\} \\ &+ \left(C^-(l) - C_D^-\right)\mathrm{Re}\left\{\Omega\left(z, e^{j\omega}\right)\left[H\tilde{B}\right]\right\} \\ &- \left(S^-(l) - S_D^-\right)\mathrm{Im}\left\{\Omega\left(z, e^{j\omega}\right)\left[H\tilde{B}\right]\right\} \\ &+ C^+(l)\mathrm{Re}\left\{\Omega\left(z, e^{j\omega}\right)\left[H\tilde{B}\right]\right\} \\ &- S^+(l)\mathrm{Im}\left\{\Omega\left(z, e^{j\omega}\right)\left[H\tilde{B}\right]\right\} \end{aligned} \tag{2.50}$$

where $\bar{\Omega}\left(e^{j\phi}\right) = \mathrm{diag}\left[e^{j\phi_1}, \cdots, e^{j\phi_7}\right]$.

Substituting Eq. (2.50) into Eq. (2.36) yields the following error dynamics:

$$\tilde{B}(l+1) - \tilde{B}(l) = \epsilon\left(L(z)\left[H\tilde{B}\right] + \Psi_1^-(l) + \Psi_1^+(l) + \Psi_2(l)\right) + \delta(l) \tag{2.51}$$

where,

$$L(z) = -\frac{K}{2}\left(\bar{\Omega}\left(e^{j\phi}\right)\Omega\left(z, e^{j\omega}\right) + \bar{\Omega}\left(e^{-j\phi}\right)\Omega\left(z, e^{-j\omega}\right)\right) \tag{2.52}$$

$$\begin{aligned}\Psi_1^-(l) =& K\left(S^-(l) - S_D^-\right)\mathrm{Im}\left\{\Omega\left(z, e^{j\omega}\right)\left[H\tilde{B}\right]\right\} \\ & - K\left(C^-(l) - C_D^-\right)\mathrm{Re}\left\{\Omega\left(z, e^{j\omega}\right)\left[H\tilde{B}\right]\right\}\end{aligned} \tag{2.53}$$

$$\Psi_1^+(l) = KS^+(l)\mathrm{Im}\left\{\Omega\left(z, e^{j\omega}\right)\left[H\tilde{B}\right]\right\} - KC^+(l)\mathrm{Re}\left\{\Omega\left(z, e^{j\omega}\right)\left[H\tilde{B}\right]\right\} \tag{2.54}$$

$$\Psi_2(l) = -\frac{1}{2}KM(l)W(z)\left[\tilde{B}(l)^T H\tilde{B}(l)\right] \tag{2.55}$$

$$\delta(l) = -\epsilon KM(l)W(z)\left[E\left(B^*\right)\right] - \frac{1}{2}\epsilon KM(l)W(z)\left[S(l)^T HS(l)\right] \tag{2.56}$$

It is straightforward to observe that the error dynamics evolve according to a sum of a linear time-invariant term, $L(z)\left[H\tilde{B}\right]$, linear time-varying functions, $\Psi_1^-(l)$ and $\Psi_1^+(l)$, a nonlinear time-varying function, $\Psi_2(l)$, and a time-varying function, $\delta(l)$, which is independent of the error of the optimization variable $\tilde{B}$.

We extend the results reported in [33] to establish the convergence of the multivariable discrete-time extremum seeking scheme. We present the local exponential convergence of the homogeneous error system and then consider the full system (Eq. (2.51)), including the $\delta(l)$ term, to establish its convergence.

2.5.1 Convergence of Homogeneous Error System

The following theorem states a sufficient condition for local exponential convergence of the error system (Eq. (2.51)) regardless the $\delta(l)$ term. We deal with the homogeneous

error system which is periodic in time l

$$\tilde{B}(l+1) - \tilde{B}(l) = \epsilon\big(L(z)\left[H\tilde{B}\right] + \Psi_1^-(l) + \Psi_1^+(l) + \Psi_2(l)\big) \tag{2.57}$$

Theorem 1. *Consider the homogeneous error system* (2.57) *with modulation frequencies that satisfy* $\omega_i \neq \omega_k$ *for all distinct* $i, k \in \{1, 2, \cdots, 7\}$ *and phase values* ϕ_k *selected such that* $\mathrm{Re}\left\{e^{j\phi_k} W\left(e^{j\omega_k}\right)\right\} > 0$ *for all* $k \in \{1, 2, \cdots, 7\}$. *There exists a positive constant* ϵ^* *such that the state-space realization is locally exponentially stable at the origin for all* $0 < \epsilon < \epsilon^*$. *This theorem is proved as in [41].*

Note that the eigenvalues of H, denoted by $\lambda(H)$, play important roles in the convergence rate of the extremum seeking [41].

2.5.2 Convergence of Full Error System

The established exponential stability of the averaged homogeneous error system helps us investigate the full system (2.51). We state the convergence properties of $\delta(l)$ through the following lemma; proved as in [41].

Lemma 4. *The time-varying function* $\delta(l)$ *exponentially converges to an* $O\left(\epsilon|a|\right)$ *of zero,*

$$|\delta(l)| \leq \epsilon^{-1} + c_1\epsilon|a|, \tag{2.58}$$

where c_1 *is a constant and* $a = [a_1, \cdots, a_7]$.

Utilizing the perturbed averaged system [41],

$$\tilde{B}^{\mathrm{ave}}(l+1) = \left(I - \epsilon\bar{K}H\right)\tilde{B}^{\mathrm{ave}}(l) + \delta(l) \tag{2.59}$$

and Lemma 4, we notice that $\tilde{B}^{\text{ave}}(l)$ converges exponentially to an $O(|a|)$-neighborhood of the origin since $|\delta(l)| \leq \epsilon^{-1} + c_1\epsilon|a|$. From [14], the exponential convergence rate of $\tilde{B}$ in Eq. (2.51) tends to the rate of $\tilde{B}^{\text{ave}}$ in the average system as ϵ tends to zero. We can hence state the convergence of the overall $\tilde{B}$-system.

Theorem 2. *Consider the full system* (2.51) *with the conditions of Theorem 1 satisfied. For sufficiently small* a_k, $k \in \{1, 2, \cdots, 7\}$ *there exists* $0 < \epsilon_1^* \leq \epsilon^*$, *such that the error variable* $\tilde{B}$ *locally exponentially converges to an* $O(|a|)$*-neighborhood of the origin for all* $0 < \epsilon \leq \epsilon_1^*$.

Corollary 1. *With the conditions of Theorem 2 satisfied, the cost value* E *locally exponentially converges to an* $O(|a|^2)$*-neighborhood of the optimal cost* $E(B^*)$.

Proof. By defining

$$\tilde{E}(B) = E(B) - E(B^*) = \frac{1}{2}\tilde{B}^T H \tilde{B} + S^T H \tilde{B} + \frac{1}{2} S^T H S \tag{2.60}$$

From Theorem 2, $\tilde{B}$ locally exponentially converges to an $O(|a|)$-neighborhood of the origin. Thus, $\tilde{E}(B)$ locally exponentially converges to an $O(|a|^2)$-neighborhood of the origin.

2.5.3 Experimental Results

We used both the analytical (ES) and numerical (GA) approaches to obtain the optimal values of B_i's shown in Figs. 2.8 and 2.9, respectively. The optimal values of B_i's are listed in Table 2.7 indicating negligible differences between the methods.

Table 2.7: Optimal trajectories' coefficients

Joint Name	Optimized B using ES	Optimized B using GA
S_0	0.0078	0.00703
S_1	0.0071	0.00700
E_0	0.1354	0.1400
E_1	0.00703	0.00700
W_0	0.1306	0.1398
W_1	0.0703	0.0650
W_2	0.1222	0.1212

It is straightforward to observe that the optimal values of B_1, B_2, and B_4 shown in Figs. 2.8(a), 2.8(b), and 2.8(d), respectively, are lower than the nominal ones indicating that their corresponding links move slower than those of the nominal trajectories. This subsequently leads to a significant reduction in the energy consumed. Note that the joint S_1, as expected, takes the biggest share of energy consumption and therefore, its lower angular velocities would lead to a lower amount of the cost function defined.

Although, the optimal values of B_3, B_5, B_6, and B_7 presented in Figs. 2.8(c), 2.8(e), 2.8(f), and 2.8(a), respectively, are higher than those of the nominal ones resulting in higher angular velocities of the optimal trajectories than the nominal ones.

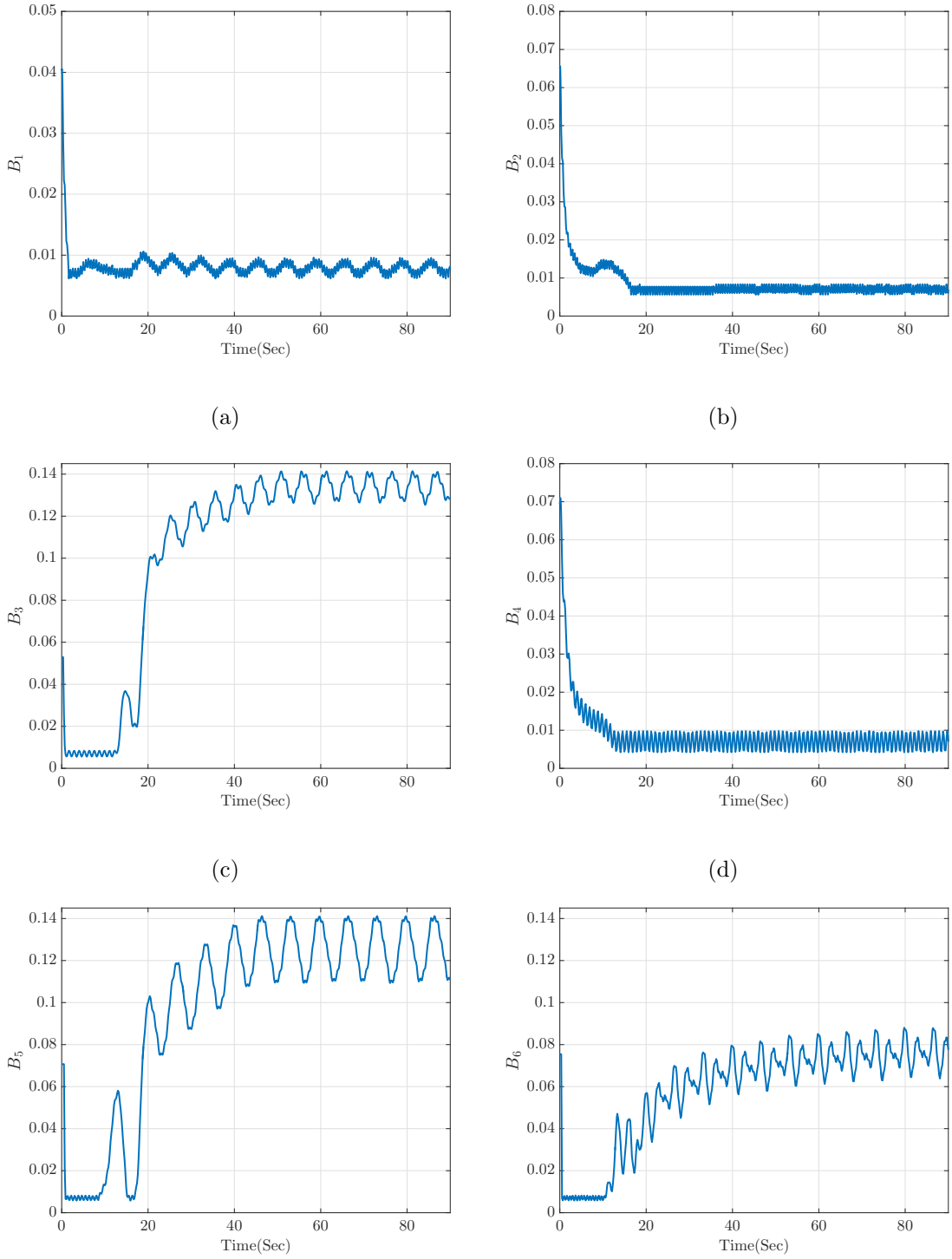

Figure 2.8: The optimal values of B's using the ES

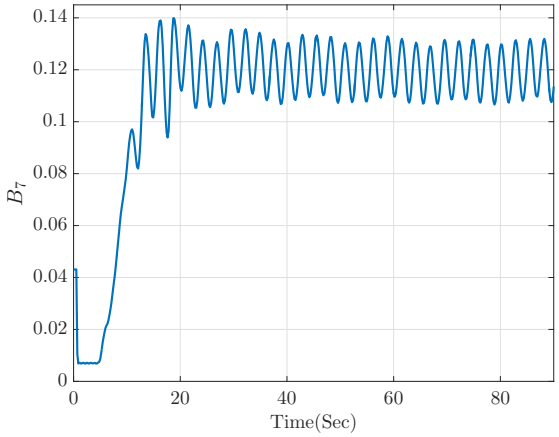

(g)

Figure 2.8: The optimal values of B's using the ES, continued

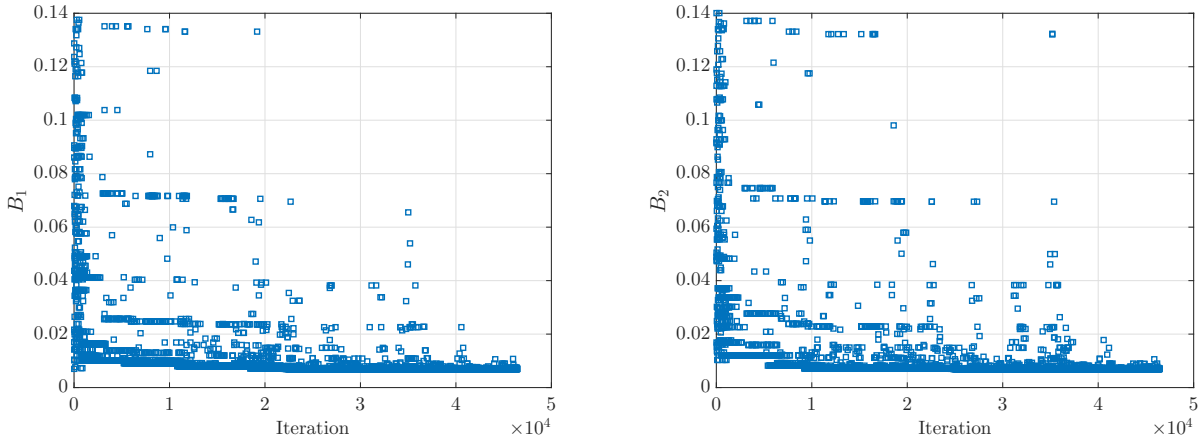

(a) (b)

Figure 2.9: The optimal values of B's using the GA

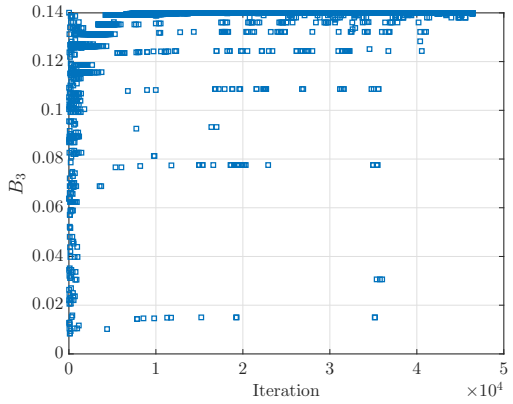

(c)

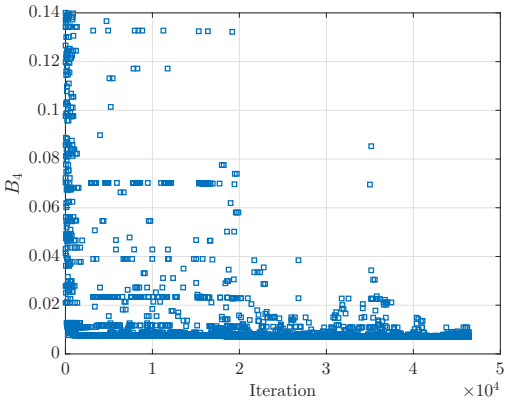

(d)

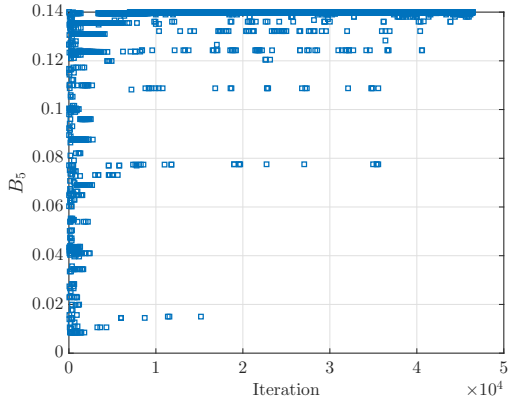

(e)

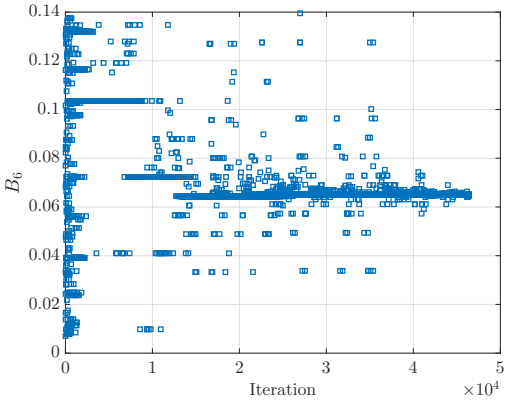

(f)

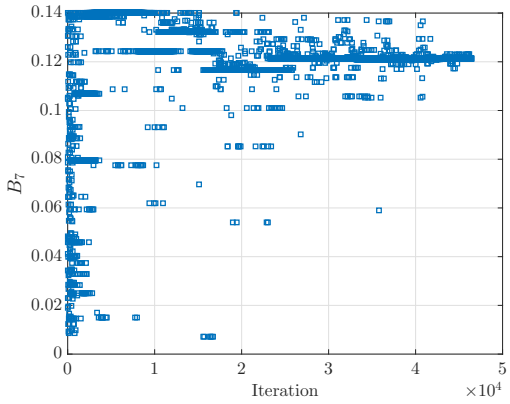

(g)

Figure 2.9: The optimal values of B's using the GA, continued

Shown in Figs. 2.10 and 2.11 are the energy consumptions minimized using both the ES and GA, respectively. Fig. 2.10(a) presents the energy optimization process versus time while the energy consumed sharply decreases to almost 37 J and then gradually converges to the optimal value of 36.627 J (at $t = 84.75$s). Shown in Fig. 2.10(a) reveals that the optimization of energy consumption fluctuates stochastically, as all the seven parameters (B_i's) are oscillating with seven different frequencies satisfying the mentioned conditions. Therefore, the value of optimal energy is not transparent to be compared with that of the GA one. We hence calculated its mean value over a running average window of one cycle of the specified fundamental low frequency (Fig. 2.10(b)) to obtain the amount of energy saved:

$$\Delta E_{\text{ES}} = \frac{\overbrace{E_{\text{nominal}}}^{45.34(J)} - \overbrace{E_{\text{optimal}}}^{36.527(J)}}{E_{\text{nominal}}} \times 100 = 19.44\% \tag{2.61}$$

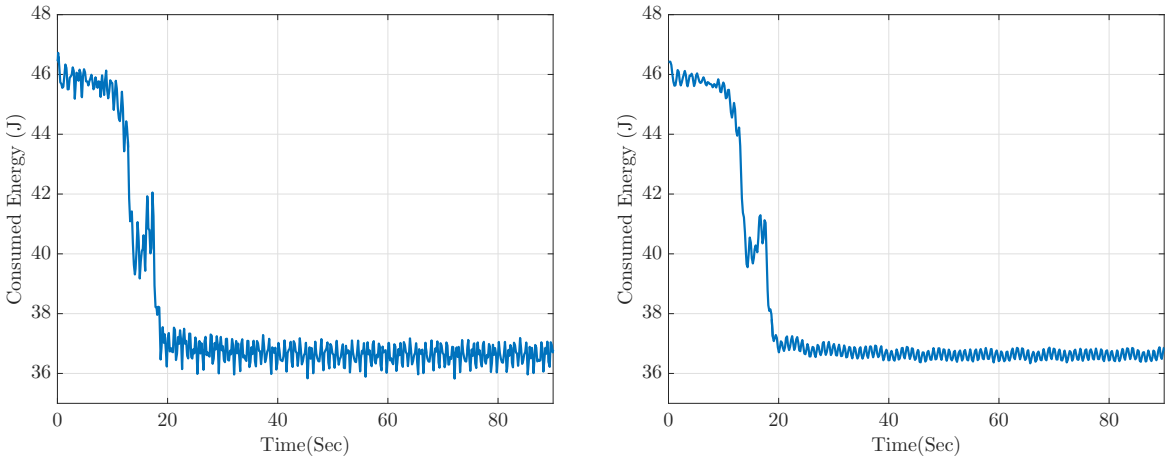

(a) (b)

Figure 2.10: The (a) actual and (b) mean value of energy optimized using the ES

Shown in Fig. 2.11(a) is the energy consumption minimized using the GA, and its best value is 36.631 (J) shown in Fig. 2.11(b).

$$\Delta E_{\text{GA}} = \frac{\overbrace{E_{\text{nominal}}}^{45.34(J)} - \overbrace{E_{\text{optimal}}}^{36.631(J)}}{E_{\text{nominal}}} \times 100 = 19.21\% \tag{2.62}$$

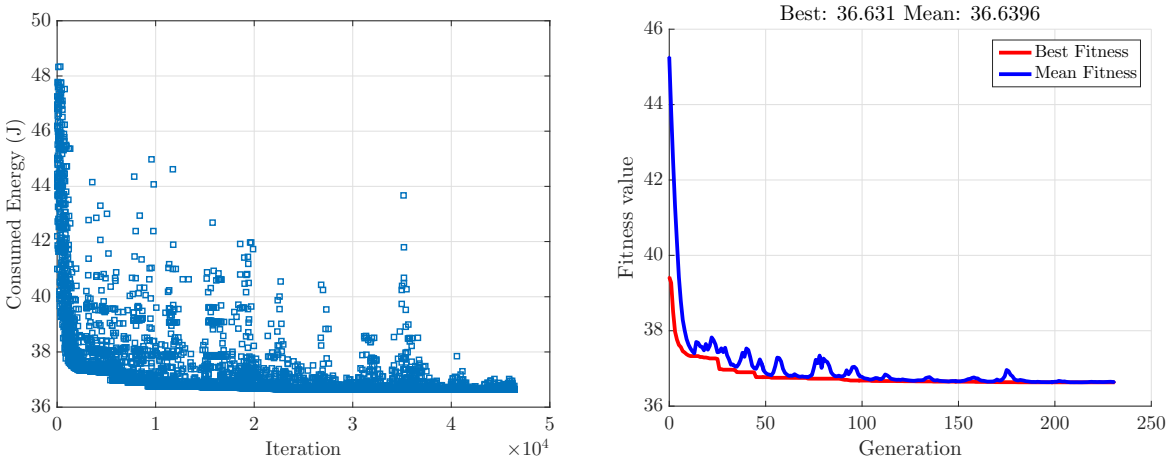

(a) (b)

Figure 2.11: (a) The energy optimized using the GA and (b) the convergence history of the GA

From another aspect, Fig. 2.11 presents considerable computational cost (iterations) of 46400 for the GA which looks logical concerning the scale of the coupled dynamic equations resulting in a significant computational time of 2876s in comparison with 137s of the ES method. Although Figs. 2.10 and 2.11 reveal a negligible difference (less than 1%) for the energy savings of both the schemes, the ES yields the better performance. Such a superior performance of the ES can be justified as follows. The ES carries out optimization by continuously sliding on the cost function in gradient direction rather than

finding optimal points discretely with a certain step size of the GA.

We have also carried out experimental validation of the nonlinear analytical approach examining both the actual (inefficient) and optimal trajectories. The actual (inefficient), nominal fitted to the actual, and optimal trajectories are presented in Fig. 2.12 revealing the differences expected.

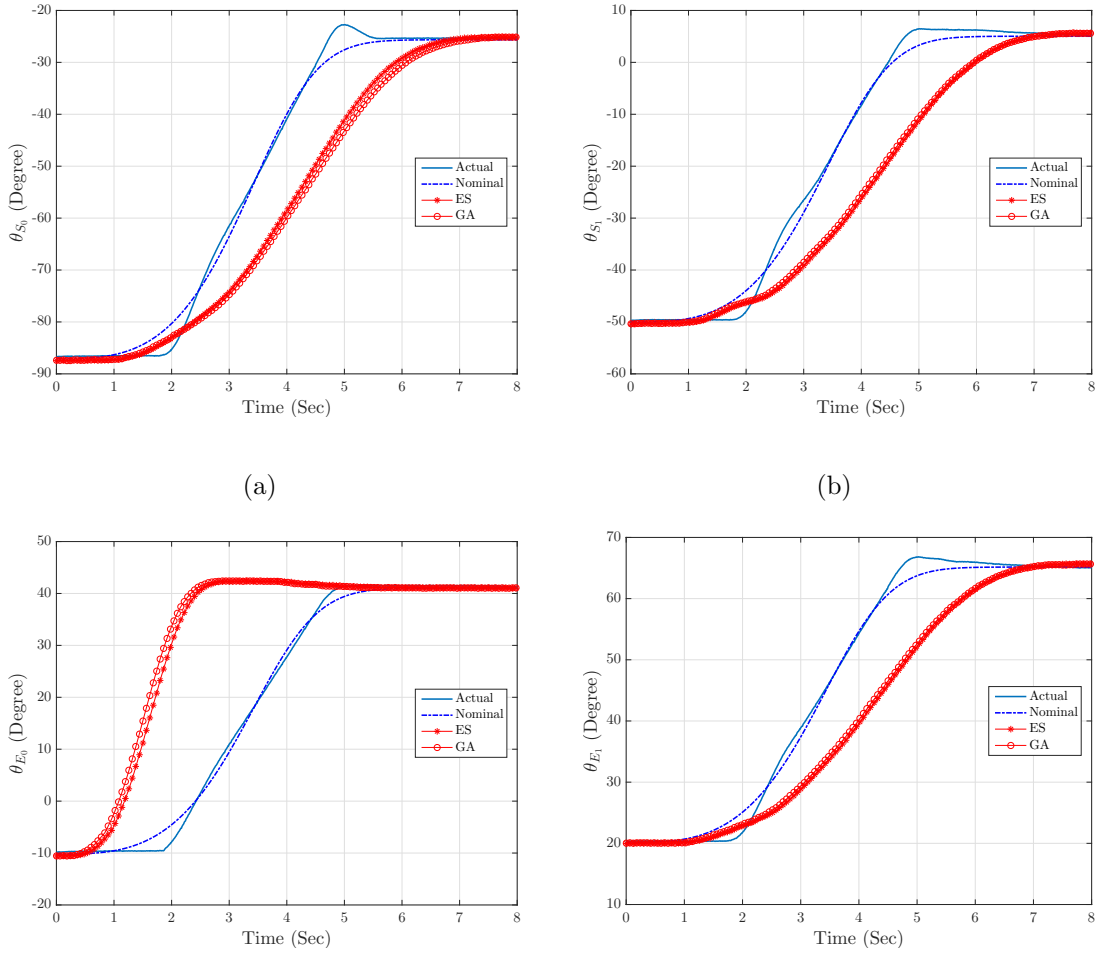

Figure 2.12: The actual (inefficient), nominal fitted to the actual, and optimal trajectories using the ES and GA: (a) S_0; (b) S_1; (c) E_0; (d) E_1; (e) W_0; (f) W_1; (g) W_2

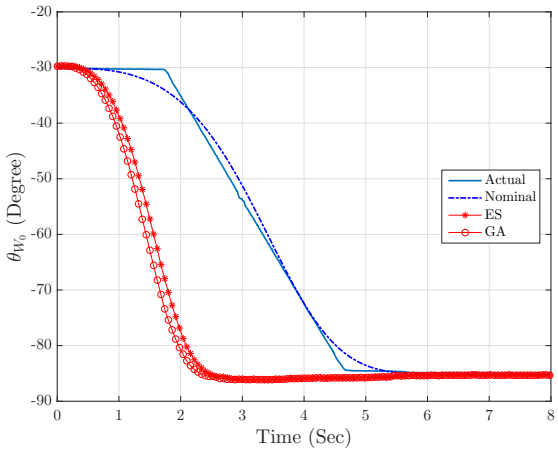

(e)

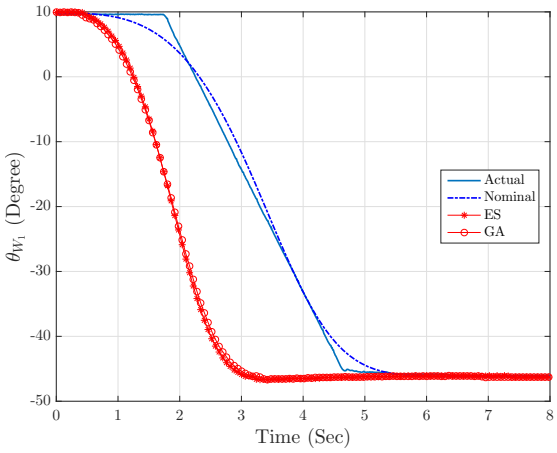

(f)

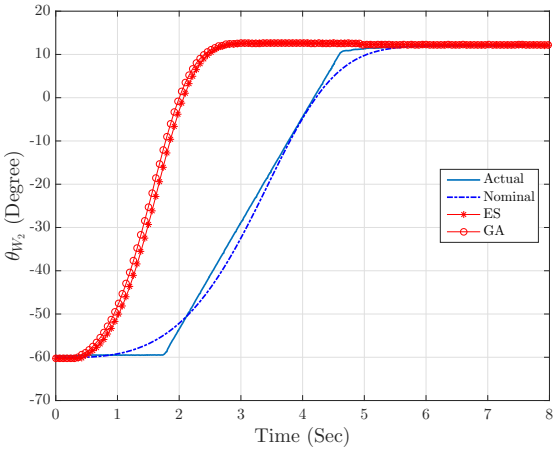

(g)

Figure 2.12: The actual (inefficient), nominal fitted to the actual, and optimal trajectories using the ES and GA: (a) S_0; (b) S_1; (c) E_0; (d) E_1; (e) W_0; (f) W_1; (g) W_2, continued

Shown in Figs. 2.12(a), 2.12(b), and 2.12(d) indicate that the optimal angular velocities of joints S_0, S_1, and E_1 are lower than those of the nominal ones. As mentioned earlier, the joint S_0 takes the biggest share (Fig. 2.4(a)) among the other ones to consume

the lumped amount of energy and therefore, its lower angular velocity would lead to a lower amount of the cost function defined. From another aspect, the effects of such higher values of the B_i's (i = 3, 5, 6, 7) can be visualized in Figs. 2.12(c), 2.12(a), 2.12(b), and 2.12(c), respectively. Logically, the smooth optimal trajectories shown in Figs. 2.12(a)-2.12(c), in comparison with the actual jerky ones, would expectedly demand lower driving torques to be used in the robot operation.

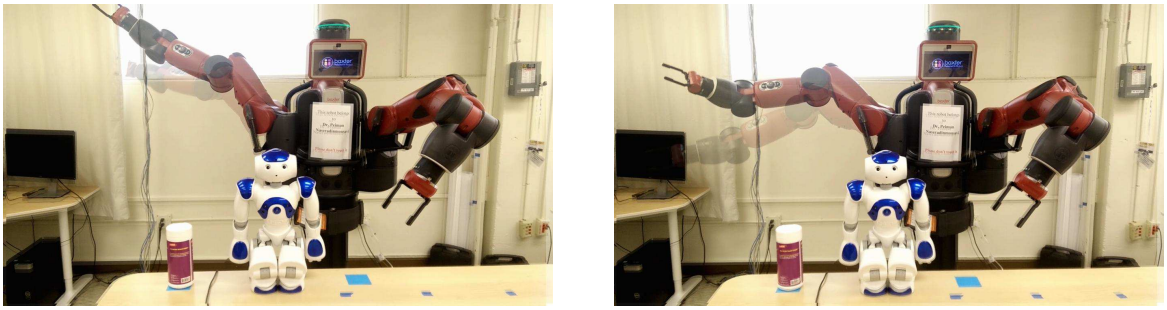

(a)

(b)

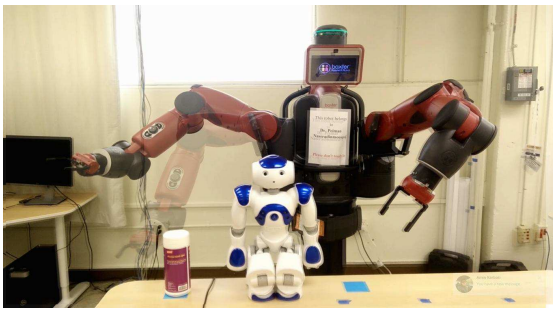

(c)

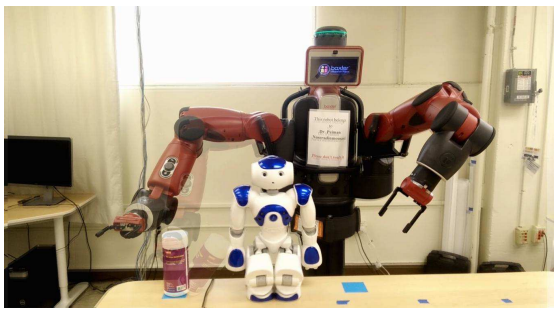

(d)

Figure 2.13: The experimental nominal and optimal trajectories using the ES in sample times of (a) $t = 1s$, (b) $t = 3s$, (c) $t = 5s$, and (d) $t = 6s$; *at* $t = 6s$ *the robot's end-effector through the nominal trajectory collides with another object due to the jerky motion while the optimal one avoids such a collision throughout the whole operational time*. The shadow frames present the nominal trajectory.

Fig. 2.13 presents the experimental work, for sample operation times of $t = 1s$, $t = 3s$, $t = 5s$, and $t = 6s$, revealing smoother motions of the joints/links for the optimal path than the actual (inefficient) one. The jerky motion of the actual trajectory caused an undesirable collision between the robot's end-effector and another object at $t = 6s$, while the optimal one avoids such a collision throughout the whole operational time. Note that

the shadow motions/frames stand for the actual (inefficient) operation.

In summary, the nominal operation shown in Fig. 2.13 is considerably faster than the optimal one, expectedly consumes more energy, and causes the collision at $t = 6s$. For the optimal case, the manipulator is fast enough, moves toward the end-point safely, and no jerky motion can be observed.

2.6 Time-Energy Optimization

Within this Section, we define the following time-energy cost function without any upper and lower bounds.

$$TE = \sum_{i=1}^{7} TE_i = \sum_{i=1}^{7} \sum_{k=0}^{N-1} \left| \tau_i(k) \dot{\theta}_i(k) \right| \Delta t + \gamma t_f \tag{2.63}$$

where t_f is the operation time as mentioned earlier, and $\gamma > 0$ is a weighting coefficient indicating the importance of operational time t_f versus consumed energy E. It is worth mentioning that t_f depends on the B_i's and we still try to find the optimal values for B_i's. From the following equality, t_f can be found based on the B_i's.

$$t_f = 2.3572 \left(\min_{i \in \{1,\cdots,7\}} (B_i) \right)^{-0.3043} \times \exp \left(-3.3883 \left(\min_{i \in \{1,\cdots,7\}} (B_i) \right)^{0.6957} \right) \tag{2.64}$$

The optimal values of B_i's with $\gamma = 5$ are listed in the following table and compared with the optimal values of the energy optimization case.

Table 2.8: Optimal trajectories' coefficients using ES

Joint Name	Energy Optimization	Time-Energy Optimization
S_0	0.0078	0.0741
S_1	0.0071	0.0685
E_0	0.1354	0.1124
E_1	0.00703	0.0323
W_0	0.1306	0.1180
W_1	0.0703	0.0643
W_2	0.1222	0.1059

The optimal operation time in accordance with these B_i's is $t_f = 4.9087s$ and, as expected, the consumed energy is $E = 41.4273J$. The optimization process for the B_i's and cost function defined in (2.63) are shown in Fig. 2.14 and Fig. 2.16, respectively.

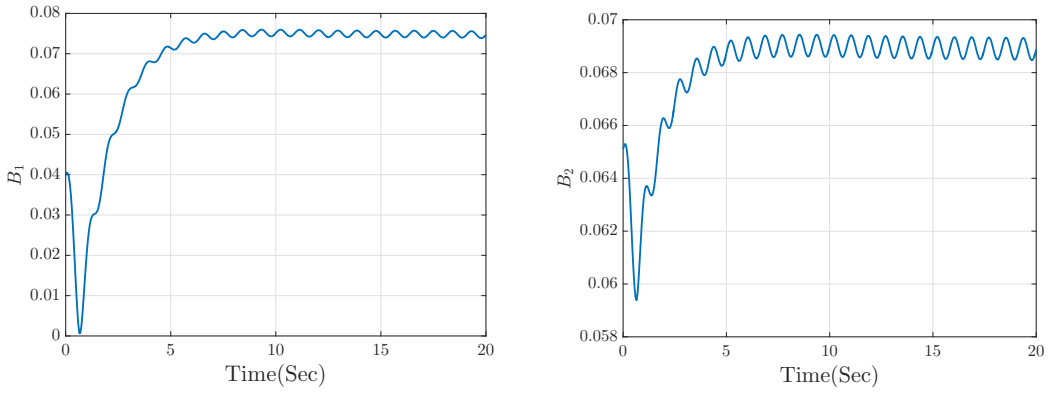

(a) (b)

Figure 2.14: The optimal values of B_i's using the ES for (a) S_0; (b) S_1; (c) E_0; (d) E_1; (e) W_0; (f) W_1; (g) W_2

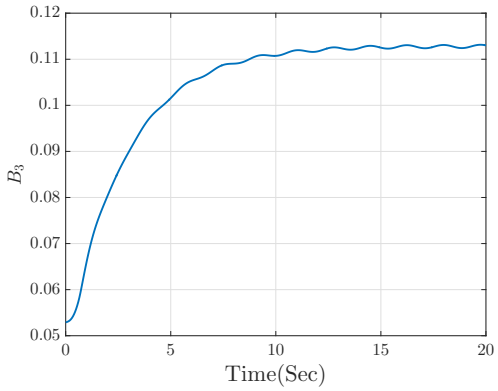

(c)

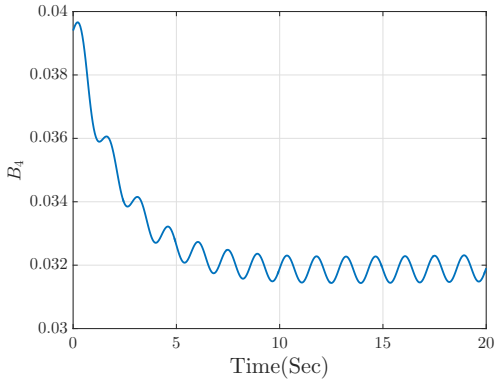

(d)

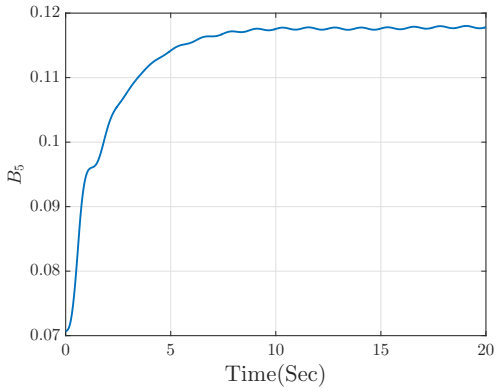

(e)

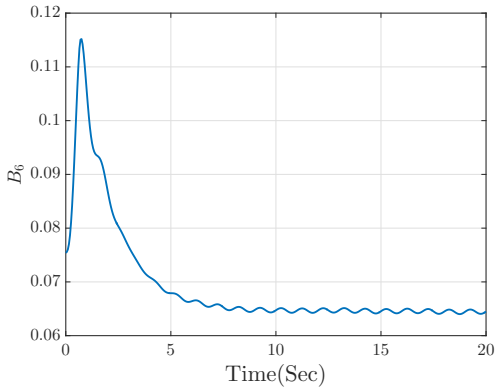

(f)

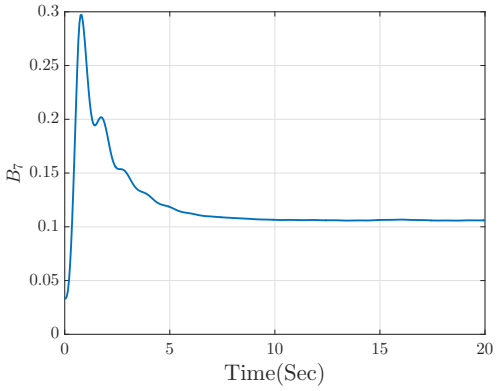

(g)

Figure 2.14: The optimal values of B_i's using the ES for (a) S_0; (b) S_1; (c) E_0; (d) E_1; (e) W_0; (f) W_1; (g) W_2, continued

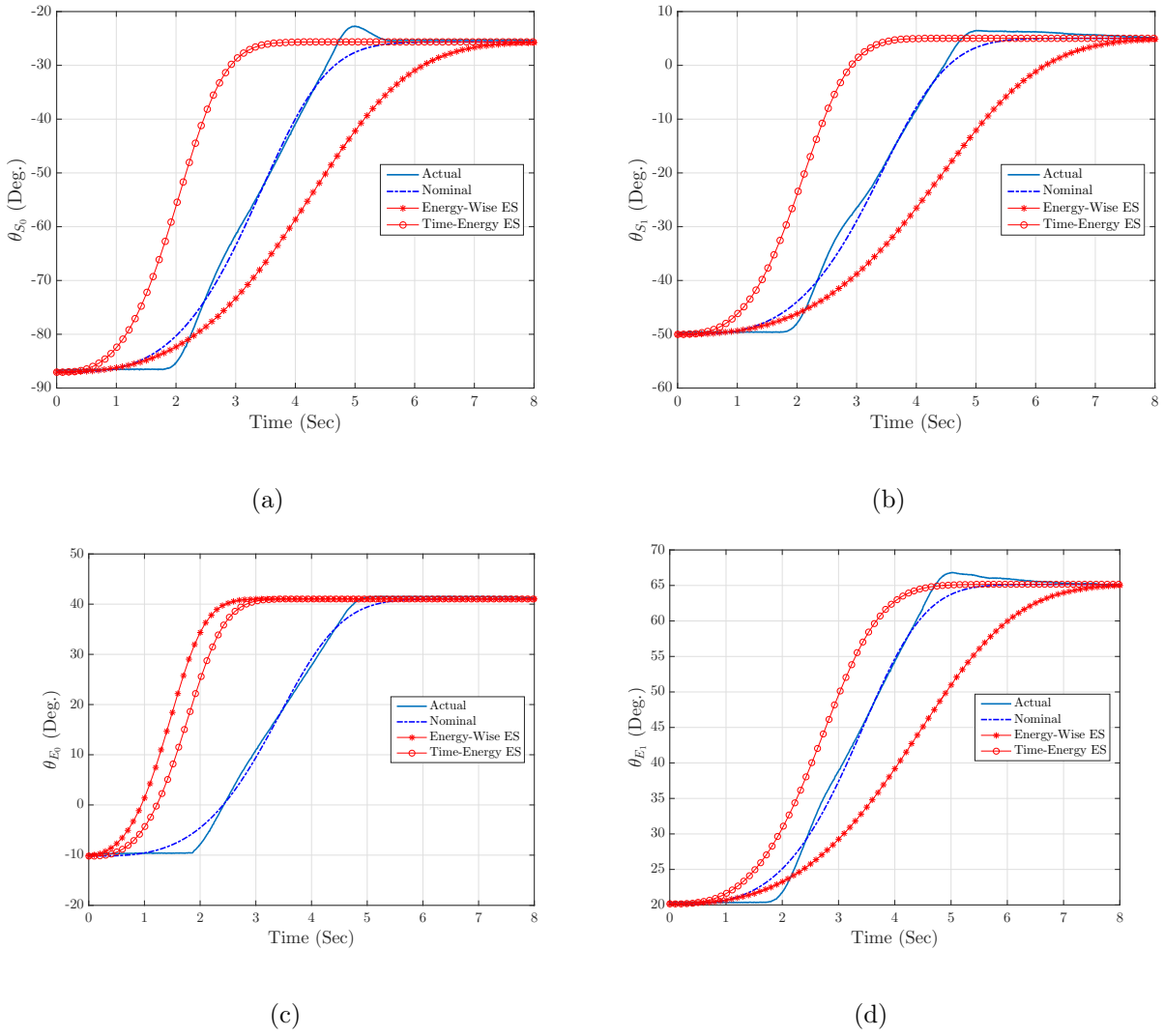

Figure 2.15: The actual (inefficient), energy-wise optimal, and time-energy optimal trajectories using the ES and GA: (a) S_0; (b) S_1; (c) E_0; (d) E_1; (e) W_0; (f) W_1; (g) W_2

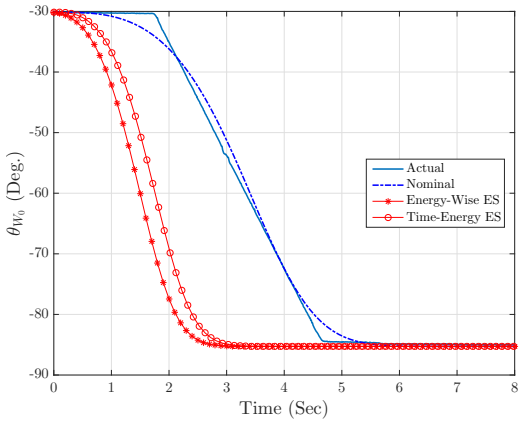

(e)

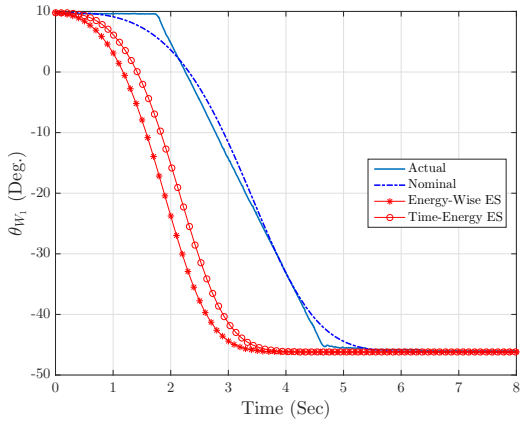

(f)

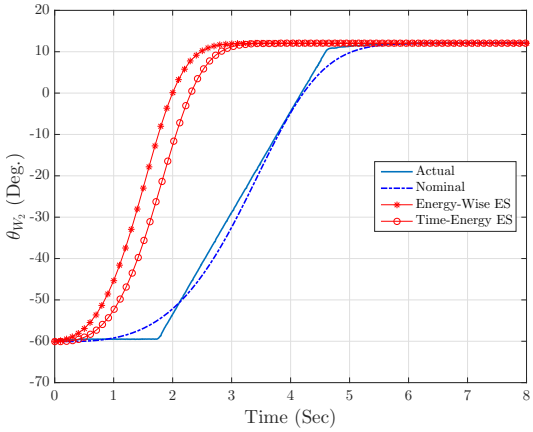

(g)

Figure 2.15: The actual (inefficient), energy-wise optimal, and time-energy optimal trajectories using the ES and GA: (a) S_0; (b) S_1; (c) E_0; (d) E_1; (e) W_0; (f) W_1; (g) W_2, continued

Fig. 2.15 reveals that all time-energy optimal trajectories reach to the end-point in less than $5s$, since the operational time is $t_f = 4.9087s$ as mentioned earlier. Shown in Fig. 2.16 is the cost function defined in (2.63) versus time and also minimization process

using the ES.

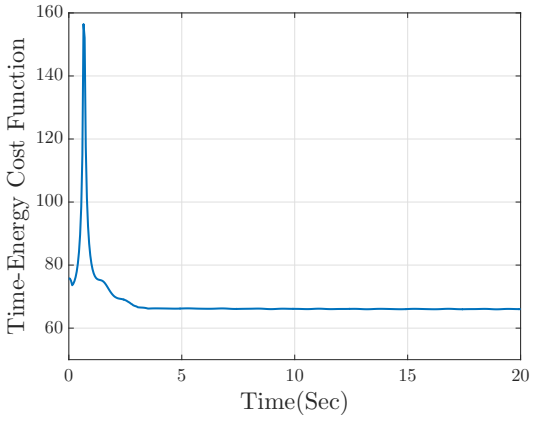

Figure 2.16: The cost function optimization process using the ES

According to Eq. (2.64), the operation time t_f decreases for the minimum value of B_i's, although it dramatically increases for when one of the B_i's gets close to zero at the beginning of optimization process. Fig. 2.16 presents that, after a notable surge, the cost function sharply decreases and then gradually converges to the optimal value of 65.9708 (at $t = 18.9500s$). Note that shown in Fig. 2.10(a) reveals that the optimization process is subject to stochastic fluctuations, as all the seven parameters (B_i's) are oscillating with seven different frequencies satisfying the mentioned conditions.

$$\Delta TE_{\text{ES}} = \frac{\overbrace{TE_{\text{nominal}}}^{76.8108} - \overbrace{TE_{\text{optimal}}}^{65.9708}}{TE_{\text{nominal}}} \times 100 = 14.11\% \tag{2.65}$$

To summarize, through the time-energy optimization process, the cost function decreases from 76.8108 to 65.9708 (14.11%) and consequently, the consumed energy increases from $36.8108J$ to $41.4273J$ (11.14%) while the operational time decreases from $8s$

to 4.9087s (38.64%). Finally, the results of time-energy optimization process are compared with the energy-wise optimization process:

Table 2.9: Comparing energy and time-energy optimization using ES

	Nominal Opr.	Energy Opt.	Time-Energy Opt.
Opr. Time (s)	8.0	8.0	4.9087
Consumed Energy (J)	45.34	36.631	41.4273
Saving Consumed Energy	–	19.44%	8.63%
Saving Opr. Time	–	0	38.64%

Based on Eq. (2.63), γ is an indicator to reveal the significant role of operation time for the minimization process; the higher values of γ would expectedly yield the higher amount of energy saved.

2.7 Conclusions

Through this chapter, we presented the interconnected trajectory optimization of a 7-DOF Baxter manipulator using both the extremum seeking and heuristic-based methods to avoid being trapped in several possible local minima. The coupled dynamic equations of the robot were derived utilizing the Lagrangian method and then validated through the experimental work. We then optimized the joints' trajectories to generate smooth paths to avoid being exposed to the jerky motions of the nominal ones in addition to minimizing energy consumption.

The global sensitivity analysis was then carried out to evaluate the effects of changes in the optimization variables on the cost function defined leading to select the most effective

ones. Based on the sensitivity analysis, the B_i's were optimized to considerably decrease the operation's energy consumed and also to address the crucial issue of jerky motion.

Finally, the optimal trajectory was experimentally implemented and compared with the actual (inefficient) one. The results revealed that the proposed scheme yields the minimum energy consumption in addition to overcoming the robot's jerky motion observed in an inefficient path, and also demonstrated that the manipulator safely follows the optimized trajectory and, as expected, tends to the end-point. The principal results of this chapter can be summarized as follows:

- ✓ Using the *multivariable discrete-time Extremum Seeking* results in a significant decrease in computational cost, an almost twenty-fold reduction relative to Genetic Algorithm.
- ✓ A considerable amount of energy is saved (upward of 19%).
- ✓ The jerky motion and the subsequent collision between the robot's end-effector and another object close to the end-point are removed using the optimal trajectory, which is noted in experimental results.
- ✓ The time-energy optimization results in the energy saving of 8.63% along with 38.64% reduction in the operation time.

2.8 Notes and References

In this chapter, the model of 7-DOF Baxter robot was presented and then experimentally verified. Based on the model, the operational optimization using both the multi-variable discrete-time Extremum Seeking (ES) and Genetic Algorithm (GA) was carried out.

One possible future work would be the modeling of friction in the joints to derive a high fidelity model and also defining various cost functions based on the applications of the manipulator. It is also of great interest to study real-time optimization.

Chapter 2 contains reprints or adaptions of the following papers: 1) M. Bagheri, M. Krstić, and P. Naseradinmousavi, "Multivariable Extremum Seeking for Joint-Space Trajectory Optimization of a High-Degrees-of-Freedom Robot," *ASME Journal of Dynamic Systems, Measurement, and Control*, Vol. 140, Issue 11, pp. 111017-111017-13, 2018; 2) M. Bagheri, M. Krstić, and P. Naseradinmousavi, "Joint-Space Trajectory Optimization of a 7-DOF Baxter Using Multivariable Extremum Seeking," *IEEE American Control Conference (ACC 2018)*, pp. 2176-2181, June 27-29, Milwaukee, WI, USA, 2018; 3) M. Bagheri, P. Naseradinmousavi, "Novel Analytical and Experimental Trajectory Optimization of a 7-DOF Baxter Robot: Global Design Sensitivity and Step Size Analyses," *The International Journal of Advanced Manufacturing Technology*, Vol. 27, Issue 9, pp. 1-15, 2017. The dissertation author is the primary investigator and author of these papers, and would like to thank Miroslav Krstić and Peiman Naseradinmousavi for their contributions.

Chapter 3

Nonlinear Predictor Feedback for Multi-Input Nonlinear Systems With Input Delay

Through this Chapter, we formulate a robust predictor-based controller for a high-DOF manipulator to compensate a time-invariant input delay during a pick-and-place task. Robot manipulators are widely used in telemanipulation systems on the account of their reliable, fast, and precise motions while they are subject to large delays. Using common control algorithms on such delay systems can cause not only poor control performance, but also catastrophic instability in engineering applications.

Therefore, delays need to be compensated for designing robust control laws. As a case study, we focus on a 7-DOF Baxter manipulator subject to three different input delays. Using the verified model in Chapter 2, we formulate a predictor-based controller,

in the presence of input delay, to track desired trajectories. Finally, the effects of input delays in the absence of a robust predictor are investigated, and then the performance of the predictor-based controller is experimentally evaluated to reveal the robustness of the algorithm formulated.

3.1 Background

Robot manipulators are widely used in various applications to track desired trajectories, particularly in telemanipulation systems such as moving debris and turning valves [6]. Remote manipulators provide the capability of executing tasks safely at an unreachable/dangerous location while they are subject to large input delays as with many engineering systems. Interest in delay, as a common dynamic phenomenon, is driven by applications in modeling and control of traffic systems [99], teleoperators [38, 48, 74], vehicles [1], chemical process control, and robot manipulators [31, 40]. Moon *et. al* presented a characteristic motion profile acquired by the recorded human hesitation motions in [81], and investigated its efficacy in a fast-paced human-robot interaction experiment. It is also interesting that Kazuaki *et. al* focused on "delays in initiating actions" and investigated its effect in learning efficiency [105].

The detrimental impact of time delay is well-established, which plays the most significant role in degrading remote perception and manipulation. Large input delays often arise from communication delay between sensor and actuator, or from the time-consuming computational burden of multi-agent networks. For instance, the foremost

concern of vision-based control is tackling the delay introduced by image acquisition and image processing. One of the earliest challenges in engineering has been the control of systems subject to delays. Note that a common approach to tackle this problem is the use of predictive algorithms. In 1959, Smith presented the delay compensator known as the Smith predictor [98]. However, in some cases, the Smith predictor – a modification of a nominal controller designed to stabilize the delay-free system – may fail to achieve the closed-loop stability when the plant is unstable [67].

Many studies in recent years were carried out for linear systems subject to the input delays [16–19, 28, 58, 69, 113, 114]. Tsubakino *et al.* [106] proposed a predictor-based state feedback controller for multi-input linear time-invariant (LTI) systems with different time delays in each individual input channel using the modified backstepping transformation due to the differences among delays. In addition to many researches on linear systems, the further recent developments of predictor-based control laws for nonlinear systems with input delays can be found in [20–22, 29, 32, 59, 61, 65, 66, 68]. Motivated by the harmful consequences of input delays on the stability and performance of such control systems, we formulate and implement a predictor-feedback controller [23] for the compensation of large input delays in a multi-input highly nonlinear system – the 7-DOF Baxter manipulator as a case study. We reasonably assume that all input channels induce the same delay due to the fact that it is practically impossible to have different delays for the robot with highly coupled dynamics.

This chapter is organized as follows. We formulate the predictor-feedback control law and present the global asymptotic stability of the closed-loop system using the

predictor-feedback control law and necessary assumptions [7, 11, 12]. Finally, a section is devoted to the results of experiments (pick-and-place task) in order to reveal the significance of predictor for the system stabilization in the presence of three different input delays.

3.2 Designing the Predictor-Based Controller

Using the verified model in Chapter 2, and noting that the inertia matrix $M(q)$ is symmetric, positive definite, and consequently invertible, the multi-input nonlinear system (2.5) can be written as 14^{th}-order ODEs with the following general state-space form,

$$\dot{X} = f_0(X, U) \tag{3.1}$$

where $X = [q_1, \cdots, q_7, \dot{q}_1, \cdots, \dot{q}_7]^{\mathrm{T}} \in \mathbb{R}^{14}$ is the vector of states and $U = \tau_{7\times 1} \in \mathbb{R}^7$ is the input of nonlinear system (3.1).

Since we intend to design a predictor-based controller leading to perfect tracking, we derive error dynamics and then design the controller to stabilize the error dynamics making the origin asymptotically stable.

$$\dot{E} = f(E, U) \tag{3.2}$$

where $E = [e_1^{\mathrm{T}}, e_2^{\mathrm{T}}]^{\mathrm{T}} \in \mathbb{R}^{14}$ is the vector of error states and $e_1(q,t),\ e_2(q,\dot{q},t) \in \mathbb{R}^7$ are defined as

$$e_1 = q_{\text{des}} - q \tag{3.3}$$

$$e_2 = \dot{e}_1 + \alpha\, e_1 \tag{3.4}$$

where $\alpha \in \mathbb{R}^7$ is a constant positive definite matrix, and the following assumption is held for the desired joint trajectories.

Assumption 1. *The desired joint trajectories are assumed to be designed such that* $q_{\text{des}}(t)$, $\dot{q}_{\text{des}}(t)$, *and* $\ddot{q}_{\text{des}}(t) \in \mathbb{R}^7$ *exist and are bounded for all* $t \geq 0$.

Note that dealing with highly nonlinear and coupled dynamic equations could cause a complicated problem of designing a computationally efficient control scheme to avoid the large delay. Therefore, we derive a predictor-based controller for a multi-input nonlinear system, in the presence of input delay, to stabilize the closed-loop system.

In order to demonstrate the generality of our approach, consider the following general multi-input nonlinear system with m inputs, n states, and constant input delay D,

$$\dot{X}(t) = f\left(X(t), U_1(t-D), \cdots, U_m(t-D)\right) \tag{3.5}$$

where, $X \in \mathbb{R}^n$ is the vector of states, $U_1, \cdots, U_m \in \mathbb{R}$ are the control inputs, $D > 0$ is an input delay, and $f : \mathbb{R}^n \times \mathbb{R}^m \to \mathbb{R}^n$ is a locally Lipschitz vector field. We assume that a feedback law $U_i(t) = \kappa_i(X(t))$ is known such that the functions $\kappa_i : \mathbb{R}^n \to \mathbb{R}$ globally asymptotically stabilize the delay-free system – the closed-loop system $\dot{X}(t) = f(X(t), \kappa(X(t)))$ is globally asymptotically stable in the absence of delay. Therefore, in the delay system, the control law needs to be as follows:

$$U_i(t-D) = \kappa_i(X(t)) \tag{3.6}$$

which can be expressed as

$$U_i(t) = \kappa_i(X(t+D)) = \kappa_i(P(t)) \tag{3.7}$$

where $P(t)$ is the D-time units ahead predictor of $X(t)$. The predictor law for the system (3.5) is given by,

$$P(t) = X(t) + \int_{t-D}^{t} f\big(P(\theta), U_1(\theta), U_2(\theta), \cdots, U_m(\theta)\big)\, d\theta \tag{3.8}$$

with the following initial conditions for the integral (3.8),

$$P(\theta) = X(0) + \int_{-D}^{\theta} f\big(P(s), U_1(s), U_2(s), \cdots, U_m(s)\big)\, ds \tag{3.9}$$

where $\theta \in [-D, 0]$. Note that using the following equality,

$$\begin{aligned}\int_{t-D}^{t} f(x)dx &= \int_{0-D}^{0} f(x+t)d(x+t) = \int_{-D}^{0} f(x+t)d(x) \\ &= -\int_{0}^{-D} f(x+t)d(x) = -\int_{0}^{D} f(-x+t)d(-x) \\ &= \int_{0}^{D} f(t-x)d(x)\end{aligned} \tag{3.10}$$

The predictor $P(t)$ can be written as follows,

$$P(t) = X(t) + \int_{0}^{D} f(P(t-\theta), U_1(t-\theta), U_2(t-\theta), \cdots, U_m(t-\theta))\, d\theta \tag{3.11}$$

It is worth mentioning that $P(t)$ is defined in terms of its past values, however a solution $P(t)$ to Eq. (3.8) does not always exist since the control applied after $t = D$ has no effect on the plant over the time interval $[0, D]$; consequently the system (3.5) can exhibit finite escape before $t = D$.

Therefore, in order to ensure the global existence of the predictor state, we need to be sure that, for all initial conditions and all locally bounded input signals, the system's solutions exist for all time. This property is the so-called "forward completeness". For designing the predictor-based controller, we utilize the results of [23].

3.2.1 Equivalent Representation of the Plant Using Transport PDEs for the Actuator's States

Delay, as a common dynamic phenomenon, can be represented by a partial differential equation (PDE) of transport type, which evolves in one spatial dimension, with one derivative in space and one derivative in time. To prepare for our subsequent stability analysis, we introduce the representations of the plant using transport PDEs.

ODEs with delays are interconnected systems of ODEs and transport PDEs. A control system with ODE plant in the presence of input delay has a cascade PDE-ODE structure, where the control signal enters through a boundary condition of the PDE [67]. Since a system with input delay is a PDE-ODE cascade with the control signal $U(t)$ entering through a boundary condition of the PDE, a system with an input delay is a boundary control system.

The system (3.5) can be written equivalently as the following PDE system,

$$\dot{X}(t) = f(X(t), u_1(0,t), \cdots, u_m(0,t)) \tag{3.12}$$

$$\partial_t u_i(x,t) = \partial_x u_i(x,t), \quad x \in (0,D), \quad i = 1, \cdots, m \tag{3.13}$$

$$u_i(D,t) = U_i(t) \qquad i = 1, \cdots, m \tag{3.14}$$

Note that the solutions to (3.13) and (3.14) are given by

$$u_i(x,t) = U_i(t+x-D), \;\; x \in [0,D] \qquad i = 1, \cdots, m \tag{3.15}$$

3.2.2 Transport PDE Representation of the Predictor States

The predictor states $P(\theta)$ can be written as

$$p(x,t) = X(t) + \int_0^x f\left(p(y,t), u_1(y,t), \cdots, u_m(y,t)\right)\, dy \tag{3.16}$$

where $x \in [0, D]$. Based on Eq. (3.16), the functions $p(x,t)$ satisfy the following ODE in x:

$$\partial_x p(x,t) = f\left(p(x,t), u_1(x,t), \cdots, u_m(x,t)\right) \quad x \in [0, D] \tag{3.17}$$

with initial solution,

$$p(0,t) = X(t) \tag{3.18}$$

We intend to reveal that the solution to (3.17) and (3.18) is

$$p(x,t) = X(t+x), \quad x \in [0, D] \tag{3.19}$$

Note that the function $X(t+x)$ satisfies the ODE in x (3.17) due to the (3.5):

$$\dot{X}(t+x) = f\left(X(t+x), U_1(t+x-D), \cdots, U_m(t+x-D)\right), \tag{3.20}$$

for all $t \geq 0$ and $0 \leq x \leq D$. This is resulted from the uniqueness of solutions to the ODE (3.5). Therefore, by defining

$$p(D,t) = P(t) \tag{3.21}$$

and using the fact that p is a function of one variable, namely $x+t$, one can conclude that

$$P(t+x-D) = p(x,t), \quad x \in [0, D] \tag{3.22}$$

Through the change of variables $x = \theta + D - t$ in Eq. (3.16), and utilizing Eqs. (3.15), (3.18), and (3.22) result in

$$P(\theta) = X(t) + \int_{t-D}^{\theta} f\left(P(s), U_1(s), \cdots, U_m(s)\right) ds \tag{3.23}$$

where $t - D \leq \theta \leq t$. Finally, with this representation, the following holds

$$U_i(t) = u_i(D, t) = \kappa_i(p(D, t)), \quad i = 1, \cdots, m \tag{3.24}$$

We define the backstepping transformation of u_i and its inverse backstepping based on the following lemmas:

Lemma 5. *The direct backstepping transformations of* $u_i,\ i = 1, \cdots, m$, *are defined by*

$$w_i(x, t) = u_i(x, t) - \kappa_i(p(x, t)) \tag{3.25}$$

with $x \in [0, D]$, $p(x, t)$ *is defined in* (3.16) *and transforms system* (3.12)-(3.14) *to the following "target system":*

$$\dot{X}(t) = f\big(X(t), w_1(0, t) + \kappa_1(X(t)), w_m(0, t) + \kappa_m(X(t))\big) \tag{3.26}$$

$$\partial_t w_i(x, t) = \partial_x w_i(x, t), \quad x \in (0, D) \tag{3.27}$$

$$w_i(D, t) = 0 \tag{3.28}$$

Lemma 6. *The inverse backstepping transformations of* (3.25) *are defined by*

$$u_i(x, t) = w_i(x, t) + \kappa_i(\pi(x, t)), \quad i = 1, \cdots, m \tag{3.29}$$

with $x \in [0, D]$ *and* $\pi(x, t)$ *is defined as follows*

$$\pi(x, t) = X(t) + \int_0^x f\big(\pi(y, t), w_1 + \kappa_1(\pi(y, t)), \cdots, w_m + \kappa_m(\pi(y, t))\big)\, dy \tag{3.30}$$

Therefore,

$$\partial_x \pi(x,t) = f\left(\pi(x,t), \kappa_1(x,t) + w_1(x,t), \cdots, \kappa_m(x,t) + w_m(x,t)\right) \tag{3.31}$$

where $x \in [0, D]$, with the following initial solution,

$$\pi(0,t) = X(t) \tag{3.32}$$

It is worth mentioning that the ultimate purpose of the p-system and the π-system is to generate the plant predictor and the target predictor, respectively, in the following forms

$$P(t) = p(D,t) \tag{3.33}$$

$$\Pi(t) = \pi(D,t) \tag{3.34}$$

Lemma 7. *The functions $(X(t), u(x,t))$ satisfy Eqs. (3.12), (3.13) if and only if the functions $(X(t), w(x,t))$ satisfy Eqs. (3.26), (3.27), where the three functions $X(t), u(x,t)$, and $w(x,t)$ are related as mentioned above.*

Proof. This result is immediate by noting that $u(x,t)$ and $w(x,t)$ are functions of only one variable, $x + t$, and therefore so are $p(x,t)$ and $\pi(x,t)$ based on the ODEs (3.17), (3.18), (3.31), and (3.32). This implies that

$$p_t(x,t) = p_x(x,t) \tag{3.35}$$

$$\pi_t(x,t) = \pi_x(x,t) \tag{3.36}$$

From this observation it follows that

$$w_t(x,t) - w_x(x,t) = u_t(x,t) - \frac{\partial \kappa(p(x,t))}{\partial p} p_t(x,t) - \left(u_x(x,t) - \frac{\partial \kappa(p(x,t))}{\partial p} p_x(x,t) \right) = 0 \tag{3.37}$$

$$u_t(x,t) - u_x(x,t) = w_t(x,t) - \frac{\partial \kappa(\pi(x,t))}{\partial \pi} \pi_t(x,t) - \left(u_x(x,t) - \frac{\partial \kappa(\pi(x,t))}{\partial \pi} \pi_x(x,t) \right) = 0 \tag{3.38}$$

which completes the proof.

Also, based on the necessary ISS assumption for the system, we can mention the following lemma,

Lemma 8. *There exists a class $\mathcal{KL}$ function β_1 such that the following holds*

$$\bar{\Xi}(t) \leq \beta_1 \left(\bar{\Xi}(0), t \right), \qquad \text{for all } t \geq 0 \tag{3.39}$$

where

$$\bar{\Xi}(t) = |X(t)| + \sum_{i=1}^{m} \|w_i(.,t)\|_\infty \tag{3.40}$$

The following lemmas help the proof of closed-loop system stability [23],

Lemma 9. *There exist class $\mathcal{K}_\infty$ functions ρ such that*

$$\|p(.,t)\|_\infty \leq \rho(\Xi(t)) \tag{3.41}$$

where

$$\Xi(t) = |X(t)| + \sum_{i=1}^{m} \|u_i(.,t)\|_\infty \tag{3.42}$$

Lemma 10. *There exist class $\mathcal{K}_\infty$ functions $\bar{\rho}$ such that*

$$\|\pi(.,t)\|_\infty \leq \bar{\rho}(\bar{\Xi}(t)) \tag{3.43}$$

where $\bar{\Xi}$ is defined in (3.40).

Lemma 11. *There exist class $\mathcal{K}_\infty$ functions ρ and $\bar{\rho}$ such that*

$$\bar{\Xi}(t) \leq \rho(\Xi(t)) \tag{3.44}$$

$$\Xi(t) \leq \bar{\rho}(\bar{\Xi}(t)) \tag{3.45}$$

Finally, based on the mentioned lemmas, the following theory can be utilized, which is proved in [23].

Theorem 3. *Consider the closed-loop system consisting of the plant* (3.12) – (3.14) *and the control laws* (3.24). *Under Assumptions of forward completeness for open-loop system and the Input-to-State Stability (ISS) for closed-loop one, there exists a β function which belongs to class $\mathcal{KL}$ such that for all initial conditions $X_0 \in \mathbb{R}^n$ and $u_{i_0} \in C[0, D],\ i = 1, \cdots, m$, which are compatible with the feedback laws, that is, they satisfy $u_{i_0}(D) = \kappa_i(p(D, 0)),\ i = 1, \cdots, m$, the closed-loop system has a unique solution $X(t) \in C^1[0, \infty)$ and $u_i(x, t) \in C\left([0, D] \times [0, \infty)\right),\ i = 1, \cdots, m$, and the following holds for all $t \geq 0$,*

$$\Xi(t) \leq \beta\left(\Xi(0), t\right), \qquad \text{for all } t \geq 0 \tag{3.46}$$

where $\Xi(t)$ defined in (3.42).

Proof of Theorem 3: By combining Eq. (3.45) with Eq. (3.39), we get that $\Xi(t) \leq \bar{\rho}\left(\beta_1(\bar{\Xi}(0), t)\right)$, for all $t \geq 0$, and hence, with Eq. (3.45) we arrive at Eq. (3.46) with

$\beta(s,t) = \bar{\rho}\left(\beta_1(\rho(s),t)\right)$. The proof of existence and uniqueness of a solution $X(t) \in C^1[0,\infty)$ and $u_i(x,t) \in C([0,D]\times[0,\infty)),\ i = 1,\cdots,m$, is shown as follows. Using relation (3.17) for $t = 0$, the compatibility of the initial conditions $u_{i_0}, i = 1,\cdots,m$, with the feedback laws (3.24) guarantee that $p(x,0) \in C^1[0,D]$. Hence, using relations (3.16) and (3.18), and the fact that $u_{i_0} \in C[0,D],\ i = 1,\cdots,m$, it also follows from (3.25) that $w_{i_0} \in C[0,D],\ i = 1,\cdots,m$. The solutions to (3.27) and (3.28) are given for all $i = 1,\cdots,m$ by

$$w_i(x,t) = \begin{cases} w_{i_0}(t+x), & 0 \le x+t \le D \\ 0, & x+t \ge D \end{cases} \tag{3.47}$$

There is a unique solution for (3.47) due to the uniqueness of the solution to (3.27) and (3.28). Hence, the compatibility of the initial conditions $u_{i_0},\ i = 1,...,m$, with the feedback laws (3.24) guarantee the existence of a unique solution $w_i(x,t) \in C\left([0,D]\times[0,\infty)\right),\ i = 1,\cdots,m$. Also, it follows that $X(t) \in C^1[0,\infty)$ from the target system (3.26). The fact that $\pi(x,t) = X(t+x)$, for all $t \ge 0$ and $x \in [0,D]$, along with the inverse backstepping transformations (3.29) guarantee that $u_i(x,t) \in C\left([0,D]\times[0,\infty)\right),\ i = 1,\cdots,m$. The proof is completed.

Notation: We denote by $\mathcal{K}$ the set of strictly increasing continuous functions $\alpha : [0,\infty) \to [0,\infty)$ with $\alpha(0) = 0$. α belongs to $\mathcal{K}_\infty$ if $\alpha \in \mathcal{K}$ and $\lim_{r\to\infty}\alpha(r) = \infty$. We denote by $\mathcal{KL}$ the set of functions $\beta : [0,\infty)\times[0,\infty) \to [0,\infty)$ such that, for each $s \in [0,\infty),\ r \to \beta(r,s)$ is nondecreasing and continuous and $\beta(0,s) = 0$ and, for each $r \in [0,\infty),\ s \to \beta(r,s)$ is monotonically decreasing with $\beta(r,s) \to 0$ as $s \to \infty$.

Finally, in the form of standard delay notation, the backstepping transformation

that we associate with this control law and its inverse transformation are given by

$$W_i(t) = U_i(t) - \kappa_i(P(t)) \tag{3.48}$$

$$U_i(t) = W_i(t) + \kappa_i(\Pi(t)) \tag{3.49}$$

where $P(t)$ is defined above and $\Pi(t)$ is defined via the integral equation

$$\Pi(t) = X(t) + \int_{t-D}^{t} f(\Pi(\theta), \kappa_1(\Pi(\sigma)) + W_1(\sigma), \cdots, \kappa_m(\Pi(\sigma)) + W_m(\sigma))\, d\theta \tag{3.50}$$

with initial condition

$$\Pi(\theta) = \int_{-D}^{\theta} f(\Pi(\sigma), \kappa_1(\Pi(\sigma)) + W_1(\sigma), \cdots, \kappa_m(\Pi(\sigma)) + W_m(\sigma))\, d\sigma + X(0), \quad \theta \in [-D, 0] \tag{3.51}$$

The purpose of this backstepping transformation is that it results in a closed-loop system (target system) of the form

$$\dot{X}(t) = f(X(t), \kappa_1(X) + W_1(t-D), \cdots, \kappa_m(X) + W_m(t-D)) \tag{3.52}$$

$$W(t) \equiv 0\,, \quad \text{for } t \geq 0 \tag{3.53}$$

where $W(t)$ for $t \in [-D, 0]$ is defined by Eqs. (3.48) and (3.9). Clearly, the nonzero values of $W(t)$, which occur only over the interval $[-D, 0]$, depend only on the initial condition $X(0)$ and the initial actuator state, $U(\sigma), \sigma \in [-D, 0]$.

Note that $P = \Pi$, however, they play different roles because they are driven by different inputs (U versus W). The mapping (3.48) represents the direct backstepping transformation $U \to W$, whereas Eq. (3.49) represents the inverse backstepping transformation $W \to U$. Both transformations are nonlinear and infinite-dimensional.

For global stabilization via predictor feedback, we require all of the following three ingredients [66]:

- ✓ The target system is globally asymptotically stable;
- ✓ The direct backstepping transformation is globally well defined;
- ✓ The inverse backstepping transformation is globally well defined.

As the system is forward-complete and is globally stabilizable in the absence of input delay, both the plant-predictor and target-predictor systems, as well as both the direct and inverse backstepping transformations (Eqs. (3.48) and (3.49)), will be globally well defined. Consequently, the predictor feedback will be globally stabilizing within this class.

By using (3.15) and Theorem 4 as a result of [23], we have the following theorem in the form of standard delay notation,

Theorem 4. *Consider the closed-loop system consisting of the plant* (3.5) *with input delay. If there exist control laws* (3.7)–(3.8) *such that* $\dot{X}(t) = f(X(t), \kappa(X(t)))$ *becomes asymptotically stable, subject to the assumptions of open-loop system forward completeness and the Input-to-State Stability (ISS) of closed-loop system* $\dot{X}(t) = f(X(t), \kappa(X(t)) + \omega)$ *with respect to* ω*, the following holds for all* $t \geq 0$*,*

$$\Omega(t) \leq \beta\left(\Omega(0), t\right) \tag{3.54}$$

where

$$\Omega(t) = |X(t)| + \sum_{i=1}^{n} \sup_{t-D \leq \theta \leq t} |U_i(\theta)| \tag{3.55}$$

3.2.3 Error System Development

The control objective includes converging joint position and velocity errors to zero implying the generalized coordinates track the desired time-varying joint trajectories, $q_{\text{des}}(t) \in \mathbb{R}^7$. A state-space model for the tracking error (Eq. (3.2)) is developed based on Eqs. (3.3) and (3.4). Then a controller is formulated to improve tracking performance indices, converging errors to zero, subject to the assumption of knowing the system dynamics, as mentioned earlier.

A state-space model, based on the tracking error, is formulated using Eq. (3.4) and its time derivative,

$$\dot{e}_1 = \dot{q}_{\text{des}} - \dot{q} \tag{3.56}$$

$$\dot{e}_2 = \ddot{q}_{\text{des}} - \ddot{q} + \alpha\, \dot{e}_1 \tag{3.57}$$

Premultiplying the inertia matrix by the time derivative of Eq. (3.57), while Eqs. (2.5) and (3.4) are substituted,

$$\begin{aligned} -M(q)\dot{e}_2 + (M(q)\alpha - C(q,\dot{q}))e_2 + \left(-M(q)\alpha^2 + C(q,\dot{q})\alpha\right) e_1 \\ + M(q)\ddot{q}_{\text{des}} + C(q,\dot{q})\dot{q}_{\text{des}} + G(q) = \tau \end{aligned} \tag{3.58}$$

which yields,

$$\dot{e}_2 = \alpha e_2 + h - M^{-1}\tau \tag{3.59}$$

where $h \in \mathbb{R}^7$ is a nonlinear function defined as

$$h = \ddot{q}_{\text{des}} - \alpha^2 e_1 + M^{-1}C\left(\dot{q}_{\text{des}} + \alpha e_1 - e_2\right) + M^{-1}G \tag{3.60}$$

and the state-space model of error dynamics becomes,

$$\dot{E} = f(E, \tau) = \begin{bmatrix} e_2 - \alpha e_1 \\ \alpha e_2 + h - M^{-1}\tau \end{bmatrix} \tag{3.61}$$

As we mentioned through Theorem 4, the forward completeness and ISS properties for the nonlinear system should be established. The forward-complete systems include all linear systems both stable and unstable, as well as various nonlinear systems with bounded nonlinearities. The mathematical model of robot manipulators contains trigonometric nonlinearities as a result of rotational motions, which implies that $q(t)$ and consequently $e_1(t)$ do not escape to infinity within a finite time. Therefore, robot manipulators are the forward-complete nonlinear systems [66]. We can also utilize the following theorem [2] to establish that the system is forward complete,

Theorem 5. *System $\dot{x} = f(x, d)$ is forward complete if and only if there exists a proper and smooth function $V : \mathbb{R}^n \to \mathbb{R}_{\geq 0}$ such that the following exponential growth condition is verified:*

$$DV(x)f(x, d) \leq V(x), \quad \forall x \in \mathbb{R}^n, \forall d \in \mathcal{D} \tag{3.62}$$

So, this theorem by [2] ensures that the assumption of Theorem 3 holds if we can establish (3.62). We now establish (3.62) by first considering the following Lyapunov function,

$$V(E) = \frac{1}{2} e_1^T e_1 + \frac{1}{2} e_2^T e_2 \tag{3.63}$$

We have,

$$\begin{aligned}\dot{V} &= e_1^T(e_2 - \alpha e_1) + e_2^T(\alpha e_2 + h - M^{-1}\tau) \\ &= e_1^T e_2 - e_1^T \alpha e_1 + e_2^T \alpha e_2 + e_2^T h - e_2^T M^{-1}\tau \end{aligned} \tag{3.64}$$

Since M, M^{-1}, and C include trigonometric functions, we get

$$e_1^T e_2 - e_1^T \alpha e_1 + e_2^T \alpha e_2 \leq \frac{1}{2}\left(e_1^T e_1 + e_2^T e_2\right) - \lambda_m e_1^T e_1 + \lambda_M e_2^T e_2 \tag{3.65}$$

$$\begin{aligned} e_2^T h \leq & e_2^T\Big(\ddot{q}_{des} - \alpha^2 e_1 + M^{-1}C\dot{q}_{des} + M^{-1}G + M^{-1}C\alpha e_1 - M^{-1}Ce_2\Big) \\ \leq & \frac{1}{2}\left(e_2^T e_2 + \ddot{q}_{\text{des}}^T \ddot{q}_{\text{des}}\right) + \frac{\gamma_1}{2}\left(e_2^T e_2 + e_1^T e_1\right) \\ & + \frac{\gamma_2}{2}\left(e_2^T e_2 + \dot{q}_{\text{des}}^T \dot{q}_{\text{des}}\right) + \frac{\gamma_3}{2}\left(e_2^T e_2 + \Gamma^2\right) \\ & + \frac{\gamma_4}{2}\left(e_2^T e_2 + e_1^T e_1\right) - \gamma_5\left(e_2^T e_2\right) \end{aligned} \tag{3.66}$$

$$-e_2^T M^{-1}\tau \leq \frac{\gamma_6}{2}\left(e_2^T e_2 + \tau^T \tau\right) \tag{3.67}$$

where λ_M and λ_m denotes the maximum and minimum eigenvalues of matrix α, respectively. Also, $\gamma_i' s > 0$ $(i = 1, 2, 3, 4, 5, 6)$ and Γ is the L_2-norm of gravitational vector.

Substituting Eqs. (3.65), (3.66), and (3.67) into Eq. (3.64) yields,

$$\begin{aligned} \dot{V} \leq & (1 - 2\lambda_m + \gamma_1 + \gamma_4)\left(\frac{1}{2}e_1^T e_1\right) \\ & + (2 + 2\lambda_M + \gamma_1 + \gamma_2 + \gamma_3 + \gamma_4 - 2\gamma_5 + \gamma_6)\left(\frac{1}{2}e_2^T e_2\right) \\ & + \frac{1}{2}\left(\ddot{q}_{\text{des}}^T \ddot{q}_{\text{des}}\right) + \frac{\gamma_2}{2}\left(\dot{q}_{\text{des}}^T \dot{q}_{\text{des}}\right) + \frac{\gamma_3}{2}\Gamma^2 + \frac{\gamma_6}{2}|\tau|^2 \\ \leq & \gamma_6\left(\frac{1}{2}e_1^T e_1 + \frac{1}{2}e_2^T e_2\right) + \gamma_7 \end{aligned} \tag{3.68}$$

where,

$$\gamma_6 = \max\Big\{\big(1 - 2\lambda_m + \gamma_1 + \gamma_4\big), \big(2 + 2\lambda_M + \gamma_1 + \gamma_2 + \gamma_3 + \gamma_4 - 2\gamma_5 + \gamma_6\big)\Big\} \tag{3.69}$$

$$\frac{1}{2}\left(\ddot{q}_{\text{des}}^T \ddot{q}_{\text{des}}\right) + \frac{\gamma_2}{2}\left(\dot{q}_{\text{des}}^T \dot{q}_{\text{des}}\right) + \frac{\gamma_3}{2}\Gamma^2 + \frac{\gamma_6}{2}|\tau|^2 \leq \gamma_7 \tag{3.70}$$

since τ, $\ddot{q}_{\text{des}}$ and $\dot{q}_{\text{des}}$ are bounded, we get,

$$\dot{V} \leq \gamma_6 V(E) + \gamma_7 \tag{3.71}$$

Consequently, $(V(E) + \frac{\gamma_7}{\gamma_6})^{\frac{1}{\gamma_6}}$ is a smooth Lyapunov function satisfying (3.62). With this function, which differs from classical Lyapunov functions because it is not positive definite because it is not zero at zero (note that this property is not required anyway in Theorem 5), we have established that the following assumption of Theorem 3 is verified.

Assumption 2. *The system $\dot{E} = f\left(E, \tau_1, \cdots, \tau_7\right)$ is forward complete.*

Forward-completeness ensures that, for every initial condition and locally bounded input signal, the corresponding solution is defined for all $t \geq 0$.

Then, we design a predictor feedback law for (3.61), which achieves global asymptotic stability for the delay-free system, as mentioned in Theorem 4 – the closed-loop system $\dot{E}(t) = f(E(t), \kappa(E(t)))$ should be asymptotically stable. Since the dynamics of system (2.5) is known, the controller is formulated, based on Eq. (3.59), as

$$\tau = \kappa(E) = M(h + (\beta + \alpha)e_2) \tag{3.72}$$

where $\beta \in \mathbb{R}^7$ is a constant positive definite matrix. Substituting Eq. (3.72) into Eq. (3.59) and using the invertible property of inertia matrix result in the closed-loop error

signal for $e_2(t)$ as

$$\dot{e}_2 = -\beta e_2 \tag{3.73}$$

Finally, the state-space model of closed-loop system, with respect to Eqs. (3.4) and (3.73), is derived as follows,

$$\dot{E} = f(E, \kappa(E)) = AE(t) \tag{3.74}$$

where $A \in \mathbb{R}^{14\times 14}$ is defined as

$$A = \begin{bmatrix} -\alpha & I_{7\times 7} \\ 0_{7\times 7} & -\beta \end{bmatrix} \tag{3.75}$$

Note that $I_{7\times 7}$ and $0_{7\times 7}$ are identity and zero matrices, respectively. Since A is an upper triangular block matrix and is also Hurwitz for any positive definite α and β matrices, closed-loop system (3.74) is hence exponentially stable.

Note that the control law is formulated such that the error dynamics becomes exponentially and subsequently asymptotically stable. Now the only property we need to establish, before using Theorem 4, is the input-to-state (ISS) stability of the following closed-loop system with respect to $\omega = [\omega_1, \cdots, \omega_m]^T$.

$$\dot{E} = f(E, \kappa(E) + \omega) = \begin{bmatrix} e_2 - \alpha e_1 \\ \alpha e_2 + h - M^{-1}(\kappa(E) + \omega) \end{bmatrix} = AE(t) - \begin{bmatrix} 0_{7\times 7} \\ M^{-1}\omega \end{bmatrix} \tag{3.76}$$

The ISS property, as a required assumption for Theorem 4, means that no matter what is the initial state, if the inputs are small, then the system's states must eventually be small.

Definition 1. A system is *Input-to-State Stable (ISS)* if there exist $\gamma \in \mathcal{K}, \beta \in \mathcal{KL}$ such that for all $x_0,\ u$, and $t \geq 0$

$$|x(t)| \leq \beta(|x_0|, t - t_0) + \gamma\left(\sup_{t_0 \geq \tau \geq t} |u(\tau)|\right) \tag{3.77}$$

for all t_0 and t such that $t \geq t_0 \geq 0$

The ISS property for system (3.76) can be shown using the following theorem in [66].

Theorem 6 (Lyapunov characterization of ISS)**.** *For the system $\dot{x} = f(x, u)$ the following properties are equivalent:*

1. *the system is ISS;*

2. *there exists a smooth ISS-Lyapunov function;*

3. *there exists a smooth, positive definite, and radially unbounded function V and class $\mathcal{K}_\infty$ functions ρ_1 and ρ_2 such that the following passivity inequity is satisfied:*

$$\frac{\partial V}{\partial x} f(x, u) \leq -\rho_1(|x|) + \rho_2(|u|). \tag{3.78}$$

Consider the following smooth, positive definite, and radially unbounded function V as follows,

$$V(E) = \frac{1}{2} e_1^T e_1 + \frac{1}{2} e_2^T e_2 \tag{3.79}$$

Therefore, using the closed-loop state-space model (3.75) and (3.76), we have,

$$\begin{aligned}\dot{V}(E) &= -e_1^T \alpha e_1 - e_2^T \beta e_2 + e_1^T e_2 - e_2^T M^{-1} \omega \\ &\leq E^T \begin{bmatrix} -\alpha & 0_{7\times 7} \\ 0_{7\times 7} & -\beta \end{bmatrix} E + \frac{1}{2}\left(|e_1|^2 + |e_2|^2\right) + \frac{\gamma_1}{2}\left(|e_2|^2 + \omega^T\omega\right) \\ &\leq -\left(\gamma_2 - \frac{1}{2} - \frac{\gamma_1}{2}\right)|E|^2 + \frac{\gamma_1}{2}|\omega|^2 \end{aligned} \tag{3.80}$$

where $\gamma_1 > 0$ and γ_2 is the minimum of eigenvalues of α and β. Note that α and β should be chosen such that $\left(\gamma_2 - \frac{1}{2} - \frac{\gamma_1}{2}\right)$ is positive.

Equivalently, ISS property can be also shown using the following Lemma in [62].

Lemma 12. *Suppose $\dot{x} = f(t, x, u)$ is continuously differentiable and globally Lipschitz in (x, u), uniformly in t. If the unforced system $\dot{x} = f(t, x, 0)$ has a globally exponentially stable equilibrium point at the origin, then the system is input-to-state (ISS) stable.*

The exponential stability of the unforced close-loop system (3.74) can be investigated using the fact that matrix A defined in (3.75) is Hurwitz. Finally, due to the fact that $\dot{E} = f(E, \kappa(E) + \omega)$ is continuously differentiable and globally Lipschitz in (E, ω), therefore, the closed-loop system (3.76) is ISS with respect to ω by using Lemma 12.

Hence, the following assumption for our system is verified,

Assumption 3. *The system $\dot{E} = f(E,\ \kappa_1(E) + \omega_1,\ \cdots,\ \kappa_7(E) + \omega_7)$ is Input-to-State Stable (ISS) with respect to $\omega = [\omega_1, \cdots, \omega_7]^T$.*

Finally, as Assumptions 2 and 3 are held for our system, we can employ Theorem 4 to design a predictor-based controller for our system in order to compensate any large

input delay, asymptotically stabilize the error, and make the robot to follow the desired joint trajectories.

3.3 Experimental Results

We experimentally implement the predictor-based controller for the 7-DOF Baxter manipulator as a case study, through a pick-and-place task, while input delays are reasonably similar in all input channels.

We reveal the destabilizing effect of input delay on the control of the manipulator, as shown in Fig. 3.1, and also discuss the effect of incremental delay on the stability of the robot. We intentionally apply the following input delays and then operate the manipulator without any predictor:

- ✓ $D = 0.01s$: indicates minimum feasible input delay with respect to the sampling rate ($t_s = 0.01s$) of Baxter.
- ✓ $D = 0.02s$: the increased delay to determine a crucial value causing the robot operational failure.
- ✓ $D = 0.04s$: the increased delay to study the significant effect of a relatively large input delay.

Figure 3.1: The robot fails to track the desired trajectory without a predictor in the presence of input delay

Figure 3.2: A stable obstacle-avoidance pick-and-place task with input delay using the predictor-based controller

The joint trajectories and torques, for the three cases mentioned above, are presented in Figs. 3.3 and 3.4, respectively, and also compared with the experimental results of delay-free system.

Note that we did not plot the joint trajectories of delay-free system since the manip-

ulator almost perfectly tracks the desired trajectories. As shown in Fig. 3.3, for $D = 0.01s$, the manipulator can still follow the desired trajectories while the joint torques are more than those of the delay-free system (Fig. 3.4). The results also reveal that the joint torques, in particular for the joint 5 (Fig. 3.4(a)), oscillate since the manipulator approaches its singular configuration while passing over the obstacle ($2.5s \leq t \leq 3.5s$).

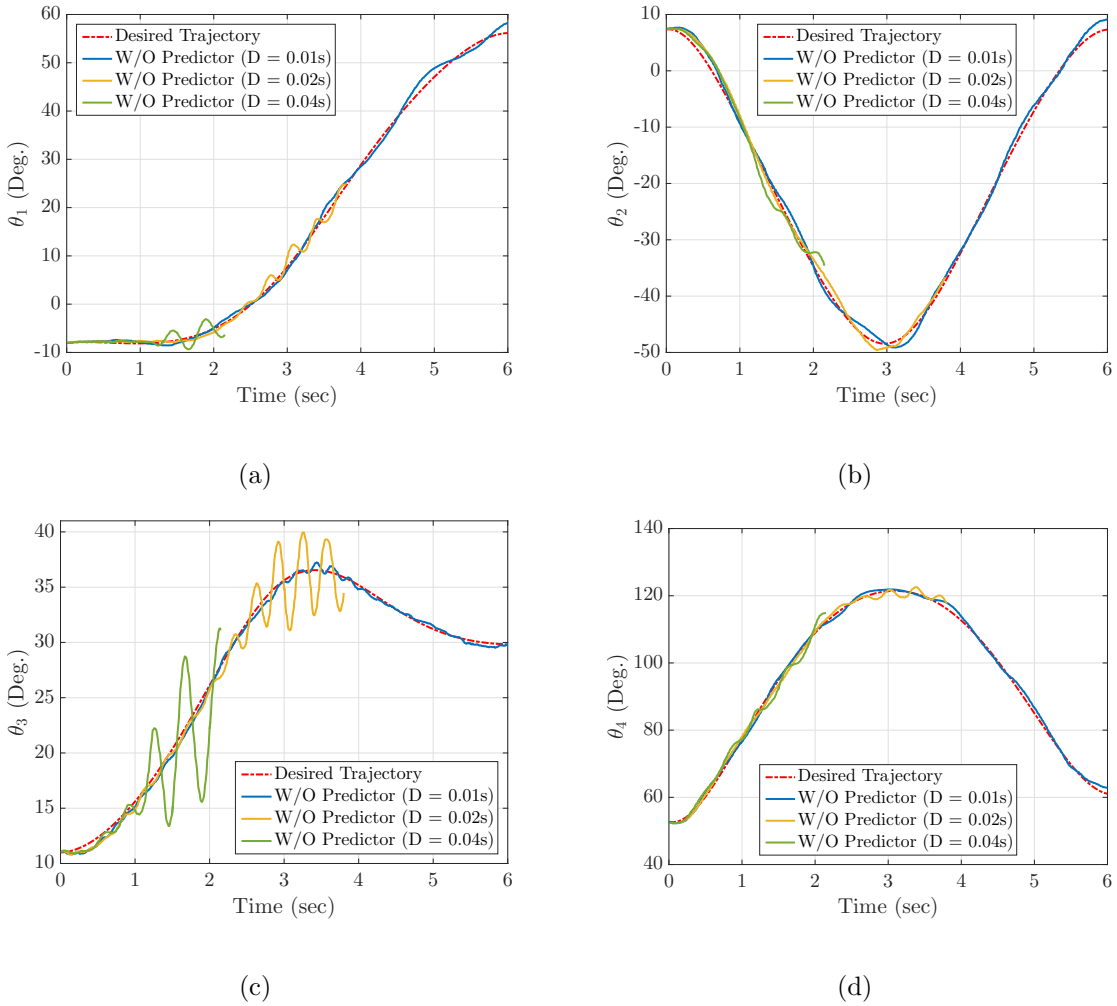

Figure 3.3: The experimental (a) S_0, (b) S_1, (c) E_0, (d) E_1, (e) W_0, (f) W_1, and (g) W_2 joint trajectories in the presence of $D = 0.01s$ (blue line), $D = 0.02s$ (orange line), and $D = 0.04s$ (green line) input delays without a predictor

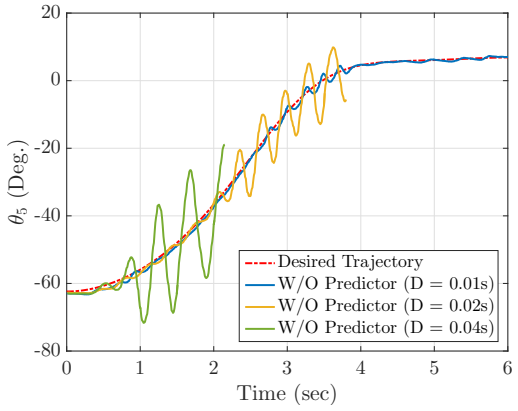

(e)

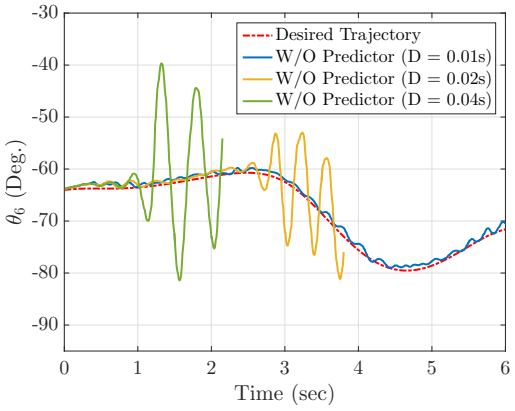

(f)

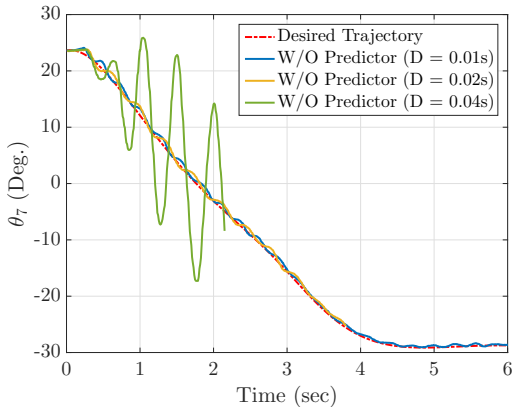

(g)

Figure 3.3: The experimental (a) S_0, (b) S_1, (c) E_0, (d) E_1, (e) W_0, (f) W_1, and (g) W_2 joint trajectories in the presence of $D = 0.01s$ (blue line), $D = 0.02s$ (orange line), and $D = 0.04s$ (green line) input delays without a predictor, continued

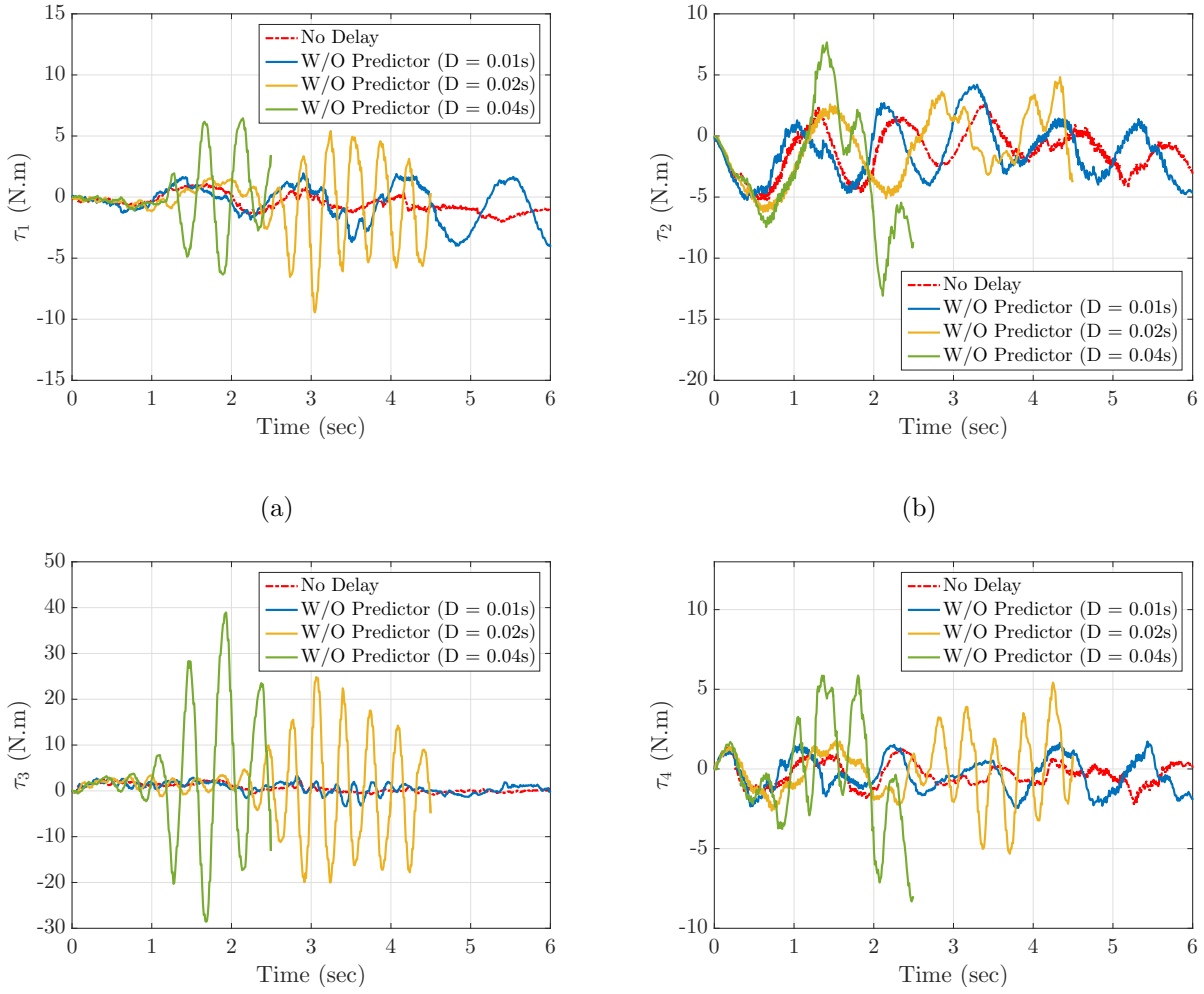

Figure 3.4: The experimental joint torques of (a) S_0, (b) S_1, (c) E_0, (d) E_1, (e) W_0, (f) W_1, and (g) W_2 in the presence of $D = 0.01s$ (blue line), $D = 0.02s$ (orange line), and $D = 0.04s$ (green line) input delays without a predictor

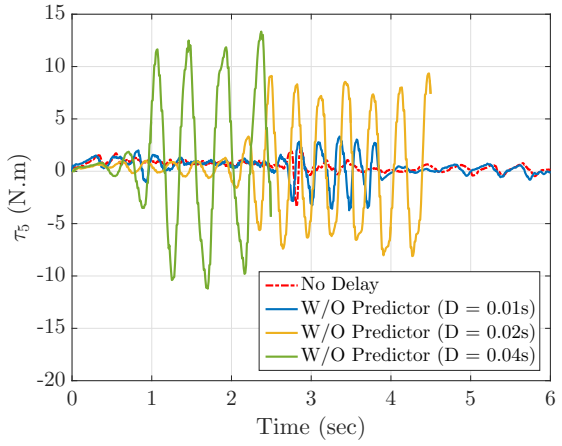

(e)

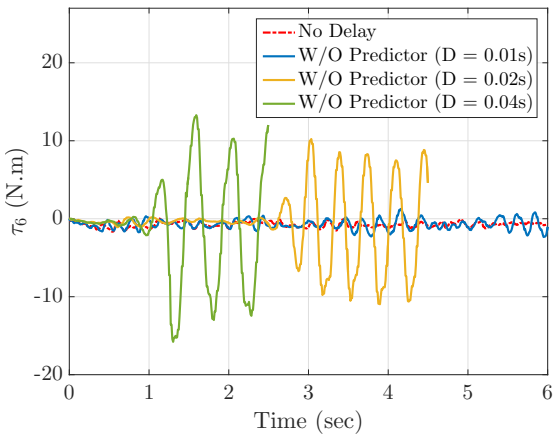

(f)

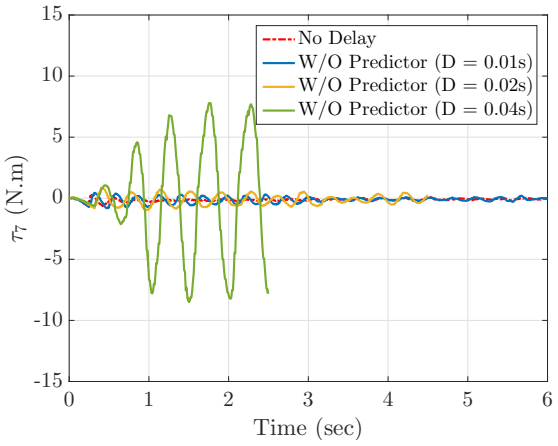

(g)

Figure 3.4: The experimental joint torques of (a) S_0, (b) S_1, (c) E_0, (d) E_1, (e) W_0, (f) W_1, and (g) W_2 in the presence of $D = 0.01s$ (blue line), $D = 0.02s$ (orange line), and $D = 0.04s$ (green line) input delays without a predictor, continued

By increasing the delay from $0.01s$ to $0.02s$, the manipulator becomes unstable and expectedly cannot follow the desired trajectories (Fig. 3.3). Note that the joint 2 (S_1) does not oscillate like the other ones because of the supporting spring mounted at this

joint (Fig. 2.1). We also examine the robot's performance in the presence of $0.04s$ input delay. The results illustrate that the manipulator harmfully oscillates and then fails to properly operate. Therefore, the robot, as expected, becomes unstable within a shorter time interval through increasing the amount of delay. It is clear that the instability of one link results in the robot failure due to the highly dynamic interconnections among the links.

It is worth mentioning that we operate the manipulator using joint torque control mode, as an advanced control scheme, which grants the access to the lowest control levels and puts much responsibility on the control algorithm. Consequently, for both $0.02s$ and $0.04s$ input delays, we could not capture more data since Baxter moves stochastically leading to the catastrophic malfunction. The AVI files of the experiments are accessible through our Dynamic Systems and Control Laboratory (DSCL) website.

In summary, as shown in Fig. 3.3, the closed-loop system becomes unstable for small input delays. Therefore, implementing the predictor-based controller is a necessity to be carried out. We hence take the advantage of the predictor-based controller, using Theorem 4, in order to globally asymptotically stabilize the manipulator due to the fact that all the assumptions are valid for the robot's arm.

Therefore, we formulate the predictor along with the controller, and then thoroughly investigate their performances in compensating the destabilizing input delays. In order to examine the effects of delay's magnitude, experiments are carried out in the presence of three different large input delays: $0.8s$, $0.9s$, and $1.0s$. Note that exposing the robot to the input delays more than $1.0s$ is not logical since the whole operational time is

6.0s.

Shown in Figs. 3.5 and 3.6 are the joint angles and torques, respectively.

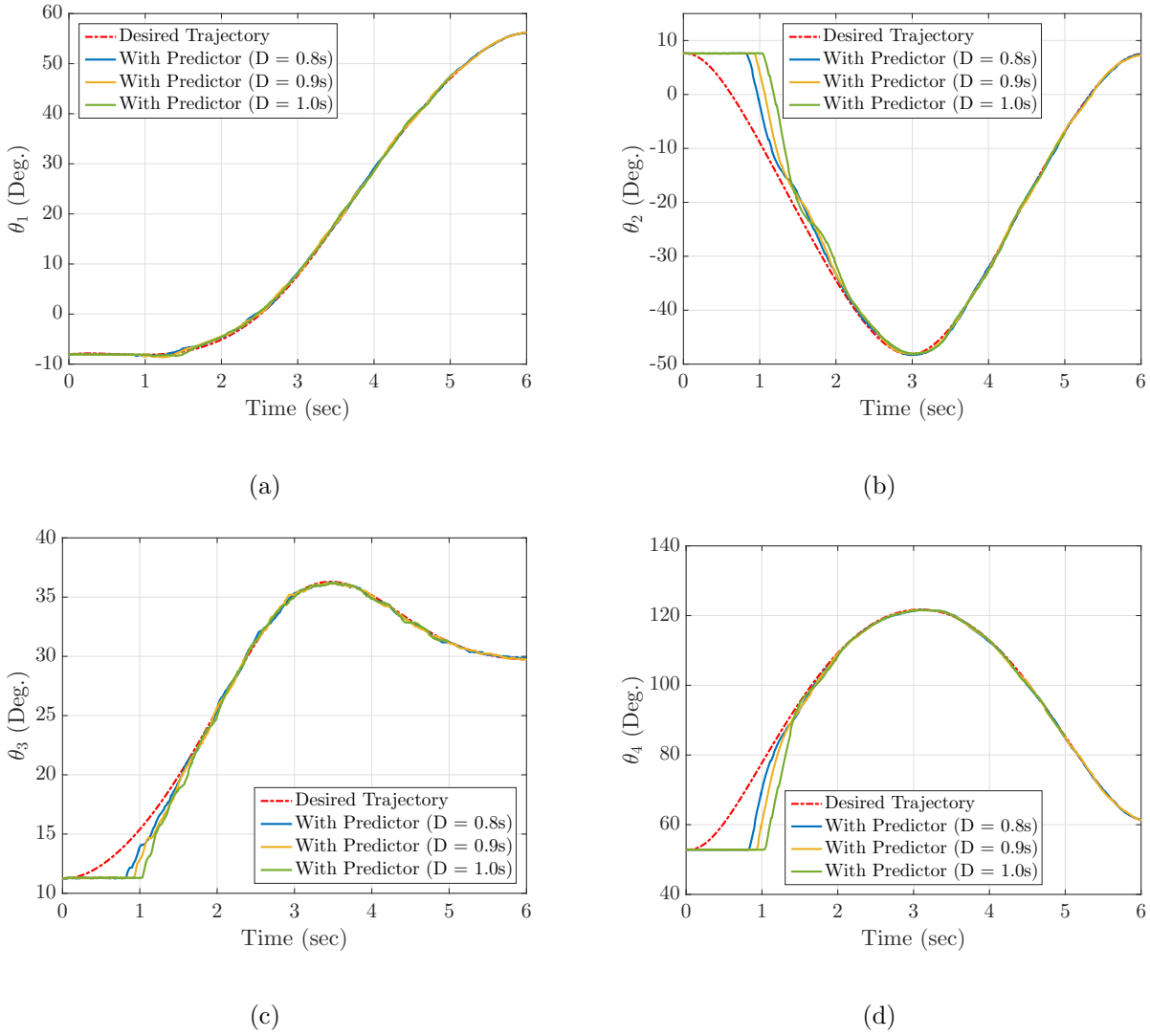

Figure 3.5: The experimental (a) S_0, (b) S_1, (c) E_0, (d) E_1, (e) W_0, (f) W_1, and (g) W_2 joint trajectories in the presence of $D = 0.8s$ (blue line), $D = 0.9s$ (orange line), and $D = 1.0s$ (green line) input delays using the predictor-based controller

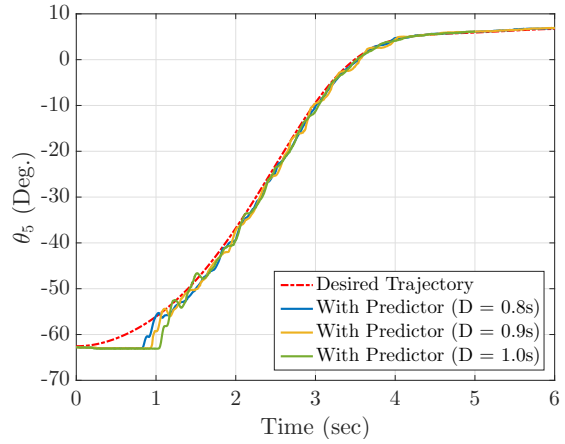

(e)

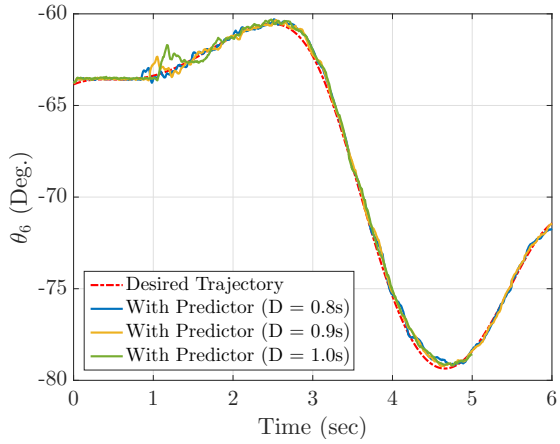

(f)

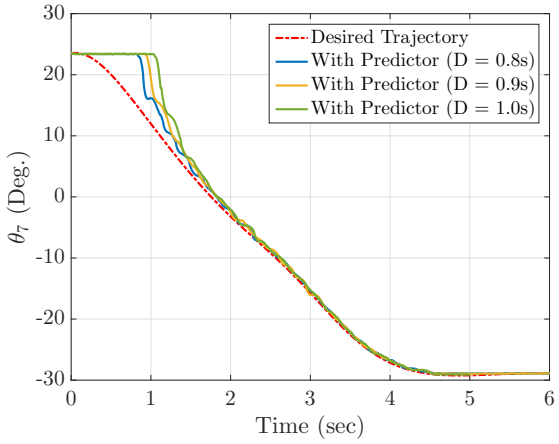

(g)

Figure 3.5: The experimental (a) S_0, (b) S_1, (c) E_0, (d) E_1, (e) W_0, (f) W_1, and (g) W_2 joint trajectories in the presence of $D = 0.8s$ (blue line), $D = 0.9s$ (orange line), and $D = 1.0s$ (green line) input delays using the predictor-based controller, continued

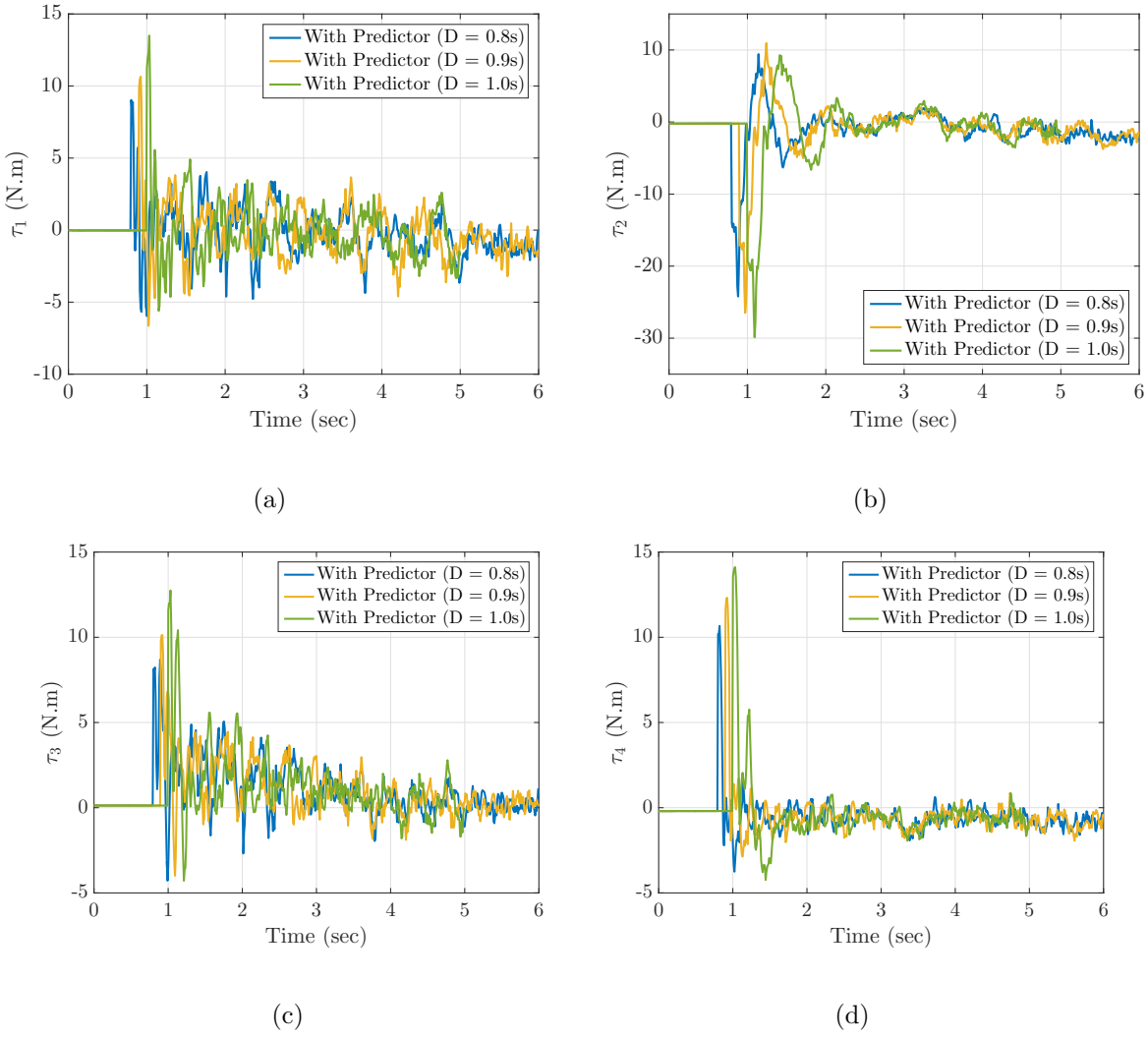

Figure 3.6: The experimental joints' torques of (a) S_0, (b) S_1, (c) E_0, (d) E_1, (e) W_0, (f) W_1, and (g) W_2 joints in the presence of $D = 0.8s$ (blue line), $D = 0.9s$ (orange line), and $D = 1.0s$ (green line) input delays using the predictor-based controller

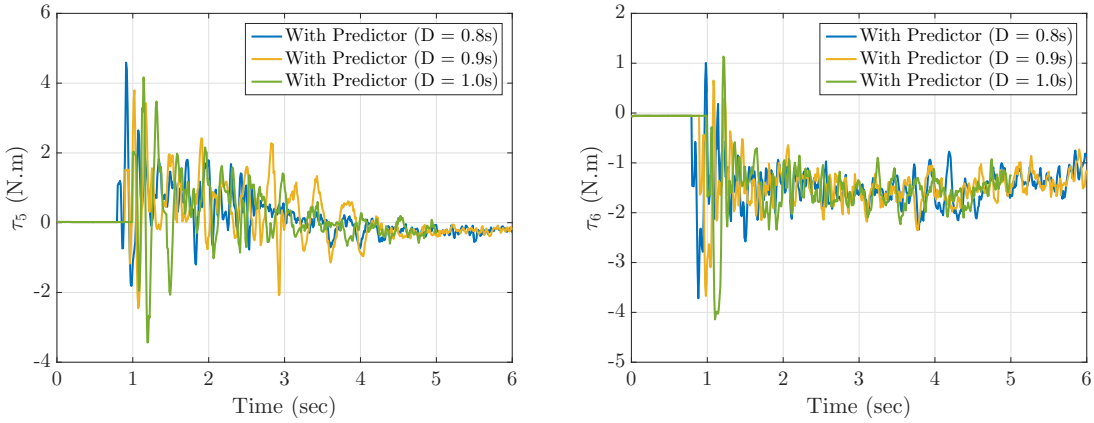

(e)

(f)

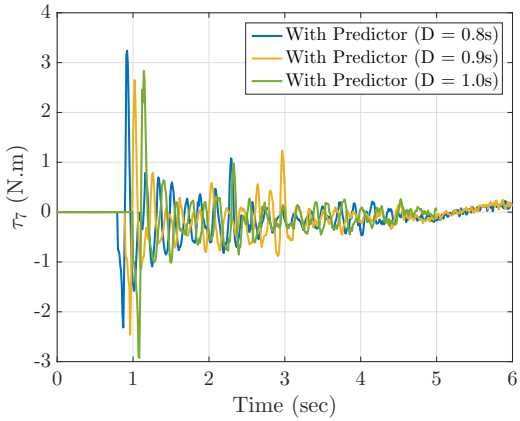

(g)

Figure 3.6: The experimental joints' torques of (a) S_0, (b) S_1, (c) E_0, (d) E_1, (e) W_0, (f) W_1, and (g) W_2 joints in the presence of $D = 0.8s$ (blue line), $D = 0.9s$ (orange line), and $D = 1.0s$ (green line) input delays using the predictor-based controller, continued

As shown in Fig. 3.6, there is no control torque before $t = D$ and consequently, the robot remains stationary (Fig. 3.5). Therefore, the errors expectedly emerge within $t \in [0, D)$, in particular for the joints 2 (S_1), 4 (E_1), and 7 (W_2) (Fig. 3.5). At $t = D$, the manipulator begins following the desired trajectories using the predictor-based controller

by applying high amounts of torques. Figs. 3.2 and 3.5 present an acceptable performance of the predictor-based controller since the tracking errors converge to zero after $4.0s$.

From another aspect, Figs. 3.5(a) and 3.5(a) reveal that the tracking errors of the joints 1 (S_0) and 6 (W_1) are not considerably high, for $0 \leq t \leq D$, despite the other ones. It is obvious that the less tracking error typically demands the less control torque to be applied with respect to the ranges of joint rotation angles. Increasing the input delay expectedly imposes higher tracking errors at the onset of the robot operation and consequently, much more control torques are needed to be applied (Fig. 3.6).

After $t = D$, the manipulator begins to perfectly track the desired trajectories using the considerable initial control torques. The control torques peak at $t = D$ and then decline by the decremental tracking errors (Fig. 3.6). As mentioned earlier, the manipulator approaches its singular configuration around $t = 3.0s$, which subsequently results in the incremental oscillation-like joint torques, in particular for the joint 5 (W_0), as shown in Fig. 3.6(a).

As shown in Fig. 3.6, comparing the control torques at $t = D$ reveals that τ_2, τ_3, and τ_4 take higher values than the other ones since the joints 2 (S_1), 3 (E_0), and 4 (E_1) are subject to more tracking errors and loads (based on the manipulator structure) with respect to the other joints.

Finally, comparing Figs. 3.4 and 3.6 implies that even an uncompensated small delay results in harmful torques and therefore, the manipulator expectedly fails to track the desired trajectories. As can be observed in Fig. 3.5, the tracking errors begin to decrease after $t = D$, due to the fact that Theorem 4 guarantees the asymptotic convergence of

the tracking errors to zero subject to any large delay. Fig. 3.7 presents the experimental tracking errors for $D = 0.8s$.

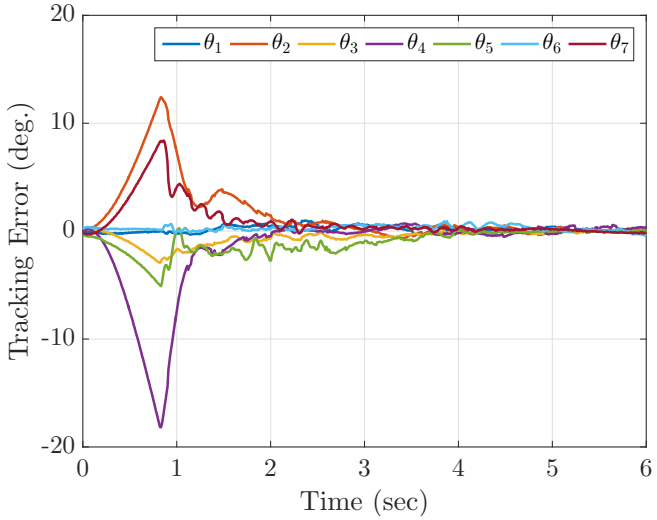

Figure 3.7: The experimental tracking errors subject to the predictor-based controller in the presence of $0.8s$ input delay

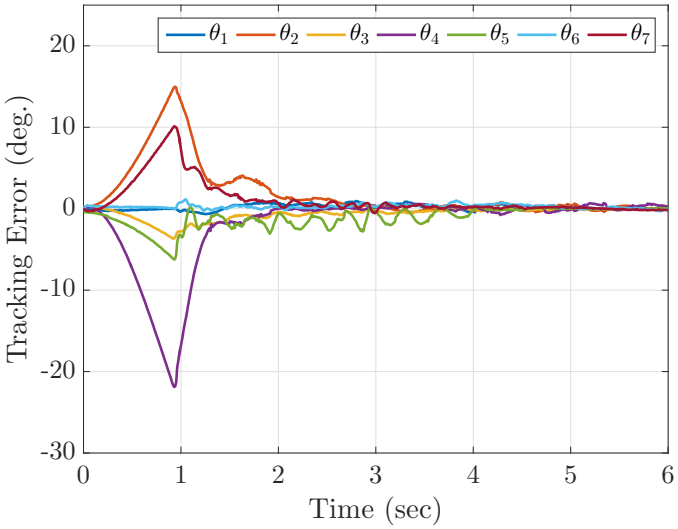

Figure 3.8: The experimental tracking errors subject to the predictor-based controller in the presence of $0.9s$ input delay

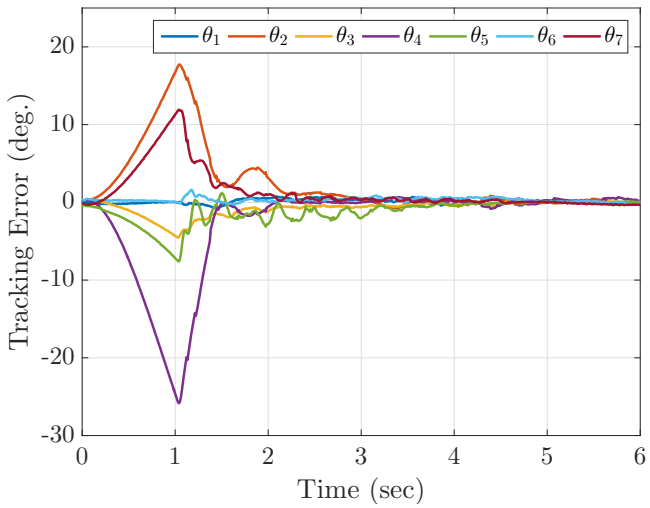

Figure 3.9: The experimental tracking errors subject to the predictor-based controller in the presence of $1.0s$ input delay

The negligible experimental tracking errors mainly root on the inaccuracy of sensors and actuators. We experimentally verified the model in a back-and-forth procedure [7,9,10] and there is an acceptable correlation between our model and Baxter's dynamics.

Moreover, unmodeled dynamics, such as friction in joints or external disturbances, may result in the prediction offset from the actual path, which we carefully considered through designing the controller. The algorithm measures the robot's joint angles at each iteration and hence making predictions begins from that measurement – the state $E(t)$ in Eq. (3.8) is measured in each iteration. Providing this measurement to the predictor endows robustness against small uncertainties and avoids any cumulative error caused by uncertainties or unmodeled dynamics.

Additionally, we established that the closed-loop system is ISS, which in turn provides the control robustness against any bounded disturbance. Based on the data provided

by Baxter's manufacturer, the series elastic actuators act as filters helping to reduce both the friction and backlash through low-cost gearbox. Therefore, as can be seen in Fig. 3.7, the tracking errors asymptomatically converge to zero. Also, Fig. 3.10 presents the simulation results for $D = 0.8s$ revealing that the tracking errors asymptomatically converge to zero, as expected.

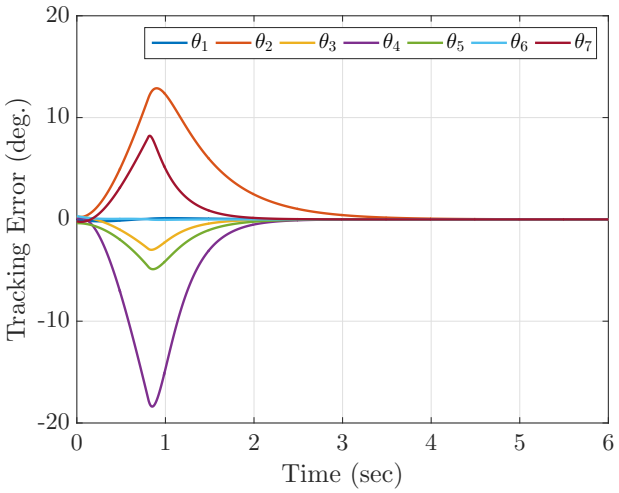

Figure 3.10: The simulated tracking errors subject to the predictor-based controller in the presence of $0.8s$ input delay

3.4 Conclusions

Throughout this chapter, we designed a predictor-based controller for a general highly interconnected nonlinear system subject to the time-invariant input delay. We investigated the destabilizing effects of three different input delays shown in Figs. 3.3 and 3.4, and then the controller was implemented for the 7-DOF Baxter manipulator as a case study. Simulation and experimental results demonstrate that the predictor-based

controller effectively compensates input delays and achieves closed-loop stability.

Toward designing the controller, we established the forward completeness of the open-loop system and Input-to-State Stability (ISS) properties of the closed-loop system. We then formulated the predictor-based controller to asymptotically stabilize the system employing Theorem 4, and then investigated the effects of large input delays on the control of the Baxter robot.

The experimental results revealed that the predictor-based controller, in the presence of large input delays, makes the robot asymptomatically stable, and the robot tracks the desired joint trajectories, as expected. We also established that the tracking errors, subject to the predictor-based controller, asymptotically converge to zero. The negligible amounts of the tracking errors, shown in Fig. 3.7, mainly root on the inaccuracy of sensors and actuators. The simulation results also presented the asymptotic convergence of the tracking errors to zero guaranteed through Theorem 4, as shown in Fig. 3.10. The principal results of this research work can be summarized as follows:

- ✓ The minimum input delay destabilizes the robot.
- ✓ Using Theorem 4, the stability of the system for any large input delay is guaranteed.
- ✓ The predictor-based controller analytically and experimentally compensates the input delay and achieves the closed-loop asymptotic stability.

It is worth mentioning that although our controller is robust against a time-invariant delay and small uncertainties, time-varying input delays and enormous uncertainties may affect the control performance; this problem has not yet been addressed. Therefore, we,

for future steps, will focus on designing a nonlinear adaptive time-delay control scheme with application to high-DOF robotic manipulators.

3.5 Notes and References

In this chapter, a predictor-based controller was formulated for a high-DOF robot manipulator in the presence of input delay. The effects of delay and also the robustness of the proposed controller were theoretically and experimentally investigated. One possible future work would be analyzing output delay along with input delay. Output delay can be caused by delay in sensors and can play a significant role in the control of the system.

Chapter 3 contains reprints or adaptions of the following papers: 1) M. Bagheri, P. Naseradinmousavi, and M. Krstić, "Feedback Linearization Based Predictor for Time Delay Control of a High-DOF Robot Manipulator," *Automatica*, Vol. 108, Oct. 2019; 2) M. Bagheri, P. Naseradinmousavi, and M. Krstić, "Time Delay Control of a High-DOF Robot Manipulator Through Feedback Linearization Based Predictor," *ASME Dynamic Systems and Control Conference (DSCC 2019)*, Paper No. DSCC2019-8915, Oct. 8 - 11, Park City, UT, USA, 2019; 3) M. Bagheri, M. Krstić, and P. Naseradinmousavi, "Analytical and Experimental Predictor-Based Time Delay Control of Baxter Robot," *ASME Dynamic Systems and Control Conference (DSCC 2018)*, Paper No. DSCC2018-9101, Sept. 30 - Oct. 3, Atlanta, GA, USA, 2018. The dissertation author is the primary investigator and author of these papers, and would like to thank Miroslav Krstic and Peiman Naseradinmousavi for their contributions.

Chapter 4

Adaptive Control Using Batch Least-Squares Identifier

In this chapter, we design a trigger-based adaptive controller for robot manipulators to efficiently estimate unknown parameters and to achieve asymptotic stability in the presence of coupled uncertainties. Robot manipulators are widely used in telemanipulation systems where they are subject to model and environmental uncertainties. Using conventional control algorithms on such systems can cause not only poor control performance, but also expensive computational costs and catastrophic instabilities.

Therefore, system uncertainties need to be estimated through designing a computationally efficient adaptive control law. We focus on robot manipulators as an example of a highly nonlinear system. As a case study, a 2-DOF manipulator subject to four parametric uncertainties is investigated. First, the dynamic equations of the manipulator are derived and the corresponding regressor matrix is constructed for the unknown parameters. For

a general nonlinear system, a theorem is presented to guarantee the asymptotic stability of the system and the convergence of parameters' estimations. Finally, simulation results are discussed for a two-link manipulator and the performance of the proposed scheme is thoroughly evaluated.

4.1 Background

Remote manipulators are widely used in various applications to track desired trajectories on the account of their reliable, fast, and precise motions in executing tasks such as moving debris and turning valves [6, 25], while, as expected, consuming a significant amount of lumped energy [8]. Remote manipulators provide the capability of executing tasks safely and autonomously at dangerous or unreachable locations. However, they inevitably operate within different environments subject to numerous uncertainties or large time delays [7, 11, 12]. These uncertainties include the length, mass, and inertia of the links, as well as the manipulator payloads, are some of the mentioned uncertainties. The detrimental impact of uncertainties is well-established, which plays the most significant role in degrading remote perception, manipulation, and destabilizing systems. Adaptive control is an effective approach to control these highly nonlinear systems under parametric uncertainties.

Considerable research efforts have been devoted to the adaptive control of linear and nonlinear finite-dimensional systems, see [63,70,97]. Adaptive controllers are designed to compensate for the detrimental effects of system uncertainties in addition to enabling

the system to follow the desired trajectory [56,82,83]. Developing adaptive control schemes for robots has received much attention in the last three decades [24, 30, 94, 102]. Using the algorithm formulated by Slotine and Li [95], Spong [101] presented the adaptive control results for flexible joint robot manipulators under the assumption of weak joint elasticity, while adaptive motion control for rigid robots was studied by Ortega and Spong in [84].

The adaptive control scheme derived in [103] requires the joints' accelerations for its implementation, through estimating the acceleration from the measured velocity, which inevitably needs sufficient encoder resolution and fast sampling. Slotine and Li [96] presented a combinatorial adaptive controller for robot manipulators, whose parameter adaptation is driven by both tracking and prediction errors. These very sophisticated schemes need the calculation of many complicated analytical expressions at each iteration leading to a considerable computational time.

The event-triggered approach has been utilized to deal with various control problems [49, 60]. Note that the closed-loop system subject to an event-triggered controller is a hybrid dynamical system. The most important advantage of the event-triggered direct adaptive control scheme [60], unlike other approaches (gradient, Lyapunov, etc.), is that it does not depend on the persistence of excitation condition to guarantee the convergence of parameter estimation. Through the proposed scheme, a novel regulation-triggered identifier is formulated allowing us to use certainty-equivalence controllers without slowing adaptation. The following main ideas are implemented into the proposed control design: 1) Utilizing piecewise-constant parameter estimates between the event-based triggers. This idea omits the crucial issue of disturbing effect of rapidly changing estimates [53, 91] and

2) The parameter estimation is regulated by error, but there is no error-based estimation leading to the parameter updating rate.

The rest of the chapter is organized as follows. We derive the model of a Euler-Lagrangian system (e.g a robot manipulator) to employ the adaptive certainty-equivalence control law using the Batch Least-Square Identifier (BaLSI). Then, we reveal that the closed-loop system is globally asymptotically stable subject to all necessary assumptions. Finally, as a benchmark, we utilize the proposed method for a two-link robot in the presence of four uncertainties, to reveal the performance and significance of the proposed scheme.

4.2 Designing BaLSI Adaptive Control Law

In this section, we formulate the adaptive control law to efficiently estimate unknown parameters along with guaranteeing perfect tracking. We design a certainty-equivalence controller combined with Batch Least-Squares Identifier to have a certainty-equivalence adaptive controller along with the event-triggered identifier.

Therefore, we need to derive the dynamic equations of the system including some parametric uncertainties, and then design the controller to stabilize the error dynamics making the origin asymptotically stable. The system (2.5) can be rewritten as follows,

$$\dot{x} = F(t, x, u) \tag{4.1}$$

where, $x = [q_1, \cdots, q_n, \dot{q}_1, \cdots, \dot{q}_n]^{\mathrm{T}} \in \mathbb{R}^{2n}$ is the vector of states, q_i and $\dot{q}_i$ are angle and angular velocity of the joints, respectively, and $u = \tau \in \mathbb{R}^n$.

Consider the general from of (4.1) where $x \in \mathbb{R}^n$ and $u \in \mathbb{R}^m$. In the case of having

parametric uncertainties in the system, (4.1) can be written in the general form of

$$\dot{x} = f(t, x, u) + g(t, x, u)\theta \tag{4.2}$$

where, both the $f : \mathbb{R}_{\geq 0} \times \mathbb{R}^{2n} \times \mathbb{R}^n \to \mathbb{R}^{2n}$ and the regressor matrix $g : \mathbb{R}_{\geq 0} \times \mathbb{R}^{2n} \times \mathbb{R}^n \to \mathbb{R}^{2n} \times \mathbb{R}^p$ are smooth mappings with $f(t, 0, 0) = 0$, $g(t, 0, 0) = 0$ hold for all $t \geq 0$ and $\theta \in \Theta \subset \mathbb{R}^p$ is a vector of unknown constant parameters: p is the number of unknown parameters taking values in a closed convex set Θ.

4.2.1 Designing Certainty-Equivalence Controller

We assume that there exists a smooth mapping $\kappa : \mathbb{R}_{\geq 0} \times \Theta \times \mathbb{R}^n \to \mathbb{R}^m$ with $\kappa(t, \theta, 0) = 0$ holds for all $t \geq 0$ and $\theta \in \Theta$ for which the following stabilizability and "uniform" coercivity property assumptions hold for $V(\theta, .) \in C^1(\mathbb{R}^n; \mathbb{R}_{\geq 0})$, a class of positive definite, radially unbounded, and continuously differentiable functions on compact sets of Θ.

Assumption 4. *For each $\theta \in \Theta$, the origin is uniformly globally asymptotically stable for the closed-loop system,*

$$\dot{x} = f(t, x, \kappa(t, \theta, x)) + g(t, x, \kappa(t, \theta, x))\,\theta \tag{4.3}$$

More specifically, the following inequality holds for all $\theta \in \Theta$, $x \in \mathbb{R}^n$, and $t \geq 0$,

$$\nabla V(x)\Big(f(t, x, \kappa(t, \theta, x)) + g(t, x, \kappa(t, \theta, x))\theta\Big) \leq -2\sigma V(\theta, x) \tag{4.4}$$

where $\sigma > 0$ is a constant.

Assumption 4 is a common stabilizability assumption, which is necessary for all possible adaptive control design approaches. Note that knowing the functions $\kappa : \mathbb{R}_{\geq 0} \times \Theta \times \mathbb{R}^n \to \mathbb{R}^m$ and $V : \Theta \times \mathbb{R}^n \to \mathbb{R}$ is not a demanding requirement, since for the design of a globally stabilizing controller, a control Lyapunov function is typically utilized.

Assumption 5. *For every non-empty and compact set $\bar{\Theta} \subset \Theta$, the following property holds: "for every $M \geq 0$ there exists $R > 0$ such that the implication $V(\theta, x) \leq M,\ \theta \in \bar{\Theta} \to |x| < R$ holds".*

Assumption 5 reveals the "uniform" coercivity property for $V(\theta, .)$ on compact sets $\Theta \subset \mathbb{R}^p$, which holds for functions in the following form,

$$\begin{aligned} V(\theta, x) =& a_1(\theta, x) x_1^2 \\ &+ \sum_{i=2}^{n} a_i(\theta, x) \left(x_i - \phi_{i-1}\left(\theta, x_1, \cdots, x_{i-1}\right)\right)^2 \end{aligned} \tag{4.5}$$

where a_i $(i = 1, \cdots, n)$ are positive continuous functions and $\phi_i : \Theta \times \mathbb{R}^i \to \mathbb{R}$ are continuous functions with $\phi_i(\theta, 0) = 0$ for all $\theta \in \Theta$ and $i = 1, \cdots, n$.

Let $t_0 \geq 0$ be the initial time and $x(t_0) = x_0$ be the given initial condition. Note that the parameter estimation $\hat{\theta} \in \mathbb{R}^p$ is kept constant within the interval between two consecutive events. Consequently, we have the following feedback control law and regulation-triggered parameter update law for $i \in \mathbb{Z}_{\geq 0}$,

$$u(t) = \kappa(t, \hat{\theta}(\tau_i), x(t)) \qquad t \in [\tau_i, \tau_{i+1}) \tag{4.6}$$

$$\hat{\theta}(t) = \hat{\theta}(\tau_i) \qquad t \in [\tau_i, \tau_{i+1}) \tag{4.7}$$

where $\tau_i \geq 0$ is the time of i^{th} event, when the following equations satisfy for $T > 0$ and $r_i > \tau_i$,

$$\tau_{i+1} = \min(\tau_i + T,\ r_i) \quad \text{for } i \in \mathbb{Z}_{\geq 0} \tag{4.8}$$

$$\tau_0 = t_0 \tag{4.9}$$

It is worth mentioning that $r_i > \tau_i$ is a time instant determined by the event-trigger, as the smallest value of time $t > \tau_i$, for which

$$V\left(\hat{\theta}(\tau_i), x(t)\right) = V\left(\hat{\theta}(\tau_i), x(\tau_i)\right) + a\left(x(\tau_i)\right) \tag{4.10}$$

where $a : \mathbb{R}^n \to \mathbb{R}_{\geq 0}$ is a continuous positive-definite function (another tunable parameter in the proposed scheme) and $x(t)$ denotes the solution of (4.2) with the certainty-equivalence controller $u(t) = \kappa\left(t, \hat{\theta}(\tau_i), x(t)\right)$. Note that defining r_i prevents states and consequently $V(\theta, .)$ from becoming too large. Therefore, the distance of time $\tau_i - \tau_{i+1}$ will be less than T if the state increases too fast.

4.2.2 Batch Least-Squares Identifier (BaLSI)

Along with designing the controller, in order to estimate the unknown vector $\theta \in \Theta$, we formulate the Batch Least-Squares Identifier (BaLSI). Based on Eq. (4.2), we notice that, for every $s, t \geq t_0$, the following equation holds:

$$\begin{aligned} x(t) - x(s) = &\int_s^t f(r, x(r), u(r))\ dr \\ &+ \left(\int_s^t g(r, x(r), u(r))\ dr\right)\theta \end{aligned} \tag{4.11}$$

Considering,

$$p(t,s) = x(t) - x(s) - \int_s^t f(r, x(r), u(r))\ dr \tag{4.12}$$

$$q(t,s) = \int_s^t g(r, x(r), u(r))\ dr \tag{4.13}$$

leads to $p(t,s) = q(t,s)\theta$ for every $s, t \geq t_0$. We define $h_i : \mathbb{R}^p \to \mathbb{R}^+$ as follows,

$$h_i(\vartheta) = \int_{t_0}^{\tau_{i+1}} \int_{t_0}^{\tau_{i+1}} |p(t,s) - q(t,s)\vartheta|^2\ ds\ dt \tag{4.14}$$

The function $h_i(\vartheta)$ has a global minimum at $\vartheta = \theta$ with $h_i(\theta) = 0$. Consequently, we get, from the Fermat's theorem for extrema, that the following equation holds:

$$Z(\tau_{i+1}) = G(\tau_{i+1})\theta \tag{4.15}$$

where

$$Z(\tau_i) = \int_{t_0}^{\tau_i} \int_{t_0}^{\tau_i} q^{\mathrm{T}}(t,s)p(t,s)\ ds\ dt \tag{4.16}$$

$$G(\tau_i) = \int_{t_0}^{\tau_i} \int_{t_0}^{\tau_i} q^{\mathrm{T}}(t,s)q(t,s)\ ds\ dt \tag{4.17}$$

Note that $G(\tau_i) \in \mathbb{R}^{p \times p}$ is a symmetric and positive semidefinite matrix, and it is invertible providing $\det(G(\tau_{i+1})) \neq 0$. Therefore, in the case of a positive definite $G(\tau_{i+1})$ $(\det(G(\tau_{i+1}) > 0)$, the vector of unknown parameters can be calculated as

$$\theta = (G(\tau_{i+1}))^{-1} Z(\tau_{i+1}) \tag{4.18}$$

However, $G(\tau_{i+1})$ is not necessarily positive definite and Eq. (4.18) is not always held. Therefore, the following convex optimization problem with linear equality constraints

has a unique solution,

$$\min_{\vartheta \in \Theta} \left| \vartheta - \hat{\theta}(\tau_i) \right|^2$$
$$\text{Subject to : } \; Z(\tau_{i+1}) = G(\tau_{i+1})\vartheta \tag{4.19}$$

Finally, the following parameter update law, the *batch least-increment least-squares parameter update law*, can be defined as:

$$\hat{\theta}(\tau_{i+1}) = \underset{\vartheta}{\operatorname{argmin}} \left\{ \left| \vartheta - \hat{\theta}(\tau_i) \right|^2 : \vartheta \in \Theta, \right.$$
$$\left. Z(\tau_{i+1}) = G(\tau_{i+1})\vartheta \right\} \tag{4.20}$$

The parameter update law (4.20) is the key difference of the proposed adaptive control scheme, however, in practice, it is better to avoid the implementation of (4.20) because of potential modeling and measurement errors. Therefore, there is no guarantee that the following set is non-empty.

$$\left\{ \vartheta \in \Theta : Z(\tau_{i+1}) = G(\tau_{i+1})\vartheta \right\} \tag{4.21}$$

Consequently, we may need to relax the minimization problem (4.20) as follows,

$$\hat{\theta}(\tau_{i+1}) = \underset{\vartheta}{\operatorname{argmin}} \left\{ \left| \vartheta - \hat{\theta}(\tau_i) \right|^2 \right.$$
$$\left. + \gamma \left| Z(\tau_{i+1}) - G(\tau_{i+1})\vartheta \right|^2 : \vartheta \in \Theta \right\} \tag{4.22}$$

We consider the plant (4.2) with the controller (4.6) - (4.9) and the parameter estimator (4.22). The main result guarantees global convergence of all states of error system to zero.

The following theorem is a direct extension of Theorem 4.1 in [57] and its proof is omitted

Theorem 7. *Consider the following control system under Assumptions 4 and 5,*

$$\dot{x} = f(t, x, \kappa(t, \theta, x)) + g(t, x, \kappa(t, \theta, x))\theta \tag{4.23}$$

Let $T \geq 0$ be a positive constant and $a : \mathbb{R}^n \to \mathbb{R}_{\geq 0}$ be a continuous positive definite function. Then there exists a mapping $\omega_{\theta,\hat{\theta}} \in \mathcal{KL}$ parameterized by $\theta, \hat{\theta} \in \Theta$ such that for every $t_0 \geq 0$, $\theta, \hat{\theta} \in \Theta$, and $x(t_0) = x_0 \in \mathbb{R}^n$, the solution of the closed-loop system is defined for all $t \geq t_0$ and satisfies,

$$|x(t)| \leq \omega_{\theta,\hat{\theta}_0}(|x_0|, t - t_0) \tag{4.24}$$

Moreover, there exist $\tau \geq 0$ and $\theta_s \in \Theta$ (both depending on $\theta, \hat{\theta}_0$, t_0, and x_0) such that $\hat{\theta}(t) = \theta_s$ for all $t \geq t_0 + \tau$ and the following equation holds for all $t \geq t_0$

$$g(t, x(t), u(t))(\theta - \theta_s) = 0 \tag{4.25}$$

Note that Theorem 7 guarantees that there is a finite settling time $\tau \geq 0$ for the parameter estimate. Also the proof of Theorem 4.1 in [57] shows that at most p switchings of the value of the parameter estimate $\hat{\theta}(t)$ can occur. It is important to notice that *no assumption for persistency of excitation* is made in Theorem 7.

4.2.3 Error System Development

The control objective includes converging joint position and velocity errors to zero implying the generalized coordinates track the desired time-varying joint trajectories,

$q_{\text{des}}(t) \in \mathbb{R}^n$. A state-space model for the tracking error is formulated based on the following equations,

$$e_1 = q - q_{\text{des}} \tag{4.26}$$

$$e_2 = \dot{q} - \dot{q}_{\text{des}} \tag{4.27}$$

where the following assumption is held for the desired joint trajectories.

Assumption 6. *The desired joint trajectories* $q_{\text{des}}(t) \in \mathbb{R}^7$ *and their derivatives* $\dot{q}_{\text{des}}(t)$, $\ddot{q}_{\text{des}}(t) \in \mathbb{R}^7$ *exist and are bounded for all* $t \geq t_0$.

Then a controller is formulated to improve tracking performance indices, converging errors to zero, subject to the assumption of knowing the system's dynamics, as mentioned earlier.

A state-space model, based on the tracking error, is formulated through premultiplying the inertia matrix by the time derivative of Eq. (4.27) while Eq. (2.5) is substituted,

$$\begin{aligned} &M(q)\dot{e}_2 + C(q,\dot{q})e_2 + M(q)\ddot{q}_{\text{des}} \\ &\qquad + C(q,\dot{q})\dot{q}_{\text{des}} + G(q) = \tau \end{aligned} \tag{4.28}$$

which yields,

$$\dot{e}_1 = e_2 \tag{4.29}$$

$$\dot{e}_2 = -\ddot{q}_{\text{des}} - M^{-1}(C\dot{q}_{\text{des}} + G + Ce_2) + M^{-1}\tau \tag{4.30}$$

Therefore, the state-space model of error dynamics becomes,

$$\dot{E} = \begin{bmatrix} e_2 \\ -\ddot{q}_{\text{des}} - M^{-1}(C\dot{q}_{\text{des}} + G + Ce_2) + M(q)^{-1}\tau \end{bmatrix} \tag{4.31}$$

where $E = [e_1^{\mathrm{T}} \;\; e_2^{\mathrm{T}}]^{\mathrm{T}} \in \mathbb{R}^{14}$ is the vector of error states.

As mentioned in Theorem 7, the nominal controller $\kappa(t, E)$ should asymptotically stabilize the closed-loop system, and the uniform coercivity property for Control Lyapunov Function (CLF) should be established. Since the dynamics of system (2.5) is known, the controller is formulated based on Eq. (4.30). In order to design a nominal controller (κ) to asymptotically stabilize the systems around the origin, we employ the backstepping approach. We implement $e_2 = \phi(e_1) = -\alpha e_1$ which is asymptotically stabilizing (4.29) since

$$V_1(e_1) = \frac{1}{2} e_1^{\mathrm{T}} e_1 \rightarrow \dot{V}_1(e_1) = -e_1^{\mathrm{T}} \alpha e_1 \tag{4.32}$$

where $\alpha \in \mathbb{R}^{n \times n}$ is a constant positive definite matrix. Now, we define a new variable $z = e_2 - \phi = e_2 + \alpha\, e_1$. Therefore, the error dynamics is rewritten based on e_1 and z as follows,

$$\dot{e}_1 = -\alpha e_1 + z \tag{4.33}$$

$$\dot{z} = \alpha(z - \alpha e_1) - h + M(q)^{-1}\tau \tag{4.34}$$

where

$$h(q,\dot{q}) = \ddot{q}_{des} + M(q)^{-1}\Big(C(q,\dot{q})\dot{q}_{des} + G(q) + C(q,\dot{q})(z - \alpha e_1)\Big) \tag{4.35}$$

The Lyapunov function candidate for new system is

$$V(e_1, z) = \frac{1}{2}e_1^{\mathrm{T}}e_1 + \frac{1}{2}z^{\mathrm{T}}z \tag{4.36}$$

and the derivative of new CLF is

$$\begin{aligned}\dot{V} =& e_1^{\mathrm{T}}(-\alpha e_1 + z) + z^{\mathrm{T}}\left(\alpha(z - \alpha e_1) - h + M(q)^{-1}\tau\right) \\ =& -e_1^{\mathrm{T}}\alpha e_1 + e_1^{\mathrm{T}}z \\ &+ z^{\mathrm{T}}\big(\alpha(z - \alpha e_1) - h(q,\dot{q}) + M(q)^{-1}\tau\big)\end{aligned} \tag{4.37}$$

The derivative of Lyapunov function would be negative definite for $E \in \mathbb{R}^n - \{0\}$ with the following input for the system,

$$\tau = M(q)(h(q,\dot{q}) - e_1 - \beta z - \alpha(z - \alpha e_1)) \tag{4.38}$$

$$\rightarrow \dot{V} = -e_1^{\mathrm{T}}\alpha e_1 - z^{\mathrm{T}}\beta z \tag{4.39}$$

where $\beta \in \mathbb{R}^{n\times n}$ is a constant positive definite matrix. Therefore, the following feedback law asymptotically stabilizes the system,

$$\tau = M(q)\big(h(q,\dot{q}) - (I_{n\times n} + \alpha\beta)\, e_1 - (\alpha + \beta)e_2\big) \tag{4.40}$$

Hence, the certainty-equivalence controller u is

$$u(t) = M(q, \hat{\theta}) \Big(h(q, \dot{q}, \hat{\theta}) - (I_{n\times n} + \alpha\beta)\, e_1 - (\alpha + \beta) e_2 \Big) \tag{4.41}$$

It is worth mentioning that finding regressor matrix $g(t, x, u)$ in Eq. (4.2) is analytically and computationally cumbersome. Therefore, we implement the proposed approach for the adaptive control of a two-link robot.

4.3 Simulation Results

We study a two-link manipulator with the following mass, Coriolis, and gravitational matrices,

$$M(q) = \begin{bmatrix} M_{11}(q) & M_{12}(q) \\ \\ M_{12}(q) & M_{22} \end{bmatrix} \tag{4.42}$$

$$C(q, \dot{q}) = \begin{bmatrix} -\dot{q}_2 C_h(q) & -(\dot{q}_1 + \dot{q}_2) C_h(q) \\ \\ \dot{q}_1 C_h(q) & 0 \end{bmatrix} \tag{4.43}$$

$$G(q) = \begin{bmatrix} -(m_1 l_{c1} + m_e l_1) g \cos(q_1) - m_e g l_{ce} \cos(q_1 + q_2) \\ \\ -m_e g l_{ce} \cos(q_1 + q_2) \end{bmatrix} \tag{4.44}$$

where,

$$M_{11}(q) = a_1 + 2a_3\cos(q_2) + 2a_4\sin(q_2)$$

$$M_{12}(q) = a_2 + a_3\cos(q_2) + a_4\sin(q_2)$$

$$M_{22} = a_2$$

$$C_h(q) = a_3\sin(q_2) - a_4\cos(q_2)$$

$$a_1 = I_1 + m_1 l_{c1}^2 + I_e + m_e l_{ce}^2 + m_e l_1^2,$$

$$a_2 = I_e + m_e l_{ce}^2$$

$$a_3 = m_e l_1 l_{ce}\cos(\delta_e), \qquad a_4 = m_e l_1 l_{ce}\sin(\delta_e)$$

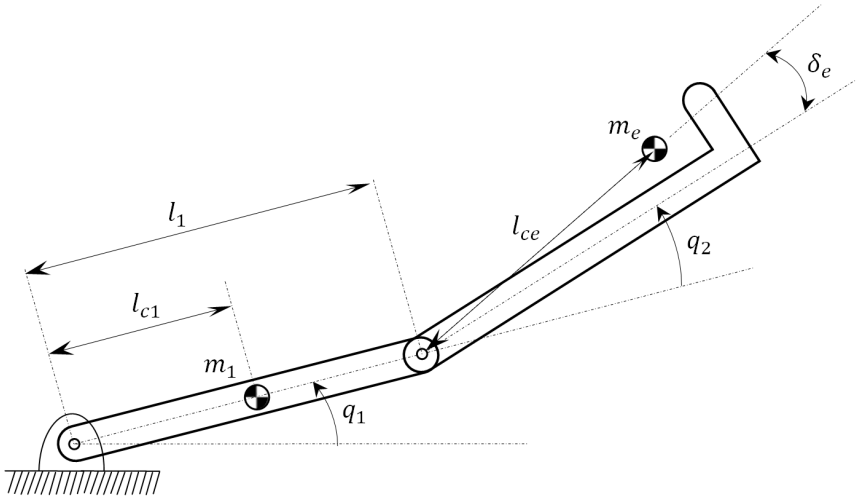

Figure 4.1: A two-link manipulator

Therefore,

$$M(q)^{-1} = \frac{1}{\text{den}} \begin{bmatrix} -a_2 & a_5 + a_2 \\ a_5 + a_2 & -2a_5 - a_1 \end{bmatrix}$$

where,

$$\text{den} = a_5^2 - a_1 a_2 + a_2^2$$

$$a_5 = a_3 \cos(q_2) + a_4 \sin(q_2)$$

and

$$M(q)^{-1} C(q, \dot{q}) = \frac{1}{\text{den}} \begin{bmatrix} -a_6(a_5 \dot{q}_1 + a_2 (\dot{q}_1 + \dot{q}_2)) & -a_2 a_6 (\dot{q}_1 + \dot{q}_2) \\ a_6 (a_5(2\dot{q}_1 + \dot{q}_2) + (a_1 \dot{q}_1 + a_2 \dot{q}_2)) & a_6(a_5 + a_2)(\dot{q}_1 + \dot{q}_2) \end{bmatrix} \tag{4.45}$$

where

$$a_6 = a_4 \cos(q_2) - a_3 \sin(q_2) \tag{4.46}$$

Finally, by having four unknown parameters (a_1, a_2, $a_3^2 - a_4^2$, and $a_3 a_4$), Eq. (4.2) can be rewritten as follows,

$$\dot{x} = f(t, x, u) + g(t, x, u)\, \theta, \qquad x = [e_1, e_2, \dot{e}_1, \dot{e}_2]^T \in \mathbb{R}^4,\ u = \tau \in \mathbb{R}^2,\ \theta \in \mathbb{R}^4 \tag{4.47}$$

$$f(t, x, u) = \begin{bmatrix} e_2 \\ \begin{bmatrix} \frac{\tau_2 a_5}{\text{den}} \\ \frac{(\tau_1 - 2\tau_2) a_5}{\text{den}} \end{bmatrix} - \ddot{q}_{\text{des}}(t) \end{bmatrix} \tag{4.48}$$

$$g(t,x,u) = \begin{bmatrix} & & 0_{2\times 4} & \\ 0 & \frac{\tau_2-\tau_1+a_6(\dot{q}_1+\dot{q}_2)^2}{\text{den}} & \frac{-\dot{q}_1^2\sin(2q_2)}{2\text{den}} & \frac{\dot{q}_1^2\cos(2q_2)}{\text{den}} \\ -\frac{\tau_2+a_6\dot{q}_1^2}{\text{den}} & \frac{\tau_1-a_6\dot{q}_2(\dot{q}_2+2\dot{q}_1)}{\text{den}} & \frac{\sin(2q_2)\left((\dot{q}_1+\dot{q}_2)^2+\dot{q}_1^2\right)}{2\text{den}} & -\frac{\cos(2q_2)\left((\dot{q}_1+\dot{q}_2)^2+\dot{q}_1^2\right)}{\text{den}} \end{bmatrix} \tag{4.49}$$

$$\theta = \begin{bmatrix} a_1 \\ a_2 \\ a_3^2 - a_4^2 \\ a_3 a_4 \end{bmatrix} \tag{4.50}$$

For a general Euler-Lagrangian system we formulated the control law (4.40), which asymptotically stabilizes the system. Note that since $M(q,\hat{\theta})$ is a function of the estimated parameters, $h(q,\dot{q},\hat{\theta})$ is subsequently a function of $\hat{\theta}$.

For the two-link manipulator shown in Fig. 4.1, we investigate the performance of designed controller stabilizing the system at the fully extended unstable equilibrium point including four unknown parameters (a_1, a_2, $a_3^2 - a_4^2$, and $a_3 a_4$). First of all, we simulate the control law (4.40) without any estimation update, $\hat{\theta} = \hat{\theta}_0$. The following values are chosen for the simulation,

$$m_1 = 1, \quad l_1 = 1, \quad l_{c1} = 0.5, \quad I_1 = 0.12$$

$$m_e = 2, \quad l_{ce} = 0.6, \quad I_e = 0.25, \quad \delta_e = 0$$

Therefore, the actual values of parameters are as follows,

$$\theta = \begin{bmatrix} 3.34 & 0.97 & 1.44 & 0 \end{bmatrix}^{\mathrm{T}}$$

while, by underestimating the mass, length, and moment of inertia of the links, the following initial guesses for the parameters are taken,

$$\hat{\theta}_0 = \begin{bmatrix} 2.338 & 0.291 & 0.72 & 0.2 \end{bmatrix}^{\mathrm{T}}$$

with the following initial conditions,

$$q_{0_1} = 0,$$

$$\dot{q}_{0_2} = -0.4 \; rad/s,$$

$$q_{0_2} = \frac{\pi}{6},$$

$$\dot{q}_{0_2} = -0.1 \; rad/s$$

4.3.1 Control Without Any Identifier

We intent to stabilize the manipulator at the fully extended unstable equilibrium point without using any identifier.

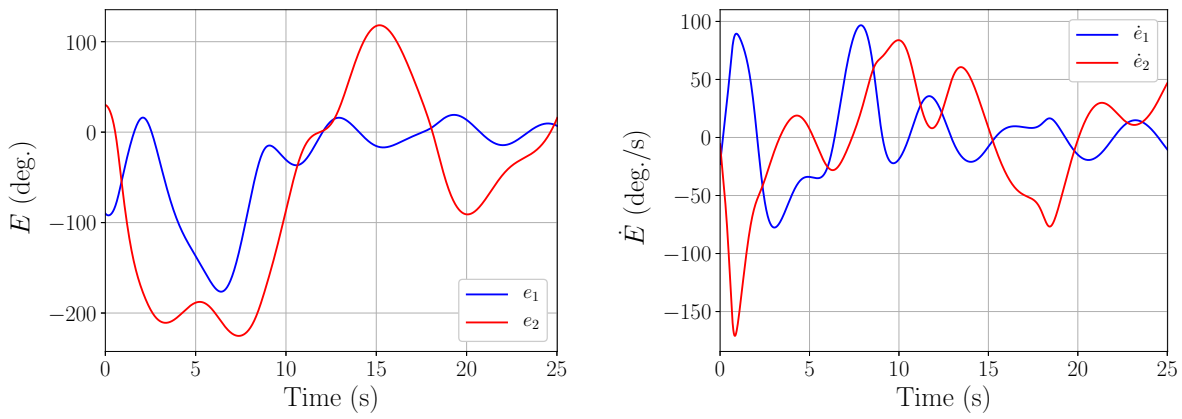

(a) (b)

Figure 4.2: The (a) tracking errors and (b) tracking errors' time derivatives without any parameter estimation update

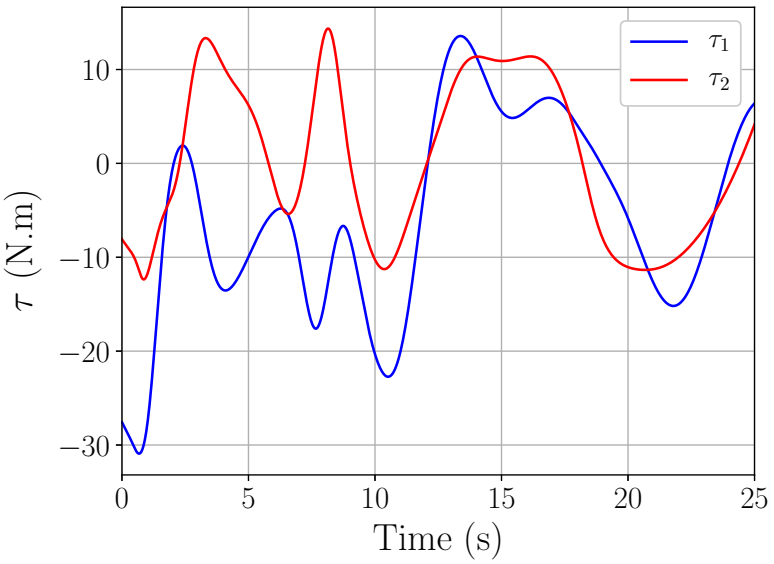

Figure 4.3: The control torques of the joints in the case of no parameter estimation update

Fig. 4.2 presents the tracking errors and their time derivatives for stabilizing the two-link robot using the proposed control scheme without any parameter estimation. The control torques of the joints are also illustrated in Fig. 4.3 revealing the instability of the robot.

As shown in Figs. 4.2 and 4.3, the system becomes completely unstable, although, by having the actual values of parameters, the control law was designed to asymptotically stabilize the system. However, in the case of updating parameter estimation using the proposed approach, the results reveal the stability of the closed-loop system.

4.3.2 Adaptive Control Using Identifier

Here we investigate the identifier (4.22) with the following parameters, along with the controller, to stabilize the manipulator at the fully extended unstable equilibrium point,

$$T = 5.0s$$

$$V(x) = \frac{1}{2}\left(|e_1|^2 + 2.5|e_2|^2\right)$$

$$a(x) = 0.8\left(|e_1|^2 + |e_2|^2\right)$$

As can be seen in Fig. 4.4, the first event-triggered parameter adaptation happens at $t = 1.44s < T$ due to the dramatic growing of the Lyapunov function, although the second one happens $5s$ after the first one (since $T = 5s$). After two estimations, the parameters converge to their actual ones and the controller properly stabilizes the system.

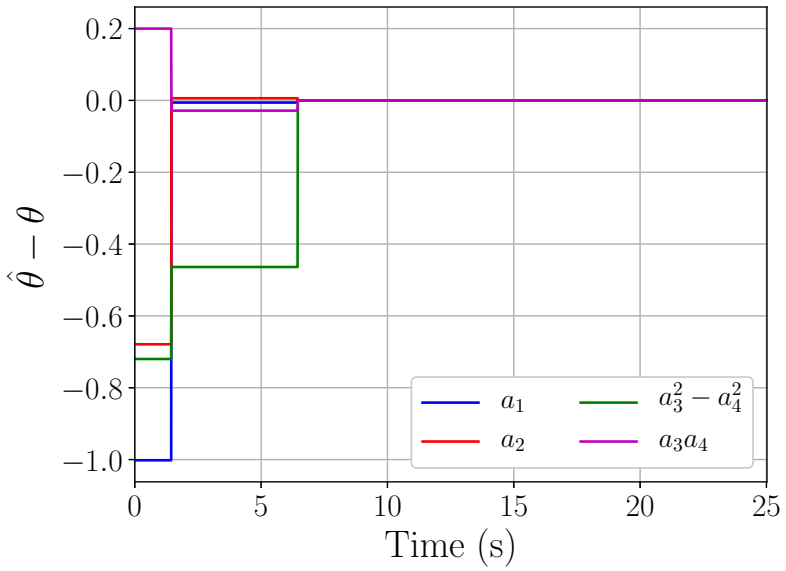

Figure 4.4: The parameter estimation process

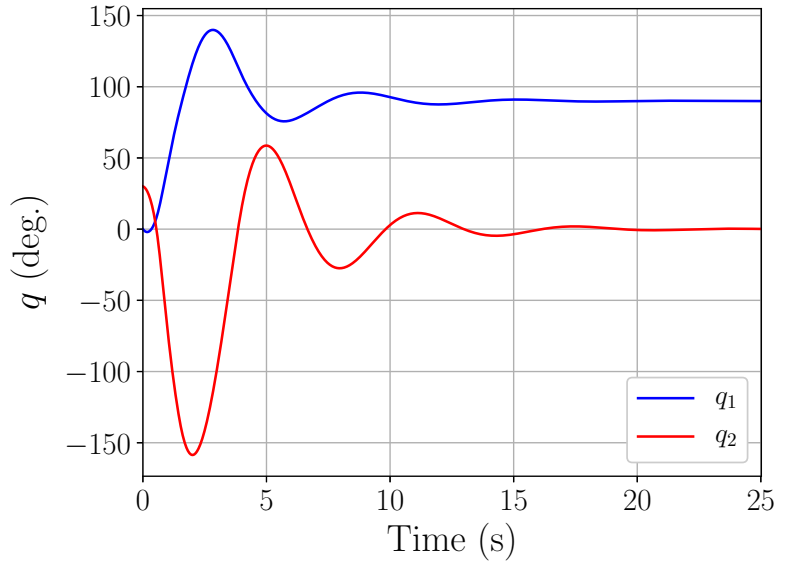

Figure 4.5: The joints' angles in the case of having parameter estimation update

Figs. 4.5 and 4.6 present the performance of the proposed adaptive scheme and also stability of the two-link robot at the fully extended unstable equilibrium point.

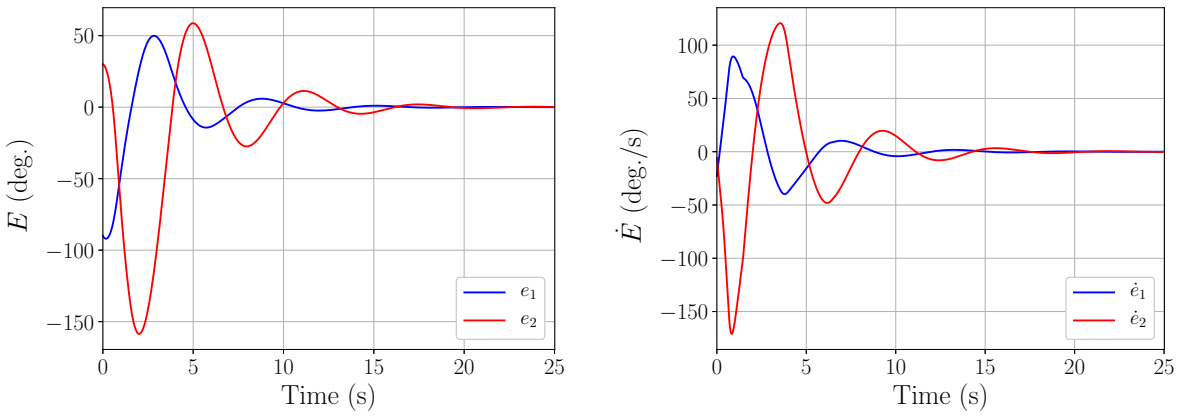

(a) (b)

Figure 4.6: The (a) tracking errors and (b) tracking errors' time derivatives with parameter estimation update

Fig. 4.6 illustrates that the tracking errors and their time derivatives asymptotically converge to zero.

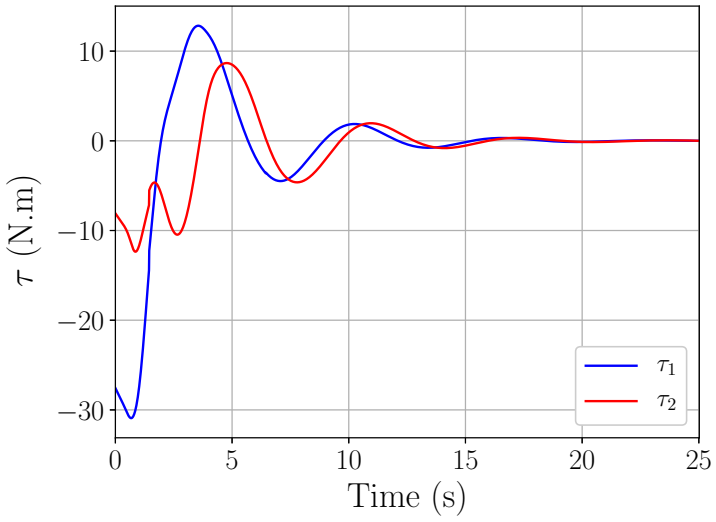

Figure 4.7: The control torques of the joints in the case of having parameter estimation update

The control torques of the joints are also illustrated in Fig. 4.7, indicating that the system becomes stable at the equilibrium point and the control torques converge to zero.

To demonstrate the importance of parameter estimation, both the phase portrait and value of Lyapunov function for both the cases (with and without parameter estimation) are shown.

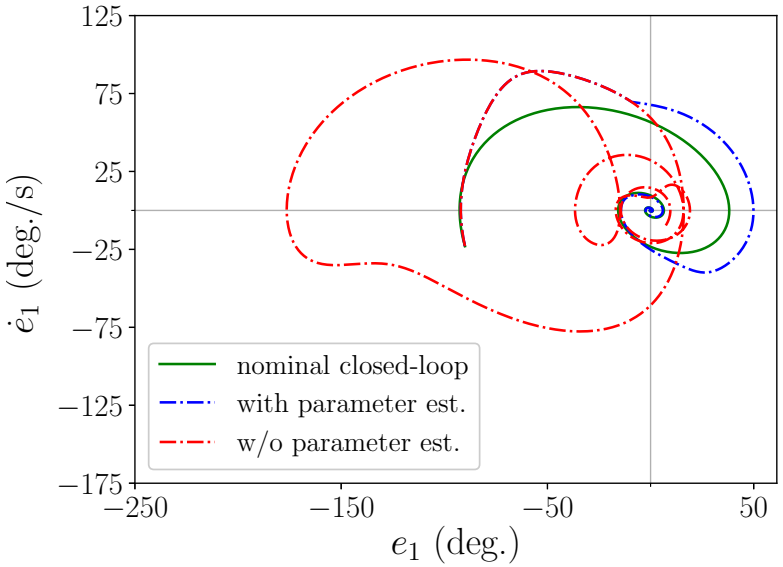

Figure 4.8: The projection on the e_1 vs. $\dot{e}_1$ plane solution of the closed-loop system with the proposed controller

Fig. 4.8 presents the phase portrait of tracking error and its time derivative for the link 1 when there is an identifier along with the controller (blue line) and there is not any identifier (red dashed line). As can be seen, the trajectory with batch parameter estimation converges to zero (blue) while the trajectory without batch parameter estimation does not (red). Fig. 4.9 presents the phase portrait of tracking error and its time derivative for link 2, again for both the cases.

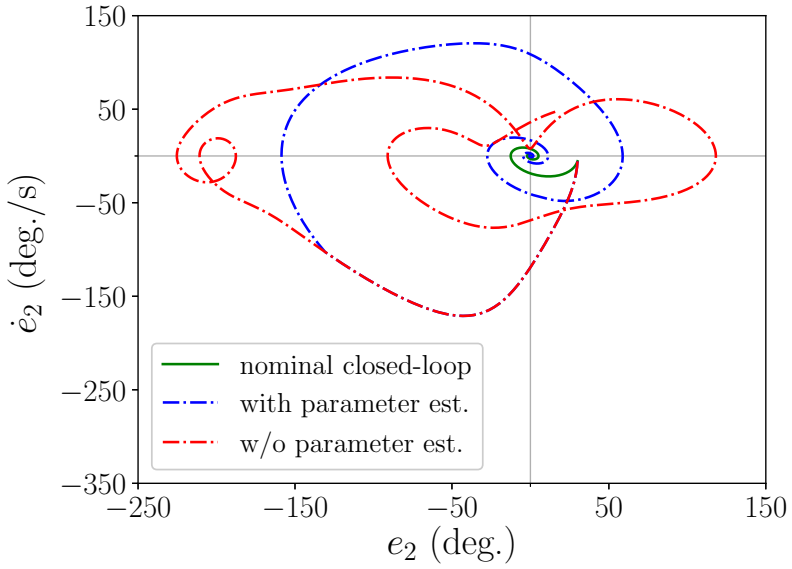

Figure 4.9: The projection on the e_2 vs. $\dot{e}_2$ plane solution of the closed-loop system with the proposed controller

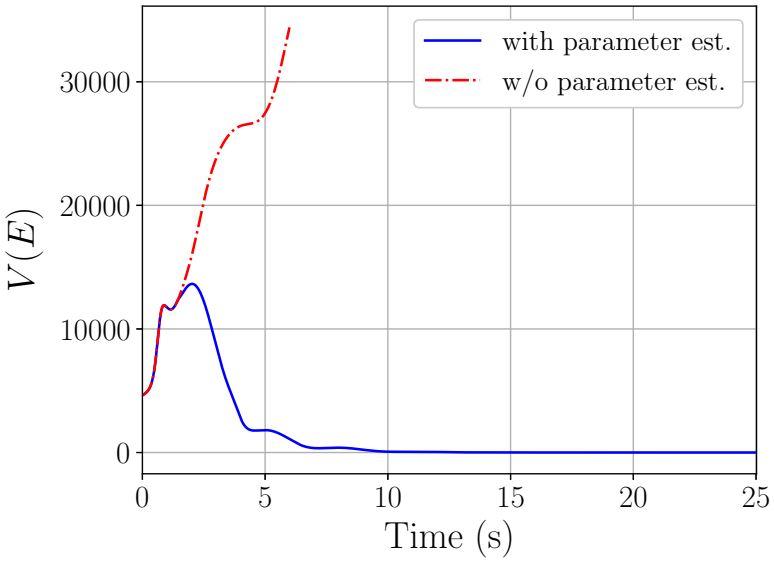

Figure 4.10: The values of Lyapunov function for the closed-loop system with the proposed controller

The phase portraits shown in Figs. 4.8 and 4.9 demonstrate the importance of parameter estimation in the stability of closed-loop system. As expected, the phase portraits of nominal closed-loop system asymptotically converge to the origin, although in the presence of uncertainty and without any parameter estimation, the phase portraits never converge to the origin.

Figs. 4.8 and 4.9 reveal that, in the case of having parameter estimation, the phase portraits converge to the nominal closed-loop ones, after the first parameter adaptation, and then asymptotically converge to the origin.

Also, the values of the Lyapunov function can be seen in Fig. 4.10, indicating that the inequality (4.10) is satisfied at around $t = 1.5s$ while the first parameter adaptation, as expected, happens at that time.

It is worth mentioning that, in the control law (4.41), selecting small α and β matrices would yield a more effective role for the model relevant part of the control scheme.

4.4 Trajectory Tracking

We now study the case that the manipulator needs to follow a time-varying desired trajectory, rather than reaching the desired position. One of the applications for trajectory tracking is executing the pick-and-place task from its initial position to a final desired position in the presence of an obstacle, typically located at the middle of the path. Then, the manipulator is supposed to follow an obstacle-avoidance trajectory while reaching the final point.

Consider the following desired trajectories, $q_{1_{\text{des}}}$ and $q_{2_{\text{des}}}$, satisfying Assumption 6,

$$q_{1_{\text{des}}} = -\frac{\pi}{8}\text{atan}(0.004t^{3.5}) + \frac{\pi}{2.5} \tag{4.51}$$

$$\dot{q}_{1_{\text{des}}} = -\frac{875\pi t^{2.5}}{8\left(t^7 + 62500\right)} \tag{4.52}$$

$$\ddot{q}_{1_{\text{des}}} = \frac{875\pi t^{1.5}\left(9t^7 - 312500\right)}{16\left(t^7 + 62500\right)^2} \tag{4.53}$$

$$q_{2_{\text{des}}} = -\frac{\pi}{36}\cos\left(\frac{\pi}{20}t\right) - \frac{\pi}{18} \tag{4.54}$$

$$\dot{q}_{2_{\text{des}}} = \frac{\pi^2}{720}\sin\left(\frac{\pi}{20}t\right) \tag{4.55}$$

$$\ddot{q}_{2_{\text{des}}} = \frac{\pi^3}{14400}\cos\left(\frac{\pi}{20}t\right) \tag{4.56}$$

4.4.1 Control Without Any Identifier

We intend to control the manipulator to track the desired trajectories without using any identifier. First, the tracking errors and control torques are presented for the case of without any parameter estimation.

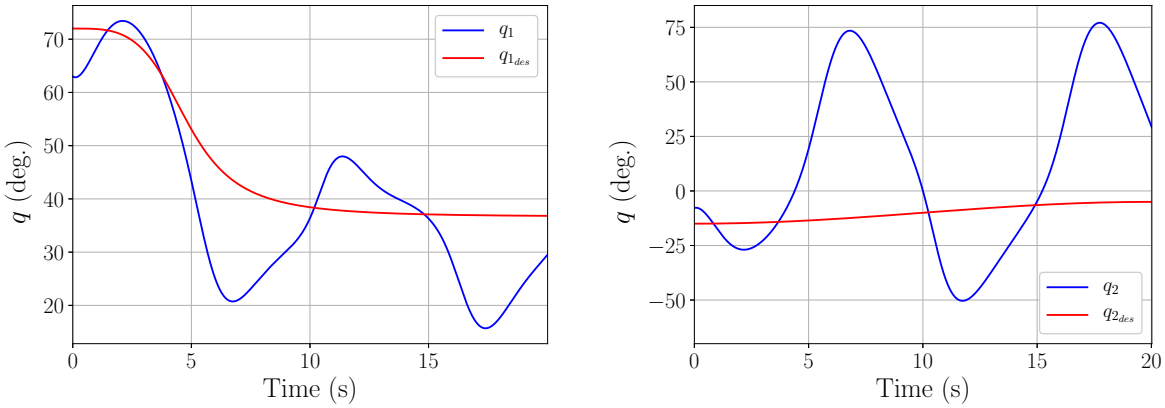

(a) (b)

Figure 4.11: The angles of joints without any parameter estimation update

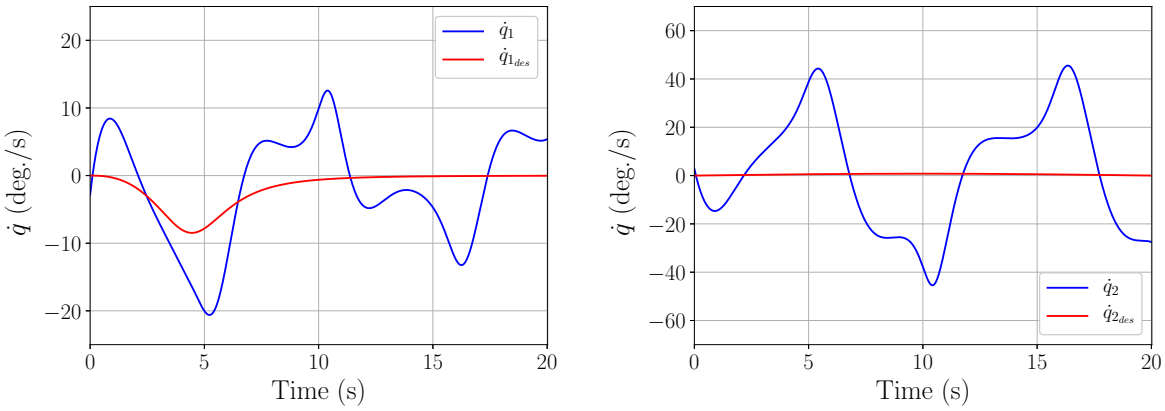

(a) (b)

Figure 4.12: The angular velocities of joints without any parameter estimation update

Figs. 4.11 and 4.12 present the angles and angular velocities of the joints, respectively, revealing the tracking performance. As can be seen, the two-link robot cannot follow the desired trajectory.

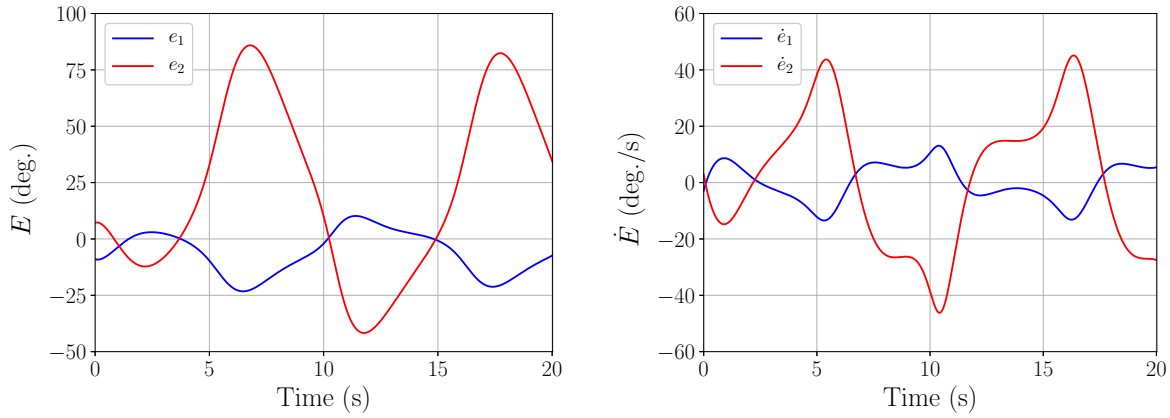

(a) (b)

Figure 4.13: The (a) tracking errors and (b) tracking errors' time derivatives without any parameter estimation update

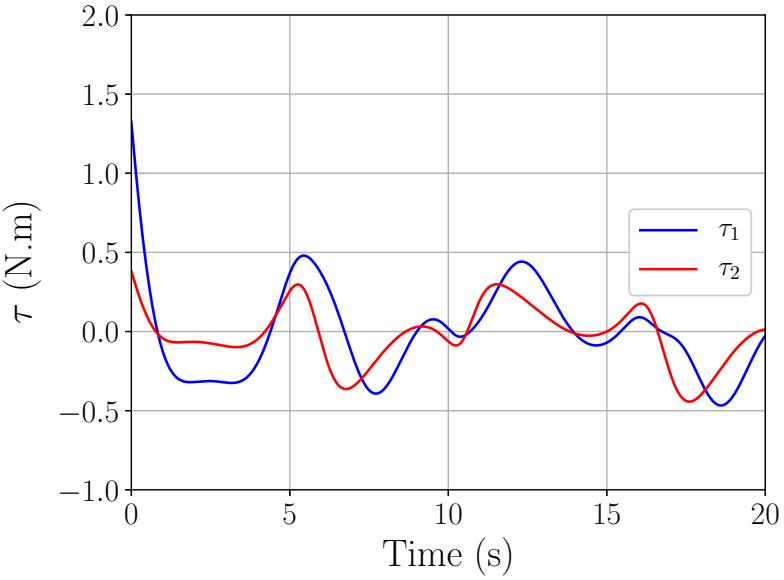

Figure 4.14: The control torques of the joints in the case of no parameter estimation update

As can be seen in Figs. 4.13 and 4.14, the system becomes completely unstable and

cannot follow the desired trajectories. By activating the parameter update law, the joints track the desired trajectories.

4.4.2 Adaptive Control Using Identifier

We here implement the identifier (4.22) with the following parameters, along with the controller, to track the desired trajectories,

$$T = 5.0s$$

$$V(x) = \frac{1}{2}\left(|e_1|^2 + 0.5|e_2|^2\right)$$

$$a(x) = 0.5\left(|e_1|^2 + |e_2|^2\right)$$

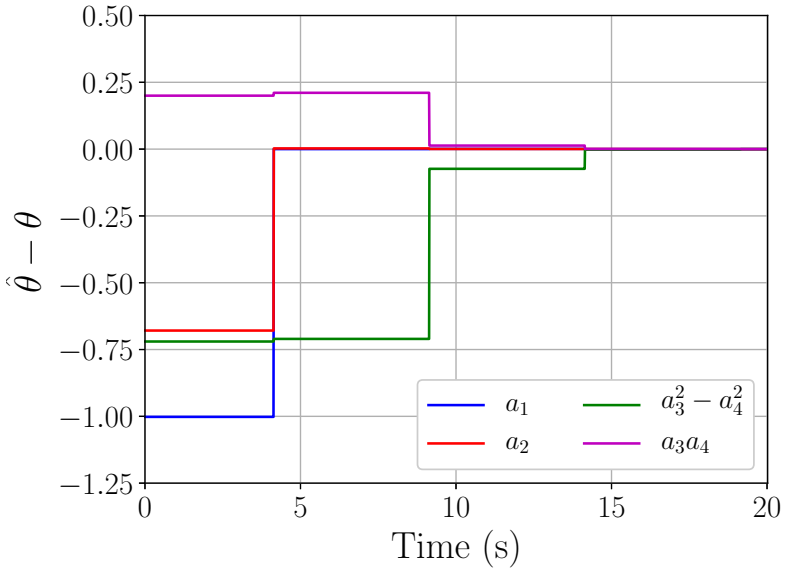

Figure 4.15: The parameter estimation process

As can be observed through Fig. 4.15, the first event-triggered parameter adapta-

tion happens at $t = 4.12s < T$ due to the dramatic growing of the Lyapunov function, although the rest of them happen every $5s$ after each other (since $T = 5s$).

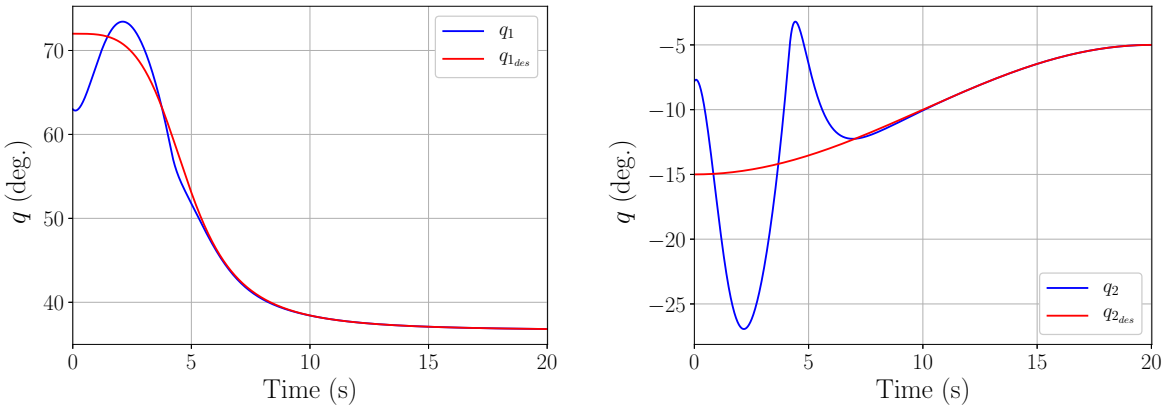

(a) (b)

Figure 4.16: The angles of joints without any parameter estimation update

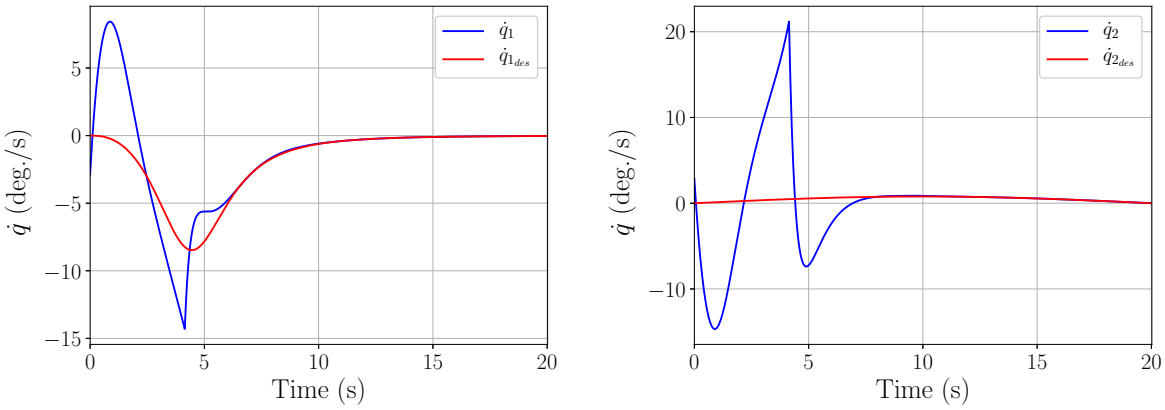

(a) (b)

Figure 4.17: The angular velocities of joints with parameter estimation update

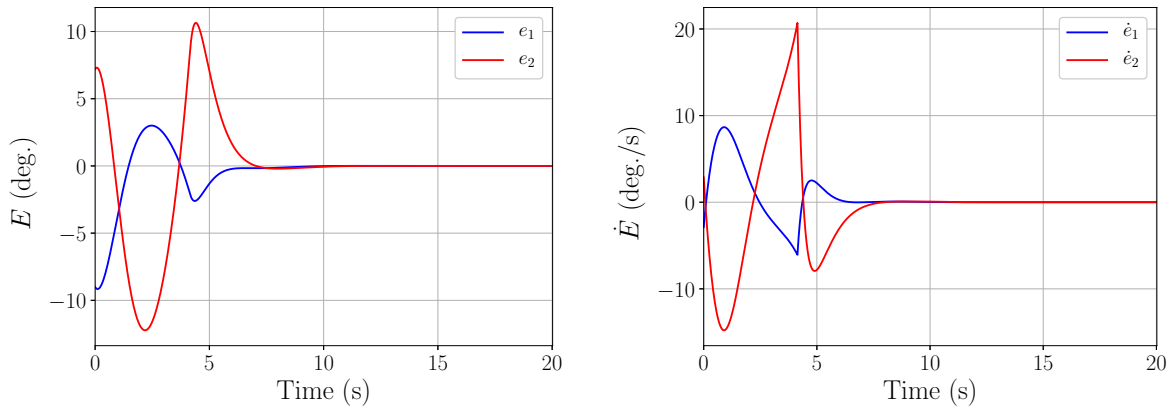

(a) (b)

Figure 4.18: The (a) tracking errors and (b) tracking errors' time derivatives with parameter estimation update

Figs. 4.16 – 4.18 present the acceptable performance of proposed adaptive scheme and also reveal that the two-link robot follows the desired trajectory after occurrence of the first parameter estimation. Fig. 4.18 illustrates that the errors and their time derivatives asymptotically converge to zero.

The control torques of the joints are also shown in Fig. 4.19,

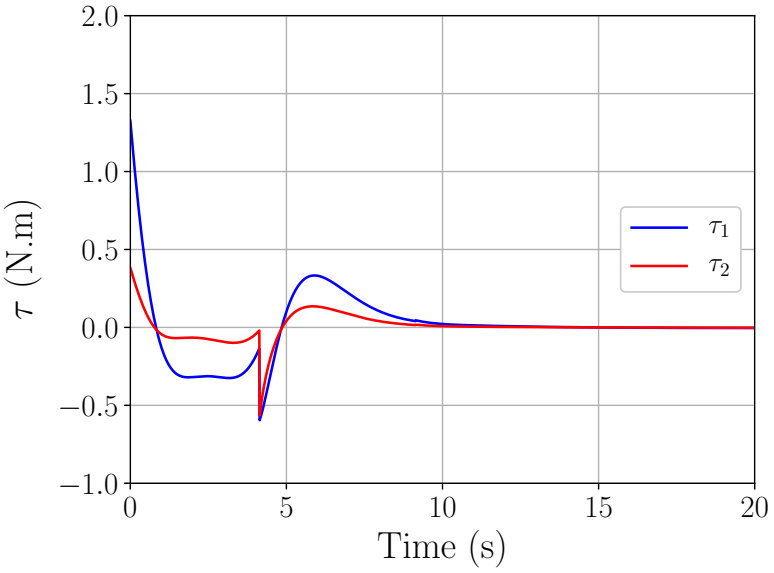

Figure 4.19: The control torques of the joints in the case of having parameter estimation update

The results reveal that the tracking errors asymptotically converge to zero and the unknown parameters are estimated as shown in Fig. 4.15. Note that the parameters' estimations do not necessarily converge to the actual values.

Fig. 4.20 presents the phase portrait of tracking errors and their time derivatives for link 1 when there is an identifier along with the controller (blue line) and there is not any identifier (red dashed line). As can be seen, the blue trajectory converges to zero, but the other one never converges. Fig. 4.21 presents the phase portrait of tracking errors and their time derivatives for link 2, again for both the cases.

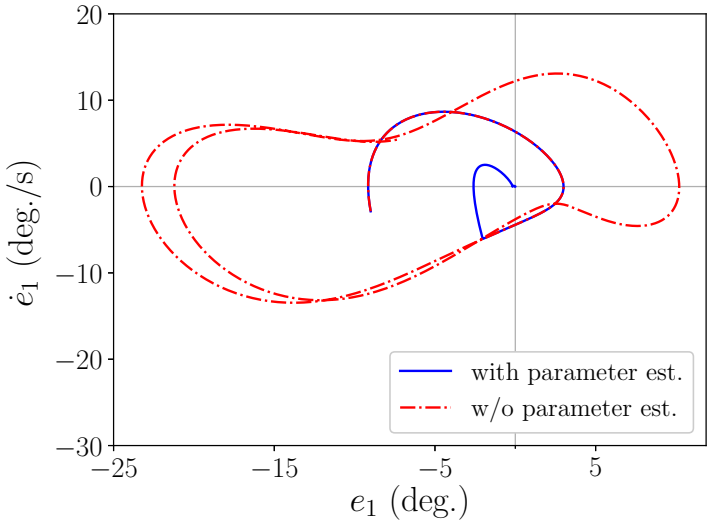

Figure 4.20: The projection on the e_1 vs. $\dot{e}_1$ plane solution of the closed-loop system with the proposed controller

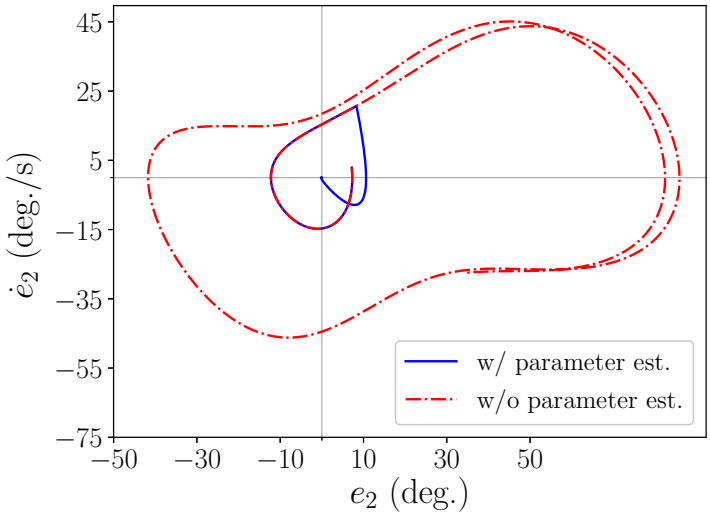

Figure 4.21: The projection on the e_2 vs. $\dot{e}_2$ plane solution of the closed-loop system with the proposed controller

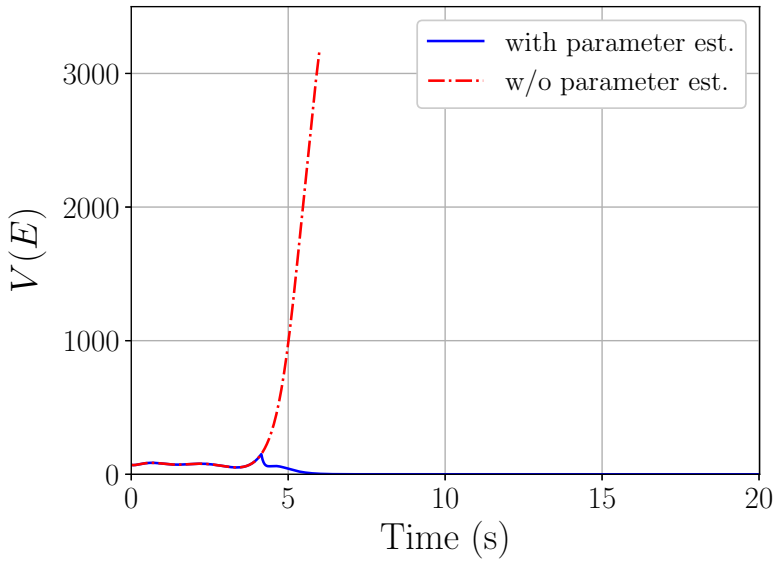

Figure 4.22: The values of Lyapunov function for the closed-loop system with the proposed controller

To investigate the performance of control law with parameter estimation, the phase portraits (illustrated through Fig. 4.20 and 4.21) and the values of Lyapunov function for both the cases (with and without parameter estimation) are presented. As can be seen in Fig. 4.22, by the incremental Lyapunov function, the unknown parameters estimation process begins through the event-triggered identifier.

It is worth mentioning that the time-varying desired trajectories do not meet the criteria of the persistence of excitation although the proposed method works well, despite the fact that the classical ones require the criteria to yield acceptable performance.

4.5 Conclusions

Throughout this chapter, we designed a triggered-based adaptive controller for robot manipulators to estimate the unknown parameters and also to achieve asymptotic stability in the presence of uncertainties. We studied a 2-DOF manipulator (Fig. 4.1) with four unknown parameters and stabilized the system at the fully extended unstable equilibrium point along with efficiently estimating the unknown parameters.

To this end, we rewrote the manipulator equations in the general form of Eq. (4.2) and extracted the unknown parameters in addition to designing the proper nominal controller. Toward designing the controller, we formulated the proper Lyapunov candidate function using the backstepping approach and then designed the nominal controller to asymptotically stabilize the system without any uncertainties. The simulation results revealed that the controller, in the presence of parametric uncertainties, makes the robot manipulator asymptomatically stable and also efficiently estimates the unknown parameters. Fig. 4.6 illustrates the convergence of tracking errors and their time derivatives to zero. Also, the parameter estimation process using the proposed scheme was shown in Fig. 4.4.

Furthermore, we investigated the performance of the proposed method for a trajectory tracking problem and the results shown in Fig. 4.18 revealed the perfect tracking and the system stabilization.

4.6 Notes and References

In this chapter, a time/event triggered-based adaptive control scheme was formulated for a robot manipulator and the performance of the proposed controller was investigated. For a two-link robot, as a case study, four unknown lumped parameters were estimated using the adaptive controller while the manipulator became stable and could track the desired trajectory.

Because of the cumbersome analytical burden of finding a regressor matrix corresponding to physical parameters of a two-link robot, we considered four lumped parameters. Therefore, one possible future work would be developing a general linear parametrization procedure for high-DOF robots, since the method is computationally efficient and can be used for highly coupled and nonlinear systems. It is also of great interest to utilize this approach along with optimal controllers to formulate a computationally efficient adaptive optimal controller.

Chapter 4 contains reprints or adaptions of the following papers: 1) M. Bagheri, I. Karafyllis, P. Naseradinmousavi, and M. Krstić, "Adaptive Control of a Two-Link Robot Using Batch Least-Square Identifier," *In preparation*, 2019. The dissertation author is the primary investigator and author of this paper, and would like to thank Iasson Karafyllis, Miroslav Krstić, and Peiman Naseradinmousavi for their contributions.

Bibliography

[1] Abdelkader Abdessameud and Abdelhamid Tayebi. Formation control of vtol unmanned aerial vehicles with communication delays. *Automatica*, 47(11):2383–2394, 2011.

[2] David Angeli. Input-to-state stability of pd-controlled robotic systems. *Automatica*, 35(7):1285–1290, 1999.

[3] Kartik B Ariyur and Miroslav Krstić. Analysis and design of multivariable extremum seeking. In *American Control Conference, 2002. Proceedings of the 2002*, volume 4, pages 2903–2908. IEEE, 2002.

[4] Kartik B Ariyur and Miroslav Krstić. Multivariable extremum seeking feedback: Analysis and design. In *Proc. of the Mathematical Theory of Networks and Systems*, 2002.

[5] Kartik B Ariyur and Miroslav Krstić. *Real-time optimization by extremum-seeking control*. John Wiley & Sons, 2003.

[6] Mostafa Bagheri, Arash Ajoudani, Jinoh Lee, Darwin G Caldwell, and Nikos G Tsagarakis. Kinematic analysis and design considerations for optimal base frame arrangement of humanoid shoulders. In *2015 IEEE International Conference on Robotics and Automation (ICRA)*, pages 2710–2715, May 26-30 2015.

[7] Mostafa Bagheri, Miroslav Krstić, and Peiman Naseradinmousavi. Analytical and experimental predictor-based time delay control of baxter robot. In *ASME 2018 Dynamic Systems and Control Conference*, pages V001T04A011–V001T04A011. American Society of Mechanical Engineers, 2018.

[8] Mostafa Bagheri, Miroslav Krstić, and Peiman Naseradinmousavi. Joint-space trajectory optimization of a 7-dof baxter using multivariable extremum seeking. In *IEEE American Control Conference (ACC 2018)*, pages 2176–2181, Milwaukee, WI, June 27-29 2018.

[9] Mostafa Bagheri, Miroslav Krstić, and Peiman Naseradinmousavi. Multivariable extremum seeking for joint-space trajectory optimization of a high-degrees-of-freedom robot. *Journal of Dynamic Systems, Measurement, and Control*, 140(11):111017, 2018.

[10] Mostafa Bagheri and Peiman Naseradinmousavi. Novel analytical and experimental trajectory optimization of a 7-dof baxter robot: global design sensitivity and step size analyses. *The International Journal of Advanced Manufacturing Technology*, 93(9-12):4153–4167, December 2017.

[11] Mostafa Bagheri, Peiman Naseradinmousavi, and Miroslav Krstić. Feedback linearization based predictor for time delay control of a high-dof robot manipulator. *Automatica*, 108:108485, 2019.

[12] Mostafa Bagheri, Peiman Naseradinmousavi, and Miroslav Krstić. Time delay control of a high-dof robot manipulator through feedback linearization based predictor. In *ASME 2019 Dynamic Systems and Control Conference*. American Society of Mechanical Engineers, 2019.

[13] Mostafa Bagheri, Peiman Naseradinmousavi, and Rasha Morsi. Experimental and novel analytical trajectory optimization of a 7-dof baxter robot: Global design sensitivity and step size analyses. In *ASME 2017 Dynamic Systems and Control Conference*, page V001T30A001. American Society of Mechanical Engineers, American Society of Mechanical Engineers, October 11-13 2017.

[14] E-W Bai, L-C Fu, and Sosale Shankara Sastry. Averaging analysis for discrete time and sampled data adaptive systems. *IEEE Transactions on Circuits and Systems*, 35(2):137–148, 1988.

[15] Eric Barnett and Clément Gosselin. Time-optimal trajectory planning of cable-driven parallel mechanisms for fully specified paths with g1-discontinuities. *Journal of Dynamic Systems, Measurement, and Control*, 137(7):071007, 2015.

[16] Nikolaos Bekiaris-Liberis, Mrdjan Jankovic, and Miroslav Krstić. Adaptive stabilization of lti systems with distributed input delay. *International Journal of Adaptive Control and Signal Processing*, 27(1-2):46–65, 2013.

[17] Nikolaos Bekiaris-Liberis and M. Krstić. Lyapunov stability of linear predictor feedback for distributed input delay. *IEEE Transactions on Automatic Control*, 56(3):655–660, March 2011.

[18] Nikolaos Bekiaris-Liberis and Miroslav Krstić. Delay-adaptive feedback for linear feedforward systems. *Systems & Control Letters*, 59(5):277–283, 2010.

[19] Nikolaos Bekiaris-Liberis and Miroslav Krstić. Stabilization of linear strict-feedback systems with delayed integrators. *Automatica*, 46(11):1902–1910, November 2010.

[20] Nikolaos Bekiaris-Liberis and Miroslav Krstić. Compensation of state-dependent input delay for nonlinear systems. *IEEE Transactions on Automatic Control*, 58(2):275–289, 2013.

[21] Nikolaos Bekiaris-Liberis and Miroslav Krstić. *Nonlinear control under nonconstant delays*, volume 25. Siam, 2013.

[22] Nikolaos Bekiaris-Liberis and Miroslav Krstić. Robustness of nonlinear predictor feedback laws to time-and state-dependent delay perturbations. *Automatica*, 49(6):1576–1590, 2013.

[23] Nikolaos Bekiaris-Liberis and Miroslav Krstić. Predictor-feedback stabilization of multi-input nonlinear systems. *IEEE Transactions on Automatic Control*, 62(2):516–531, 2017.

[24] Harry Berghuis, Romeo Ortega, and Henk Nijmeijer. A robust adaptive robot controller. *IEEE Transactions on Robotics and Automation*, 9(6):825–830, 1993.

[25] Alex Bertino, Mostafa Bagheri, Peiman Naseradinmousavi, and Miroslav Krstić. Experimental autonomous deep learning-based 3d path planning for a 7-dof robot manipulator. In *ASME 2019 Dynamic Systems and Control Conference*. American Society of Mechanical Engineers, 2019.

[26] G Bessonnet and JP Lallemand. On the optimization of robotic manipulator trajectories with bounded joint actuators or joint kinetic loads considered as control variables. *Journal of Dynamic Systems, Measurement, and Control*, 116:819–819, 1994.

[27] Paolo Binetti, Kartik B Ariyur, Miroslav Krstić, and Franco Bernelli. Formation flight optimization using extremum seeking feedback. *Journal of Guidance Control and Dynamics*, 26(1):132–142, 2003.

[28] Delphine Bresch-Pietri and Miroslav Krstić. Adaptive trajectory tracking despite unknown input delay and plant parameters. *Automatica*, 45(9):2074–2081, 2009.

[29] Nikolaos Bresch-Pietri and Miroslav Krstić. Delay-adaptive control for nonlinear systems. *IEEE Transactions on Automatic Control*, 59:1203–1217, 2014.

[30] Chien-Chern Cheah, Chao Liu, and Jean-Jacques E Slotine. Adaptive tracking control for robots with unknown kinematic and dynamic properties. *The International Journal of Robotics Research*, 25(3):283–296, 2006.

[31] Yangquan Chen, Zhiming Gong, and Changyun Wen. Analysis of a high-order iterative learning control algorithm for uncertain nonlinear systems with state delays. *Automatica*, 34(3):345–353, 1998.

[32] Joon-Young Choi and Miroslav Krstić. Compensation of time-varying input delay for discrete-time nonlinear systems. *International Journal of Robust and Nonlinear control*, 26:1755–1776, 2016.

[33] Joon-Young Choi, Miroslav Krstić, Kartik B Ariyur, and Jin Soo Lee. Extremum seeking control for discrete-time systems. *IEEE Transactions on Automatic Control*, 47(2):318–323, 2002.

[34] Jennie Cochran, Eva Kanso, Scott D Kelly, Hailong Xiong, and Miroslav Krstić. Source seeking for two nonholonomic models of fish locomotion. *IEEE Transactions on Robotics*, 25(5):1166–1176, 2009.

[35] Jennie Cochran, Antranik Siranosian, Nima Ghods, and Miroslav Krstić. 3-d source seeking for underactuated vehicles without position measurement. *IEEE Transactions on Robotics*, 25(1):117–129, 2009.

[36] D. Costantinescu and E. A. Croft. Smooth and time-optimal trajectory planning for industrial manipulators along specified paths. *Journal of robotic systems*, 17(5):233–249, 2000.

[37] Yuval Davidor. *Genetic Algorithms and Robotics: A heuristic strategy for optimization*, volume 1. World Scientific, 1991.

[38] Alper Denasi, Dragan Kostić, and Henk Nijmeijer. Time delay compensation in bilateral teleoperations using impact. *IEEE Transactions on Control Systems Technology*, 21(3):704–715, 2013.

[39] J Dong and JA Stori. A generalized time-optimal bidirectional scan algorithm for constrained feed-rate optimization. *Journal of Dynamic Systems, Measurement, and Control*, 128(2):379–390, 2006.

[40] N Fischer, A Dani, Nitin Sharma, and Warren E Dixon. Saturated control of an uncertain nonlinear system with input delay. *Automatica*, 49(6):1741–1747, 2013.

[41] Paul Frihauf, Miroslav Krstić, and Tamer Başar. Finite-horizon lq control for unknown discrete-time linear systems via extremum seeking. *European Journal of Control*, 19(5):399–407, 2013.

[42] D. P. Garg and M. Kumar. Optimization techniques applied to multiple manipulators for path planning and torque minimization. *Engineering Applications of Artificial Intelligence*, 15(3):241–252, 2002.

[43] Azad Ghaffari, Miroslav Krstić, and Dragan Nešić. Multivariable newton-based extremum seeking. *Automatica*, 48(8):1759–1767, 2012.

[44] Azad Ghaffari, Miroslav Krstić, and Sridhar Seshagiri. Power optimization and control in wind energy conversion systems using extremum seeking. *IEEE Transactions on Control Systems Technology*, 22(5):1684–1695, 2014.

[45] Azad Ghaffari, Miroslav Krstić, and Sridhar Seshagiri. Power optimization for photovoltaic microconverters using multivariable newton-based extremum seeking. *IEEE Transactions on Control Systems Technology*, 22(6):2141–2149, 2014.

[46] Azad Ghaffari, Sridhar Seshagiri, and Miroslav Krstić. Power optimization for photovoltaic micro-converters using multivariable gradient-based extremum-seeking. In *IEEE American Control Conference (ACC 2012)*, pages 3383–3388. IEEE, 2012.

[47] Azad Ghaffari, Sridhar Seshagiri, and Miroslav Krstić. Multivariable maximum power point tracking for photovoltaic micro-converters using extremum seeking. *Control Engineering Practice*, 35:83–91, 2015.

[48] Farzad Hashemzadeh, Iraj Hassanzadeh, and Mahdi Tavakoli. Teleoperation in the presence of varying time delays and sandwich linearity in actuators. *Automatica*, 49(9):2813–2821, 2013.

[49] WPMH Heemels, Karl Henrik Johansson, and Paulo Tabuada. An introduction to event-triggered and self-triggered control. In *2012 IEEE 51st IEEE Conference on Decision and Control (CDC)*, pages 3270–3285. IEEE, 2012.

[50] Andre R Hirakawa and Atsuo Kawamura. Proposal of trajectory generation for redundant manipulators using variational approach applied to minimization of consumed electrical energy. In *Advanced Motion Control, 1996. AMC'96-MIE. Proceedings., 1996 4th International Workshop on*, volume 2, pages 687–692. IEEE, 1996.

[51] Panfeng Huang, Yangsheng Xu, and Bin Liang. Global minimum-jerk trajectory planning of space manipulator. *International Journal of Control, Automation, and Systems*, 4(4):405–413, 2006.

[52] Panfeng Huang, Yangsheng Xu, and Bin Liang. Minimum-torque path planning of space robots using genetic algorithms. *International Journal of Robotics & Automation*, 21(3):229, 2006.

[53] Petros A Ioannou and Jing Sun. *Robust adaptive control*. Courier Corporation, 2012.

[54] Devesh K Jha, Yue Li, Thomas A Wettergren, and Asok Ray. Robot path planning in uncertain environments: A language-measure-theoretic approach. *Journal of Dynamic Systems, Measurement, and Control*, 137(3):034501, 2015.

[55] Qimi Jiang and Clément M Gosselin. Dynamic optimization of reactionless four-bar linkages. *Journal of Dynamic Systems, Measurement, and Control*, 132(4):041006, 2010.

[56] Mansour Kabganian, Reza Nadafi, Yasha Tamhidi, and Mostafa Bagheri. A novel mechanical attitude simulator with adaptive control for micro-satellite. In *Control, Instrumentation and Automation (ICCIA), 2011 2nd International Conference on*, pages 694–698. IEEE, 2011.

[57] Iasson Karafyllis, Maria Kontorinaki, and Miroslav Krstic. Adaptive control by regulation-triggered batch least-squares estimation of non-observable parameters. *arXiv preprint arXiv:1811.10833*, 2018.

[58] Iasson Karafyllis and Miroslav Krstić. Delay-robustness of linear predictor feedback without restriction on delay rate. *Automatica*, 49(6):1761–1767, 2013.

[59] Iasson Karafyllis and Miroslav Krstić. Numerical schemes for nonlinear predictor feedback. *Mathematics of Control, Signals, and Systems*, 26(4):519–546, 2014.

[60] Iasson Karafyllis and Miroslav Krstić. Adaptive certainty-equivalence control with regulation-triggered finite-time least-squares identification. *IEEE Transactions on Automatic Control*, 63(10):3261–3275, 2018.

[61] Iasson Karafyllis, Miroslav Krstić, Tarek Ahmed-Ali, and Francoise Lamnabhi-Lagarrigue. Global stabilisation of nonlinear delay systems with a compact absorbing set. *International Journal of Control*, 87(5):1010–1027, 2014.

[62] Hassan K. Khalil. *Noninear Systems*. Prentice Hall, third edition, 2002.

[63] M Krstić, I Kanellakopoulos, and PV Kokotović. Adaptive nonlinear control without overparametrization. *Systems & Control Letters*, 19(3):177–185, 1992.

[64] Miroslav Krstić. Performance improvement and limitations in extremum seeking control. *Systems & Control Letters*, 39(5):313–326, 2000.

[65] Miroslav Krstić. On compensating long actuator delays in nonlinear control. In *IEEE American Control Conference, 2008*, pages 2921–2926, June 11-13 2008.

[66] Miroslav Krstić. *Delay Compensation for Nonlinear, Adaptive, and PDE Systems (Systems & Control: Foundations & Applications)*. Springer, 2009.

[67] Miroslav Krstić. Compensation of infinite-dimensional actuator and sensor dynamics. *IEEE Control Systems*, 30(1):22–41, 2010.

[68] Miroslav Krstić. Input delay compensation for forward complete and strict-feedforward nonlinear systems. *IEEE Transactions on Automatic Control*, 55(2):287–303, 2010.

[69] Miroslav Krstić. Lyapunov stability of linear predictor feedback for time-varying input delay. *IEEE Transactions on Automatic Control*, 55(2):554–559, February 2010.

[70] Miroslav Krstić, I. Kanellakopoulos, and P. Kokotović. *Nonlinear and Adaptive Control Design*. Wiley-Interscience, 1995.

[71] Miroslav Krstić and Hsin-Hsiung Wang. Stability of extremum seeking feedback for general nonlinear dynamic systems. *Automatica*, 36(4):595–601, 2000.

[72] Yaoyu Li, Mario A Rotea, GT-C Chiu, Luc G Mongeau, and In-Su Paek. Extremum seeking control of a tunable thermoacoustic cooler. *IEEE Transactions on Control Systems Technology*, 13(4):527–536, 2005.

[73] Shu-Jun Liu and Miroslav Krstić. Discrete-time stochastic extremum seeking. *IFAC Proceedings Volumes*, 47(3):3274–3279, 2014.

[74] Yen-Chen Liu and Nikhil Chopra. Control of semi-autonomous teleoperation system with time delays. *Automatica*, 49(6):1553–1565, 2013.

[75] Johnson YS Luh and Chyuan S Lin. Optimum path planning for mechanical manipulators. *Journal of Dynamic Systems, Measurement, and Control*, pages 142–151, 1981.

[76] Max Lungarella, Giorgio Metta, Rolf Pfeifer, and Giulio Sandini. Developmental robotics: a survey. *Connection science*, 15(4):151–190, 2003.

[77] Moshe P Mann, Boaz Zion, Dror Rubinstein, Raphael Linker, and Itzhak Shmulevich. Minimum time kinematic motions of a cartesian mobile manipulator for a fruit harvesting robot. *Journal of Dynamic Systems, Measurement, and Control*, 136(5):051009, 2014.

[78] Chris Manzie and Miroslav Krstić. Extremum seeking with stochastic perturbations. *IEEE Transactions on Automatic Control*, 54(3):580–585, 2009.

[79] Jan Mattmüller and Damian Gisler. Calculating a near time-optimal jerk-constrained trajectory along a specified smooth path. *The International Journal of Advanced Manufacturing Technology*, 45(9):1007–1016, 2009.

[80] D. Meike and L. Ribickis. Energy efficient use of robotics in the automobile industry. In *2011 15th International Conference on Advanced Robotics (ICAR)*, pages 507–511, 2011.

[81] AJung Moon, Chris AC Parker, Elizabeth A Croft, and HF Van der Loos. Design and impact of hesitation gestures during human-robot resource conflicts. *Journal of Human-Robot Interaction*, 2(3):18–40, 2013.

[82] Peiman Naseradinmousavi, Hashem Ashrafiuon, and Mostafa Bagheri. A decentralized neuro-adaptive control scheme to suppress chaotic/hyperchaotic dynamics of smart valves network. *Journal of Computational and Nonlinear Dynamics*, 13(5), April 2018.

[83] Peiman Naseradinmousavi, Hashem Ashrafiuon, and Mostafa Bagheri. Suppressing chaotic and hyperchaotic dynamics of smart valves network using a centralized adaptive approach. In *2018 Annual American Control Conference (ACC)*, pages 1671–1676. IEEE, 2018.

[84] Romeo Ortega and Mark W Spong. Adaptive motion control of rigid robots: A tutorial. *Automatica*, 25(6):877–888, 1989.

[85] Jahng-Hyon Park and Haruhiko Asada. Concurrent design optimization of mechanical structure and control for high speed robots. *Journal of Dynamic Systems, Measurement, and Control*, 116(3):344–356, 1994.

[86] Quang-Cuong Pham and Yoshihiko Nakamura. A new trajectory deformation algorithm based on affine transformations. *IEEE Transactions on Robotics*, 31(4):1054–1063, 2015.

[87] WE Red, Hung-Veit Troung-Cao, and KH Kim. Robot path planning in three-dimensions using the direct subspace. *Journal of Dynamic Systems, Measurement, and Control*, 109(3):238–244, 1987.

[88] Rethink Robotics. Workspace guidelines. `http://mfg.rethinkrobotics.com/wiki/Workspace_Guidelines`.

[89] Mario A Rotea. Analysis of multivariable extremum seeking algorithms. In *American Control Conference, 2000. Proceedings of the 2000*, volume 1, pages 433–437. IEEE, 2000.

[90] Francisco Rubio, Carlos Llopis-Albert, Francisco Valero, and Josep Lluis Suñer. Industrial robot efficient trajectory generation without collision through the evolution of the optimal trajectory. *Robotics and Autonomous Systems*, 86:106–112, 2016.

[91] Shankar Sastry and Marc Bodson. *Adaptive control: stability, convergence and robustness*. Courier Corporation, 2011.

[92] Z. Shiller. Time-energy optimal control of articulated systems with geometric path constraints. *Journal of Dynamic Systems, Measurement, and Control*, 118(1):139–143, 1996.

[93] Bruno Siciliano, Lorenzo Sciavicco, Luigi Villani, and Giuseppe Oriolo. *Robotics: modelling, planning and control*. Springer Science & Business Media, 2010.

[94] J-JE Slotine and Li Weiping. Adaptive manipulator control: A case study. *IEEE transactions on automatic control*, 33(11):995–1003, 1988.

[95] Jean-Jacques E Slotine and Weiping Li. On the adaptive control of robot manipulators. *The international journal of robotics research*, 6(3):49–59, 1987.

[96] Jean-Jacques E Slotine and Weiping Li. Composite adaptive control of robot manipulators. *Automatica*, 25(4):509–519, 1989.

[97] Jean-Jacques E Slotine, Weiping Li, et al. *Applied nonlinear control*, volume 199. prentice-Hall Englewood Cliffs, NJ, 1991.

[98] Otto JM Smith. A controller to overcome dead time. *ISA J.*, 6:28–33, 1959.

[99] Oren Solomon and Emilia Fridman. New stability conditions for systems with distributed delays. *Automatica*, 49(11):3467–3475, 2013.

[100] M. W. Spong, S. Hutchinson, and M. Vidyasagar. *Robot Modeling and Control*. Jon Wiley & Sons Inc, 2005.

[101] Mark W Spong. Adaptive control of flexible joint manipulators. *Systems & Control Letters*, 13(1):15–21, 1989.

[102] Mark W Spong. On the robust control of robot manipulators. *IEEE Transactions on automatic control*, 37(11):1782–1786, 1992.

[103] Mark W Spong and Romeo Ortega. On adaptive inverse dynamics control of rigid robots. *IEEE Transactions on Automatic Control*, 35(1):92–95, 1990.

[104] Miloš S Stanković and Dušan M Stipanović. Discrete time extremum seeking by autonomous vehicles in a stochastic environment. In *48h IEEE Conference on Decision and Control held jointly with 28th Chinese Control Conference*, pages 4541–4546. IEEE, 2009.

[105] Kazuaki Tanaka, Motoyuki Ozeki, and Natsuki Oka. The hesitation of a robot: A delay in its motion increases learning efficiency and impresses humans as teachable. In *Proceedings of the 5th ACM/IEEE international conference on Human-robot interaction*, pages 189–190. IEEE Press, 2010.

[106] Daisuke Tsubakino, Miroslav Krstić, and Tiago Roux Oliveira. Exact predictor feedbacks for multi-input lti systems with distinct input delays. *Automatica*, 71:143–150, 2016.

[107] Gregory C Walsh. On the application of multi-parameter extremum seeking control. In *American Control Conference, 2000. Proceedings of the 2000*, volume 1, pages 411–415. IEEE, 2000.

[108] Hsin-Hsiung Wang, Simon Yeung, and Miroslav Krstić. Experimental application of extremum seeking on an axial-flow compressor. *IEEE Transactions on Control Systems Technology*, 8(2):300–309, 2000.

[109] GJ Wiens and MJ Berggren. Suboptimal path planning of robots: minimal nonlinear forces and energy. *Journal of Dynamic Systems, Measurement, and Control*, 113(4):748–752, 1991.

[110] Won Soo Yun, Dong Woo Cho, and Yoon Su Baek. Dynamic path planning for robot navigation using sonor mapping and neural networks. *Journal of Dynamic Systems, Measurement, and Control*, 119(1):19–26, 1997.

[111] Yinghua Zhang, Mario Rotea, and Nicholas Gans. Sensors searching for interesting things: Extremum seeking control on entropy maps. In *Decision and Control and European Control Conference (CDC-ECC), 2011 50th IEEE Conference on*, pages 4985–4991. IEEE, 2011.

[112] Yinghua Zhang, Jinglin Shen, Mario Rotea, and Nicholas Gans. Robots looking for interesting things: Extremum seeking control on saliency maps. In *Intelligent Robots and Systems (IROS), 2011 IEEE/RSJ International Conference on*, pages 1180–1186. IEEE, 2011.

[113] Yang Zhu and Miroslav Krstić. Adaptive output feedback control for uncertain linear time-delay systems. *IEEE Transactions on Automatic Control*, 62:545–560, 2017.

[114] Yang Zhu, Hongye Su, and Miroslav Krstić. Adaptive backstepping control of uncertain linear systems under unknown actuator delay. *Automatica*, 54:256–265, 2015.